NAUSIVIOS CHORA

A Journal in Naval Sciences and Technology

PART B:
ELECTRICAL ENGINEERING and COMPUTER SCIENCE

Volume 4/2012

ΝΑΥΣΙΒΙΟΣ ΧΩΡΑ

Περιοδική Έκδοση Ναυτικών Επιστημών

ΜΕΡΟΣ Β:
ΕΠΙΣΤΗΜΕΣ ΗΛΕΚΤΡΟΛΟΓΟΥ ΜΗΧΑΝΙΚΟΥ ΚΑΙ ΜΗΧΑΝΙΚΟΥ ΗΛΕΚΤΡΟΝΙΚΩΝ ΥΠΟΛΟΓΙΣΤΩΝ

Τεύχος 4/2012

«ΝΑΥΣΙΒΙΟΣ ΧΩΡΑ» 2012
Περιοδική Έκδοση Ναυτικών Επιστημών
Σχολή Ναυτικών Δοκίμων,
Τέρμα Χατζηκυριακού, Χατζηκυριάκειο,
Πειραιάς 18539, Ελλάδα
http://nausivios.snd.edu.gr
ΤΗΛ+302104581382/FAX+302104581604
nausivios@snd.edu.gr

"NAUSIVIOS CHORA" 2012
Journal in Naval Sciences and Technology
Hellenic Naval Academy
Hatzikiriakio, 18539 Piraeus, Greece
http://nausivios.snd.edu.gr
Tel +302104581382/fax +302104581604
nausivios@snd.edu.gr

ISSN: 1791-4469

TABLE OF CONTENTS

Χαιρετισμός Διοικητή Σχολής Ναυτικών Δοκίμων

Καλωσορίζουμε το 4ο τεύχος της «Ναυσιβίου Χώρας» που αναδεικνύει το έργο που επιτελείται στη ΣΝΔ όσον αφορά τις Ναυτικές Επιστήμες.

Σήμερα, σε μια εποχή οικονομικών και κοινωνικών προβλημάτων η έκδοση της «Ναυσιβίου Χώρας» σηματοδοτεί την προσπάθεια των καθηγητών της ΣΝΔ και άλλων εκπαιδευτικών ιδρυμάτων να δημιουργήσουν με το έργο τους θετικές προσδοκίες και εμπλουτισμό γνώσεων τόσο στους φοιτούντες στα Ανώτατα Στρατιωτικά Εκπαιδευτικά Ιδρύματα όσο και σε όλες τις Πανεπιστημιακές Σχολές που ασχολούνται με τον κλάδο των Ναυτικών Επιστημών. Στόχος τους είναι να ενημερώσουν και να προβάλλουν νέες μεθόδους και εξελιγμένες τεχνικές βασισμένες σε προσωπικές έρευνες και αναλύσεις, με αποτέλεσμα την καλύτερη εκπαίδευση και επιμόρφωση των νέων επιστημόνων.

Ως εκ τούτου, χαιρετίζω την τέταρτη έκδοση της «Ναυσιβίου Χώρας» με την ευχή να αποτελέσει ένα νέο κίνητρο για την εξέλιξη και την πρόοδο της Ναυτικής Επιστήμης τόσο στην Ελλάδα όσο και στο εξωτερικό.

Υποναύαρχος Ι. Μαΐστρος ΠΝ, Διοικητής ΣΝΔ

Welcome Address by the Commandant of the Hellenic Naval Academy

We welcome the 4th edition of the “Nausivios Chora” which illustrates the work of the Hellenic Naval Academy concerning the Naval Sciences.

Nowadays, at a time of economic and social problems, the edition of the “Nausivios Chora” underlines the effort of the staff of the Hellenic Navy Academy and other Institutes to create with their work positive expectations and knowledge enrichment both to the students of the Higher Military Educational Institutions and to other Universities that are engaged with Naval Sciences. They are targeting to inform and display new methods and sophisticated techniques based on personal research and analysis, in order to educate and train the new scientists.

Therefore, I wellcome the fourth edition of the “Nausivios Chora” with the wish for it to be a motive for the development and progress of the Naval Science not only in Greece but also abroad.

Rear-Admiral I. Maistros HN, Commandant of the Hellenic Naval Academy

International Advisory Committee

Editorial Board

Editor's Note

"Nausivios Chora" is a scientific journal published since 2006 by the Hellenic Naval Academy, the Institution that provides academic and professional training to the future officers of the Hellenic Navy. The faculty members of the Hellenic Naval Academy are devoted to the promotion of research and education on a broad range of scientific disciplines.

"Nausivios Chora" is a biannual, peer-reviewed, open access journal that publishes original articles in areas of scientific research and applications directly or indirectly related to the naval sciences and technology. The scope of the Journal is to provide a basis for the communication and dissemination of scientific results obtained in Hellenic or International academic and research institutions that may present a relevance to the sea element.

"Nausivios Chora" hosts articles belonging to various scientific disciplines and is divided in five parts, namely *Mechanical and Marine Engineering*, *Electrical Engineering and Computer Science*, *Natural Sciences and Mathematics*, *Humanities and Political Sciences* and *Naval Operations*. The present 2012 Edition Issue contains 24 articles.

The International Advisory Committee members and the Body of Reviewers, all acknowledged experts in their field of interests, cover a wide range of scientific disciplines ensuring the integrity of the peer-review process and the academic excellence of the published articles in a way that best represents the aims and scope of the Journal.

Prof Dr Elias Ar Yfantis
Editor in chief

Acknowledgments

I wish to express my special thanks to Dr Antonis Tsapalis for his excellent work as the administrator of the “Nausivios Chora” website.
Special thanks to Dr Evangelia Karagianni for her creative work on the “Nausivios Chora” 2012 Edition.

E.Ar.Yfantis

PART B:

ELECTRICAL ENGINEERING and COMPUTER SCIENCE

Availability Investigation of Free Space Optical Links with Time Diversity for Turbulence Channels Modeled with the K-Distribution

A.N. Stassinakis, G.G. Chronopoulos and H.E. Nistazakis

Department of Electronics, Computers, Telecommunications and Control, Faculty of Physics, National and Kapodistrian University of Athens, Athens, 15784, Greece
e-mails: {a-stasinakis;grigchronop;enistaz}@phys.uoa.gr

Abstract. The terrestrial free space optical (FSO) communication systems, are attaining license free, high bandwidth access and security with low installation and operation cost. On the other hand, their main disadvantage is the continuous variations of the characteristics of the electromagnetic beam's propagation path, which is the atmosphere, causing performance mitigation on system's availability and performance. A very important phenomenon which induces these variations is the atmospheric turbulence. In order to minimize its influence on the characteristics of the FSO links, many techniques have been investigated and among them, the diversity techniques have attracted significant research interest. In this work, we investigate the availability, by means of their outage probability estimation, of FSO communication links which are using the time diversity configuration, over strong atmospheric turbulence channels modelled with the K-distribution. For this setup, we derive closed form mathematical expressions for the estimation of outage probability for various atmospheric turbulence strengths. Finally, we present numerical results for many cases with various turbulence strengths and time diversity characteristics.

Keywords: K-distribution, Diversity Techniques, Atmospheric Turbulence, Outage Probability, Wireless Optical Communication Systems.
PACS: 42.79.Sz, 92.60.hk.

INTRODUCTION

The terrestrial outdoor wireless communication systems which are using the optical frequencies, i.e. the free space optical (FSO) communication systems, are combining many advantages such as, license free, high bandwidth access and security with low installation and operation cost, [1]-[4]. Obviously, the propagation path for the electromagnetic beam is the atmosphere. Thus, any change of its characteristics causes performance variations. One of them, is the atmospheric turbulence which represents a very significant availability and performance mitigation factor [1], [2], [4]-[10], affecting both, intensity and phase of the optical signal [11]. This phenomenon, for the case of a typical outdoor line-of-sight, point-to-point optical link causes even rapid fluctuations at the irradiance of the signal at the receiver's end. As a result, the optical channel is showing randomly time-varying characteristics due to the so-

called scintillation effect, [1], [2], [5]-[8], which are decreasing the FSO system's availability and performance.

In order to counterbalance the influence of the turbulence effect on the availability and performance of FSO links, the diversity techniques have attracted significant attention by many research groups [11]-[18]. This technique is used in RF communication systems and most of the times is realized in space, in time or in wavelength. For the spatial diversity, [12]-[16], the optical communication system uses multiple transmitters and/or receivers at different places which are transmitting and receiving copies of the same part of the information signal. For the links with time diversity [17]-[19], there is only one trans–receiver pair, but the information signal is retransmitted more than once at different time slots. Finally, the systems which are using the wavelength diversity, [11], [19]-[21], use a composite transmitter and the signal is transmitted at the same time at different wavelengths towards a number of wavelength-selected receivers.

In this work we investigate the availability of FSO communication systems which are using the time diversity schemes over strong atmospheric turbulence channels modelled with the K-distribution [22]-[24]. For this point-to-point configuration, which consists of one transmitter and one receiver, in each side of the link [18], [19], we study its availability by means of the outage probability estimation for various atmospheric turbulence conditions. For the estimation of this metric we derive closed form mathematical expressions.

The rest of this paper is organized as follows: in section II we analyze the basic characteristic of the FSO link with time diversity and we present the channel model. In section III, we derive the mathematical expression for the estimation of the outage probability while, in section IV we present the corresponding numerical results and in section V we outline the conclusions.

SYSTEM AND CHANNEL MODEL

In an FSO link that uses time diversity schemes, the signal is transmitted in multiple copies, M, in different time slots. Thus, every copy is transmitted through the same spatial channel but with different turbulence characteristics each time due to the fact that it is a very rapidly varying phenomenon. As mentioned above, this system is using only one transmitter and one receiver in each side of the optical link. Hence, this procedure can be emulated as to send each copy in different receivers at the same time, i.e. similar as a system with one transmitter (single input) and multiple receivers (multiple outputs) - SIMO).

This link with time diversity can be described by using a binary input and continuous output with intensity modulation – direct detection (IM/DD) and the modulation we use is on-off keying (OOK). The channel is assumed to be memoryless, stationary with independent and identically distributed intensity (i.i.d) fast fading statistics with additive Gaussian noise (AWGN). Thus, as it is mentioned above, in order to model the FSO link with time diversity which is sending M times each part of the signal, we assume that the FSO link can be studied as a communication system with one transmitter and M receivers. Thus, the statistical channel model is given as [15], [18], [19]:

$$y_m = s_m x + n = \eta_m x I_m + n, \qquad m = 1,\ldots,M \tag{1}$$

where y_m represents the signal arriving at the receiver, s_m is the instantaneous gain and is equal to ηI_m where η is the effective photo-current conversion ratio of the receiver while I_m is the instantaneous normalized irradiance at the receiver, x is the modulated signal that is transmitted and takes the values "0" or "1" and finally, n is the AWGN with zero mean and variance $N_0/2$.

For the cases of strong turbulence conditions, the induced fading can be assumed as a random process that follows the K-distribution [15], [22]-[24]. The corresponding probability density function (pdf) is given as [23]:

$$f_{I_m}(I_m) = \frac{2(b_m)^{\frac{1+b_m}{2}}}{\Gamma(b_m)} I_m^{\frac{1+b_m}{2}-1} K_{b_m-1}\left(2\sqrt{b_m I_m}\right) \tag{2}$$

where $K_v(.)$ stands for the modified Bessel function of the second kind of order v, $\Gamma(.)$ is the gamma function while the parameter b_m is related to the effective number of discrete scatterers [22]-[24].

The corresponding cumulative distribution function (cdf) for the K-distribution is calculated by integrating (2) and concludes to the following expression [15], [23]:

$$F_{I_m}(I_m) = \frac{(b_m I_m)^{\frac{1+b_m}{2}}}{\Gamma(b_m)} G_{1,3}^{2,1}\left(b_m I_m \left| \begin{matrix} \frac{1-b_m}{2} \\ \frac{1-b_m}{2}, \frac{b_m-1}{2}, -\frac{1+b_m}{2} \end{matrix} \right. \right) \tag{3}$$

where $G_{p,q}^{m,n}[\cdot]$ stands for the Meijer G-function, [25].

Next, we define the instantaneous electrical signal-to-noise ratio (SNR) as $\xi_m = (\eta I_m)^2 / N_0 = s_m^2 / N_0$, [10], [18], and the average electrical SNR as $\mu = (\eta E[I_m])^2 / N_0$, [10], [18], [26], where $E[.]$ stands for the expected value of the normalized irradiance I_m. Using the expressions of ξ_m and μ_m in (2) and after a power transformation of I_m, the pdf of K distribution for ξ_m is obtained in the following form [15], [23]:

$$f_{\mu_m}(\mu_m) = \frac{(b_m)^{\frac{1+b_m}{2}}}{\Gamma(b_m)} \frac{\xi_m^{\frac{1+b_m}{4}-1}}{\mu_m^{\frac{1+b_m}{4}}} K_{b_m-1}\left(\sqrt[4]{\frac{16 b_m \xi_m}{\mu_m}} \right) \tag{4}$$

while the corresponding cdf of K-distribution has the following form [15], [23]:

$$F_{\xi_m}(\xi_m) = \frac{(b_m)^{\frac{1+b_m}{2}}}{\Gamma(b_m)} \left(\frac{\xi_m}{\mu_m}\right)^{\frac{1+b_m}{4}} G_{1,3}^{2,1}\left(b_m \sqrt{\frac{\xi_m}{\mu_m}} \left| \begin{matrix} \frac{1-b_m}{2} \\ \frac{1-b_m}{2}, \frac{b_m-1}{2}, -\frac{1+b_m}{2} \end{matrix} \right. \right) \tag{5}$$

OUTAGE PROBABILITY OF THE FSO LINK WITH TIME DIVERSITY

The above cdf can conclude to a mathematical expression for the estimation of the outage probability of the FSO communication systems with time diversity, over turbulent channels modeled with the K distribution. This metric, represents the probability that the instantaneous electrical SNR falls below a critical threshold, ξ_{th}, which represents the receiver's sensitivity limit

and thus, it is a particularly important parameter for systems' designing [10], [18], [19]. The outage probability for each one of the *M* copies of the signal is given as [10], [18], [19], [27]:

$$P_{out,m} = \Pr(\xi_m \le \xi_{th}) = F_{\xi_m}(\xi_{th}), \tag{6}$$

In this section we will derive the expression for the outage probability of an FSO link when the turbulence channel is modeled by K-distribution and the system uses time diversity. Due to the independence of outage probability of each copy of the *M* copies of the signal that will be transmitted, the outage probability of the FSO link can be estimated as [12], [18], [19]:

$$P_{out,M} = \Pi_{m=1}^{M} \Pr(\xi_m \le \xi_{th}) = \Pi_{m=1}^{M} F_{\xi}(\xi_{th}) \tag{7}$$

Thus, from (5) and (7) we conclude the following finite product for the estimation of the probability of error for the FSO time diversity scheme over strong turbulence conditions:

$$P_{out}(\xi_{th}) = \prod_{m=1}^{M} \left[\frac{b_m^{\frac{1+b_m}{2}}}{\Gamma(b_m)} \left(\frac{\xi_{th}}{\mu_m} \right)^{\frac{1+b_m}{4}} G_{1,3}^{2,1}\left(b\sqrt{\frac{\xi_{th}}{\mu_m}} \middle| \begin{matrix} \frac{1-b_m}{2} \\ \frac{1-b_m}{2}, \frac{b_m-1}{2}, -\frac{1+b_m}{2} \end{matrix} \right) \right] \tag{8}$$

The above expression, i.e. Eq. (8), can be further simplified by taking into account that the FSO link is using time diversity. Thus, in this scheme, as mentioned above, is using only one pair of trans-receiver in each side of the optical link and as a result, the spatial propagation path, for all the copies of the information signal, is the same. Thus, we can assume accurately, that the value of b_m, of Eqs (4) and (5), as well the average electrical SNR, μ_m, remain, practically, invariable for all the *M* transmitted copies [18], [19]. Hence, in (8) we can assume $b=b_1=b_2=\ldots=b_M$ and $\mu=\mu_1=\mu_2=\ldots=\mu_M$, as well, [18], [19].

Using the above assumptions the expression of Eq. (8) results to the following closed form mathematical expression for the estimation of FSO system's availability through the estimation of its outage probability for strong atmospheric turbulence channels modeled with the K-distribution:

$$P_{out}(\xi_{th}) = \left[\frac{b^{\frac{1+b}{2}}}{\Gamma(b)} \left(\frac{\xi_{th}}{\mu} \right)^{\frac{1+b}{4}} G_{1,3}^{2,1}\left(b\sqrt{\frac{\xi_{th}}{\mu}} \middle| \begin{matrix} \frac{1-b}{2} \\ \frac{1-b}{2}, \frac{b-1}{2}, -\frac{1+b}{2} \end{matrix} \right) \right]^{M} \tag{9}$$

It is important to mention here that the expression (8) can be used for many types of diversity, such as spatial, wavelength, etc, while the expression (9) stands for the time diversity scheme. Additionally, this expression, i.e. Eq. (9), estimates the total probability of outage of an FSO link with time diversity over strong turbulence conditions. It is worth mentioning here that this result, i.e. Eq. (9), generalizes the expression of the outage probability of the single FSO point-to-point link without diversity, obtained in [23].

NUMERICAL RESULTS

Using the mathematical expressions obtained in Eqs (8) and (9), the outage probability estimation of an FSO link with time diversity under strong atmospheric turbulence conditions modelled with the K distribution, is feasible. By studying quantitatively these expressions it is clear that this technique improves the system's availability without need of extra trans-receivers, in each side of the FSO links. On the other hand, due to the finite bandwidth of the channel and the one and only spatial propagation path, the performance of the link is decreasing, as shown in [18], [19], [28]. Thus, in order to design an FSO link with time diversity, in practice, we should choose the correct diversity strength, i.e. the value of *M*, according to the requirements of each FSO link.

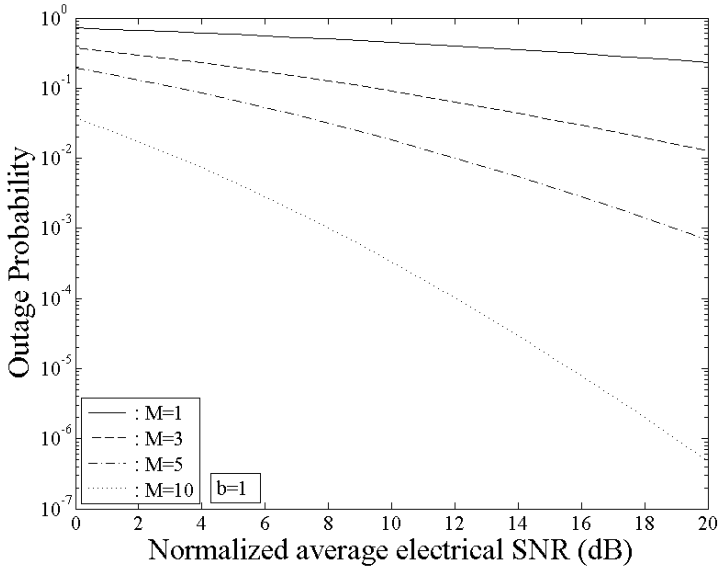

FIGURE 1. Outage probability, P_{out}, of an FSO link with time diversity, modeled with the K-distribution, versus the normalized average electrical SNR, μ/ξ_{th}, with b=1 and various values of time diversity parameter M.

In this section, we present the availability results for the FSO links with time diversity, using the extracted mathematical expressions of Eq. (9). The important parameters of the FSO link which are modelled with the K distribution, are the number of repetitions of the information signal, M, the normalized average electrical SNR at the receiver, μ/ξ_{th}, and the parameter b. For the parameter b we choose three values, i.e. 1, 7 and 15, where the smaller values correspond to stronger turbulence conditions. On the other hand, for the time diversity parameter, M, we consider the values 1, which corresponds to an FSO link without diversity, 3, 5 and 10.

In Figure (1) we present the results for the case of very strong turbulence conditions, i.e b=1. It is obvious that for the case without diversity, even the smaller value of outage probability, i.e for large value of the normalized average electrical SNR, is giving a very large value which is not acceptable for FSO communication links. Thus, the same link with strong, M=5, or stronger, M=10, time diversity achieves much better values for this probability metric. It is obvious that for larger values of M, the availability improvement would be better, but, as mentioned above, further increase of M, will result in significant decrease of the effective (practical) bit rate of the system [18], [19], [28].

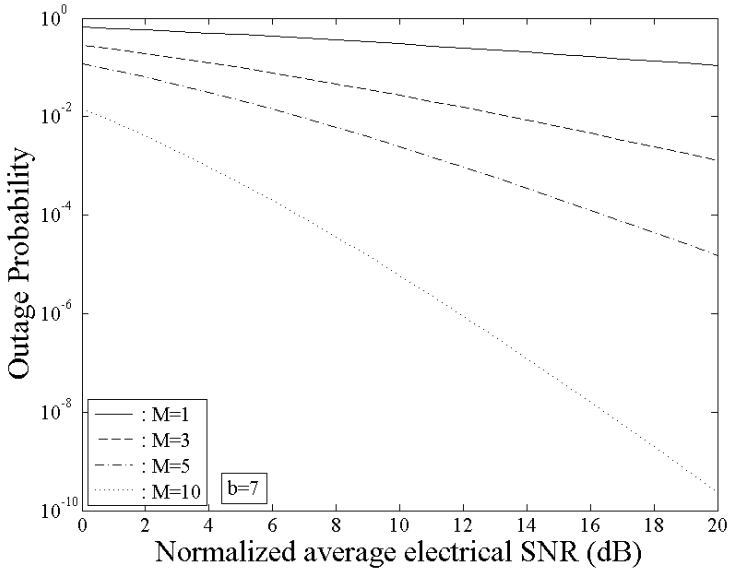

FIGURE 2. Outage probability, P_{out}, of an FSO link with time diversity, modeled with the K-distribution, versus the normalized average electrical SNR, μ/ξ_{th}, with b=7 and various values of time diversity parameter M.

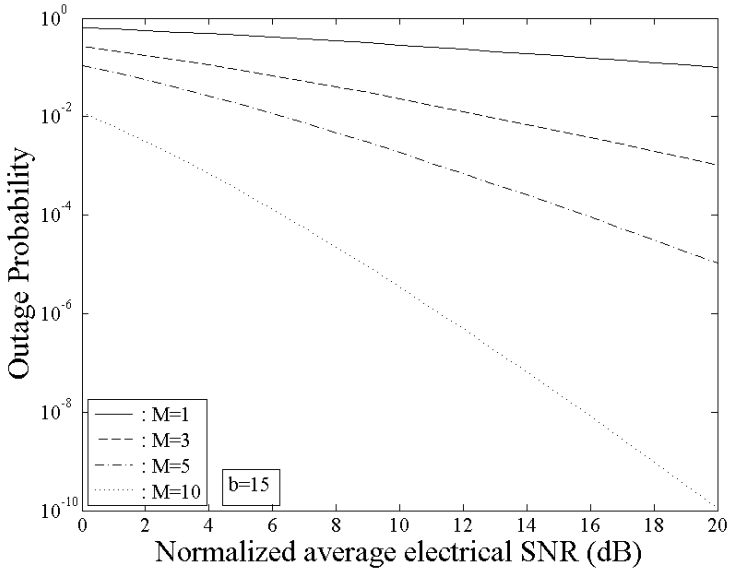

FIGURE 3. Outage probability, P_{out}, of an FSO link with time diversity, modeled with the K-distribution, versus the normalized average electrical SNR, μ/ξ_{th}, with b=15 and various values of time diversity parameter M.

The above conclusion, is clear for larger values of b, i.e. for weaker atmospheric turbulence conditions than those of Figure (1). Thus, in Figures (2) and (3) we present the corresponding results for b=7 and 15. In both cases, it is obvious that the values of outage probability, without time diversity, i.e. M=1, are smaller than those of the previous case with b=1, but they are still large and not acceptable for practical FSO links, even for large values of normalized average electrical SNR. This situation is much better when the time diversity scheme is used. As we can

observe in Figures (2) and (3), for time diversity values, M=5 and M=10, the link can easily achieve very small values of this probability and thus the system can be easily characterized as one with very high availability.

CONCLUSIONS

In this work we investigated an FSO system which is using a time diversity scheme in order to increase its availability against atmospheric turbulence effect. More specifically, we investigate the capabilities of a terrestrial, outdoor, FSO link with time diversity, which is working under strong turbulence conditions modeled with the K-distribution. For this case we extract both, general and more specific, closed form mathematical expressions for the estimation of the link's availability through the estimation of outage probability. We prove that this technique can decrease significantly the system's probability of outage without need of extra trans-receivers in each side of the link. Moreover, in the section with the numerical results, using the above derived mathematical expressions, we show that the achieved improvement of the link's availability characteristics are significant and consequently, the whole system can be described as one with very high availability.

REFERENCES

1. H. Henniger, and O. Wilfert, “An Introduction to Free-Space Optical Communications,” *Radioengineering*, vol. 19, iss. 2, pp. 203-212, 2010.
2. Z. Ghassemlooy and W.O. Popoola, "Terrestrial Free-Space Optical Communications", book chapter in "Mobile and Wireless Communications: Network Layer and Circuit Level Design", Salma Ait Fares and Fumiyuki Adachi (Ed.), ISBN: 978-953-307-042-1, InTech, 2010.
3. D. Keddar and S. Arnon, Urban Optical Wireless Communication Networks: the Main Challenges and Possible Solutions, IEEE Opt. Com. (2004) S1-S7.
4. S. Arnon, Optical Wireless Communications, Encycl. Opt. Eng., Marcel Dekker Inc. New York, (2003), pp. 1866-1886.
5. A.K. Majumdar, Free-Space Laser Communication Performance in the Atmospheric Channel, J. Opt. Fiber Commun. Rep., 2 (2005) 345-396.
6. L.C. Andrews, R.L. Phillips, C.Y. Hopen, Laser Beam Scintillation with Applications, SPIE Optical Engineering Press, (2001).
7. W.O. Popoola, Z. Ghassemlooy, C.G. Lee and A.C. Boucouvalas, Scintillation Effect on Intensity Modulated Laser Communication Systems - A Laboratory Demonstration, Optics and Laser Technology, 42, 4 (2010) 682-692.
8. L.C. Andrews, M.A. Al-Habash, C.Y. Hopen, and R.L. Phillips, Theory of Optical Scintillation: Gaussian Beam Wave Model, Waves in Random Media, 11 (2001) 271-291.
9. H.E. Nistazakis, E.A. Karagianni, A.D. Tsigopoulos, M.E. Fafalios, and G.S. Tombras, “Average capacity of optical wireless communication systems over atmospheric turbulence channels”, *IEEE/OSA Journal of Lightwave Technology*, Vol. 27, no. 8, pp. 974-979, (2009).
10. H.E. Nistazakis, T.A. Tsiftsis and G.S. Tombras, Performance Analysis of Free-Space Optical Communication Systems Over Atmospheric Turbulence Channels, IET Communications, 3, 8 (2009) 1402-1409.
11. R. Rachmani, and S. Arnon, “Wavelength Diversity in Turbulence Channels for Sensor Networks,” *IEEE 26th Convention of Electrical and Electronics Engineers in Israel, IEEEI 2010*, art. no. 5661946, pp. 915-918, 2010.
12. A.N. Stassinakis, H.E. Nistazakis, and G.S. Tombras, “Comparative Performance Study of One or Multiple Receivers Schemes for FSO Links Over Gamma Gamma Turbulence Channels”, *Taylor & Francis Group, Journal of Modern Optics*, Vol. 59, Iss. 11, pp. 1023-1031, 2012.

13. S.M. Navidpour, M. Uysal, and M. Kavehrad, “BER Performance of Free Space Optical Transmission with Spatial Diversity,” *IEEE Trans. Wireless Commun.*, vol. 6, iss. 8, pp. 2813-2819, 2007.
14. E.J. Shin, and V.W.S. Chan, “Optical Communication Over the Turbulent Atmospheric Channel using Spatial Diversity,” *Conference Record / IEEE Global Telecommunications Conference*, vol. 3, pp. 2055-2060, 2002.
15. T.A. Tsiftsis, H.G. Sandalidis, G.K. Karagiannidis, and M. Uysal, “Optical Wireless Links with Spatial Diversity Over Strong Atmospheric Turbulence Channels,” *IEEE Transactions on Wireless Communications*, vol. 8, iss. 2, art. no. 4786457, pp. 951-957, 2009.
16. Z. Wang, W.-D. Zhong, S. Fu, and C. Lin, “Performance Comparison of Different Modulation Formats Over Free-Space Optical Turbulence Links with Space Diversity Reception Technique,” *IEEE Photonics Journal*, vol. 1, iss. 6, pp. 277-285, 2009.
17. F. Xu, A. Khalighi, P. Caussé, and S. Bourennane, “Channel Coding and Time-Diversity for Optical Wireless Links,” *Optics Express*, vol. 17, iss. 2, pp. 872-887, 2009.
18. H.E. Nistazakis, “A Time-Diversity Scheme for Wireless Optical Links Over Exponentially Modeled Turbulence Channels”, *Elsevier, Optik -International Journal for Light and Electron Optics*, in press.
19. H.E. Nistazakis and G.S. Tombras, “On the use of Wavelength and Time Diversity in Optical Wireless Communication Systems over Gamma-Gamma Turbulence Channels”, *Elsevier, Journal of Optics & Laser Technology*, Vol. 44, Iss. 7, pp. 2088-2094, 2012.
20. E. Wainright, H.H. Refai, and J.J. Sluss Jr., “Wavelength Diversity in Free-Space Optics to Alleviate Fog Effects”, *Proceedings of SPIE - The International Society for Optical Engineering*, vol. 5712, art. no. 16, pp. 110-118, 2005.
21. R. Purvinskis, D. Giggenbach, H. Henniger, N. Perlot, and F. David, “Multiple Wavelength Free-Space Laser Communications,” *Proceedings of SPIE - The International Society for Optical Engineering*, vol. 4975, pp. 12-19, 2003.
22. M. Uysal, S.M. Navidpour and J. Li, “Error Rate Performance of Coded Free Space Optical Links Over Strong Turbulence Channels", IEEE Communications Letters, Vol. 8, no 10, 2004.
23. H.G. Sandalidis, T.A. Tsiftsis, “Outage probability and ergodic capacity of free-space optical links over strong turbulence”, *Electronics Lett*ers, Vol. 44, no. 1, p.p. 46 – 47, 2008.
24. H.E. Nistazakis, A.D. Tsigopoulos, M.P. Hanias, C.D. Psychogios, D. Marinos, C. Aidinis, and G.S. Tombras, Estimation of Outage Capacity for Free Space Optical Links Over I-K and K Turbulent Channels, Radioengineering, 20, 2 (2011) 493-498.
25. V.S. Adamchik, O.I. and Marichev, “The Algorithm for Calculating Integrals of Hypergeometric Type Function and its Realization in Reduce System,” *Proc. International Conference on Symbolic and Algebraic Computation*, pp. 212-224, Tokyo, Japan, 1990.
26. X. Zhu, and J.M. Kahn, Free-Space Optical Communications Through Atmospheric Turbulence Channels, IEEE Trans. on Commun., 50, 8 (2002) 1293-1300.
27. W.O. Popoola, Z. Ghassemlooy and E. Leitgeb, BER and Outage Probability of DPSK Subcarrier Intensity Modulated Free Space Optics in Fully Developed Speckle, Journal of Communications, 4, 8 (2009) pp. 546-554.
28. A.D. Tsigopoulos, "Maximum Effective Bit Rate Estimation for Wireless Optical Communication Links with Time-Diversity Over Strong Turbulence Channels", *Nausivios Chora 2012*, submitted.

Maximum Effective Bit Rate Estimation for Wireless Optical Communication Links with Time-Diversity Over Strong Turbulence Channels

Andreas D. Tsigopoulos

Dept. of Battle Systems, Naval Operations, Sea Studies, Navigation, Electronics and Telecommunications,
Hellenic Naval Academy, Hadjikyriakou ave, Piraeus 18539, Greece
e-mail: atsigo@snd.edu.gr

Abstract. The free space optical communication systems exhibit significant research and commercial interest in the last few years due to their capability of achieving optical wireless communications with high and secure data rate transmission and low installation and operational cost, without need of licensing. On the other hand, the unstable conditions of the atmosphere, which is the propagation path of the laser beam that carries the information signal, and especially the atmospheric turbulence effect, affects mainly its intensity and causes random irradiance fluctuations at the receiver's end. This phenomenon causes a significant reduction in the system's availability and performance (BER). In order to overcome this reduction, many methods have been studied, from which the diversity techniques are a very efficient solution. In this work, we investigate a time-diversity scheme for free space optical channels under strong turbulence conditions modeled with the K distribution. We concentrate on the estimation of the maximum effective bit rate of the link, which is limited by the finite capacity of the optical channel, as well as on the multiple transmission of the same part of the information signal in order to achieve much better performance characteristics using the time diversity scheme. Thus, we extract closed form mathematical expressions for the estimation of the maximum effective bit rate, for both, fast and slow, fading statistics. Finally, we present numerical results for many practical cases.

Keywords: K-distribution, Time diversity, Free Space Optical Communication Systems, Atmospheric Turbulence, Maximum Effective Bit Rate, Channel Capacity.
PACS: 42.79.Sz, 92.60.hk.

INTRODUCTION

Free space optical (FSO) communication systems enable the communication between two points with a laser beam using the atmosphere as a channel. This kind of wireless communication has many advantages compared to other methods, such as high speed of data transfer (bit-rate), no need of license to transmit in this band of frequencies, low installation and operation cost. On the other hand, the unstable conditions of the atmosphere and especially the atmospheric turbulence effect, affects the intensity of the laser beam causing random irradiance

fluctuations at the receiver's end. So, the atmosphere is a channel with randomly time varying characteristics [1]-[8].

Thus, it is obvious that the atmospheric turbulence is a mitigation factor for the performance and reliability of the FSO link, due to the induced scintillation effect [4]-[10]. In order to overcome this influence, many techniques have been investigated. The diversity schemes represent one of them [11]-[19]. In this technique, the information signal is sent more than once, using different spatial paths, i.e. spatial diversity, different wavelengths, i.e. wavelength diversity, different polarizations, i.e. polarization diversity, or different time slots, i.e. time diversity [16], [19]. Thus, each copy of the information signal propagates through a channel with different characteristics and obviously the probability of error is decreasing as well as the probability of outage of the FSO system.

In this work, we are studying an FSO communication link over atmospheric turbulence channel by assuming strong turbulence conditions modeled with the K-distribution [20]-[22], with a time diversity scheme. In this configuration, the main advantage is the requirement of one and only trans-receiver pair which is sending the same information signal more than once in different time slots. On the other hand, taking into account that the channel's capacity is finite, this technique reduces the actual effective maximum bit rate of the link. Thus, we present mathematical expressions for the estimation of this limit for both, slow and fast, fading statistics of the wireless connection.

The rest of this work is organized as follows: in Section II, we introduce the considered FSO system and channel model for the time diversity scheme. In Section III, we derive closed-form mathematical expressions for the estimation of the maximum effective bit rate of the FSO link for slow and fast fading statistics, while in Section IV, we present numerical results for the system's reliability and performance for various link's parameters. Final conclusions are presented in Section V.

THE FSO CHANNEL MODEL WITH TIME DIVERSITY

As mentioned above, for the FSO links with time diversity, only a single pair of transmitter and receiver is needed and the information signal is sent more than once using different time slots. Thus, this diversity scheme can be emulated with an FSO communication system which is using one transmitter that transmits M copies of the signal at M different time-slots and one receiver for these M copies. Hence, this operation is equivalent to the combined operation of one transmitter transmitting through M channel/branches and M receivers at the receiving end, similar with the Single Input Multiple Output (SIMO) communication systems [19].

The system's input is binary and the output continuous intensity modulation/direct detection (IM/DD), with On-Off keying (OOK) modulation. Moreover, the channel is characterized as stationary and memoryless with independent and identically distributed intensity (i.i.d) fading statistics, with additive white Gaussian noise (AWGN). In this case, the statistical channel model can be expressed as in [14], [15], [23]:

$$r_m = s_m x + n = \eta x I_m + n, \qquad m = 1,\ldots,M \tag{10}$$

where y_m is the signal at the receiver for each one of the M copies of the information signal, $s_m=\eta_m I_m$ is the instantaneous intensity gain, η is the effective photo-current conversion ratio of the receiver, I_m is the normalized irradiance arrived in each receiver, x is the modulated signal (taking the binary values "0" or "1"), and n represents the additive white Gaussian noise (AWGN) with zero mean and variance equal to $N_0/2$, [24], [25].

For strong atmospheric turbulence conditions modeled with the K distribution, the probability density function (pdf) of this model is given in [21], as:

$$f_{I_m}(I_m) = \frac{2(a_m)^{\frac{1+a_m}{2}}}{\Gamma(a_m)} I_m^{\frac{a_m-1}{2}} K_{a_m-1}\left(2\sqrt{a_m I_m}\right) \tag{11}$$

where $K_v(.)$ is the modified Bessel function of the second kind of order v and $\Gamma(.)$ is the gamma function. In addition, a_m represents a parameter that is generally associated with the number of scatterers forming the random component of the optical field [20]-[22]. By integrating (2), we conclude the corresponding cumulative distribution function (cdf), which has the following expression [21]:

$$F_{I_m}(I_m) = \frac{(a_m I_m)^{\frac{1+a_m}{2}}}{\Gamma(a_m)} G_{1,3}^{2,1}\left(b_m I_m \left| \begin{matrix} \frac{1-a_m}{2} \\ \frac{1-a_m}{2}, \frac{a_m-1}{2}, -\frac{1+a_m}{2} \end{matrix} \right. \right) \tag{12}$$

Next, we define the instantaneous electrical signal-to-noise ratio (SNR) as $\xi_m = (\eta I_m)^2 / N_0 = s_m^2 / N_0$, [25], and the average electrical SNR as $\mu_m = (\eta E[I_m])^2 / N_0$, [25], [26], with *E[.]* being the expected value of the normalized irradiance of the m_{th} copy of the information signal I_m. Thus, the pdf and the cdf of ξ_m, for the K distribution, are given as [21]:

$$f_{\xi_m}(\xi_m) = \frac{(a_m)^{\frac{1+a_m}{2}}}{\Gamma(a_m)} \frac{\xi_m^{\frac{1+a_m}{4}-1}}{\mu_m^{\frac{1+a_m}{4}}} K_{a_m-1}\left(\sqrt[4]{\frac{16 a_m^2 \xi_m}{\mu_m}} \right) \tag{13}$$

and

$$F_{\xi_m}(\xi_m) = \frac{(a_m)^{\frac{1+a_m}{2}}}{\Gamma(a_m)} \left(\frac{\xi_m}{\mu_m} \right)^{\frac{1+a_m}{4}} G_{1,3}^{2,1}\left(\sqrt{\frac{a_m^2 \xi_m}{\mu_m}} \left| \begin{matrix} \frac{1-a_m}{2} \\ \frac{1-a_m}{2}, \frac{a_m-1}{2}, -\frac{1+a_m}{2} \end{matrix} \right. \right) \tag{14}$$

where $G_{p,q}^{m,n}[\cdot]$ is the Meijer G-function, [27].

For a time diversity scheme, due to the fact that we use one pair of transmitter and receiver and consequently the spatial propagation path is the same, we can assume that the value of a_m, of Eqs (4) and (5), as well the average electrical SNR, μ_m, remain invariable for all the M copies of the transmitted signal [19]. Hence, the pdf and the cdf for ξ_m, is obtained from (4) and (5) by assuming that $a=a_1=a_2=\ldots=a_M$ and $\mu=\mu_1=\mu_2=\ldots=\mu_M$, [19] and we have the following mathematical forms, [21]:

$$f_{\xi_m}(\xi_m) = \frac{a^{\frac{1+a}{2}}}{\Gamma(a)} \frac{\xi_m^{\frac{a-3}{4}}}{\mu^{\frac{1+a}{4}}} K_{a-1}\left(\sqrt[4]{\frac{16a^2\xi_m}{\mu}}\right) \tag{15}$$

and

$$F_{\xi_m}(\xi_m) = \frac{a^{\frac{1+a}{2}}}{\Gamma(a)} \left(\frac{\xi_m}{\mu}\right)^{\frac{1+a_m}{4}} G_{1,3}^{2,1}\left(\sqrt{\frac{a^2\xi_m}{\mu}} \middle| \begin{matrix} \frac{1-a}{2} \\ \frac{1-a}{2}, \frac{a-1}{2}, -\frac{1+a}{2} \end{matrix}\right) \tag{16}$$

MAXIMUM EFFECTIVE BIT RATE OF THE LINK WITH TIME DIVERSITY

It is well known that the time diversity schemes decrease the outage probability of the FSO links, as well as their probability of error, and as a result, increase their availability, reliability and performance [16], [19]. On the other hand, due to the fact that the time diversity schemes are using one trans-receiver pair and the capacity of the channel is finite, the main disadvantage of this technique is that the multiple transmissions of the same parts of the information signal, decrease the maximum practical rate of data transmission. In this section, we will use significant mathematical expressions for FSO links without diversity, in order to investigate the maximum effective bit rate of the link with time diversity, *R′*. Obviously, this quantity is lower than the maximum bit rate of the link, *R*, due to the fact that it represents the practical rate of bit transmission, taking into account that with this technique, the same bit, occupies the trans-receiver *M* different time slots. The maximum bit rate, *R*, that can be transmitted through a single channel with fast fading statistics is determined by its average capacity, C_{av}, [19], [28]-[31], which represents the practically achievable error-free bit-rate transmission. While, for the case of slow fading statistics [19], [22], [32], [33], the value of *R* is estimated by its outage capacity, C_{out}, which stands for a metric that equals to the guaranteed capacity for channel realizations with a probability of (1-r), i.e. $\Pr[C < C_{out}] = r$, [19], [22], [32], [33]. Thus, taking into account that the time diversity scheme uses only one FSO channel, the average (outage) channel capacity of the whole scheme, coincides with *R* for the case of fast (slow) fading statistics [19].

Hence, we can derive a new mathematical expression for *R*, using the expressions obtained in [21], [22]. Thus, for *M* copies of the same bits of the information signal, the maximum effective bit rate of the time diversity FSO link, could be defined as [12], [19]:

$$R' = \frac{R}{M} \equiv \frac{C}{M} \tag{17}$$

where *C* equals either to C_{av} or to C_{out}, according to the channel's fading statistics. Thus, by substituting in Eq. (8) the results obtained in Refs [21] and [22] for average and outage channel's capacity, respectively, we conclude to the following closed form mathematical expressions for the estimation of the maximum effective bit rate, R'_{av} and R'_{out}, that are derived for both types of fading statistics, respectively:

$$R'_{av} = \frac{a^{\frac{1+a}{2}} B}{4\pi M \ln(2)\Gamma(a)\mu^{\frac{\alpha+1}{4}}} G_{2,6}^{6,1}\left(\frac{a^2}{16\mu} \middle| \begin{matrix} -\frac{1+a}{4}, \frac{3-a}{4} \\ \frac{a-1}{2}, \frac{a+1}{4}, \frac{1-a}{4}, \frac{3-a}{4}, -\frac{1+a}{4}, -\frac{1+a}{4} \end{matrix} \right) \tag{18}$$

and

$$r = \frac{\left(2^{MR'out/B}-1\right)^{\frac{a+1}{4}}}{\left(\sqrt{\mu}/\alpha\right)^{\frac{\alpha+1}{4}}\Gamma(a)} G_{1,3}^{2,1}\left(a\sqrt{\frac{2^{MR'out/B}-1}{\mu}} \middle| \begin{matrix} \frac{1-a}{2} \\ \frac{1-a}{2}, \frac{a-1}{2}, -\frac{1+a}{2} \end{matrix} \right) \tag{19}$$

with B being the channel's bandwidth, while the quantity (1-r) represents the probability of channel realizations where the capacity, C_{out}, is guaranteed.

NUMERICAL RESULTS

Using the expressions (9) and (10), we are able to present the maximum effective bit rate and the outage capacity as a function of the average electrical SNR, for the FSO link that uses time diversity scheme, for different parameter values. More specifically, we have the case without time diversity, M=1 and two cases with diversity, i.e. M=3 and M=5, for two values of parameter α, i.e. 1 and 3.

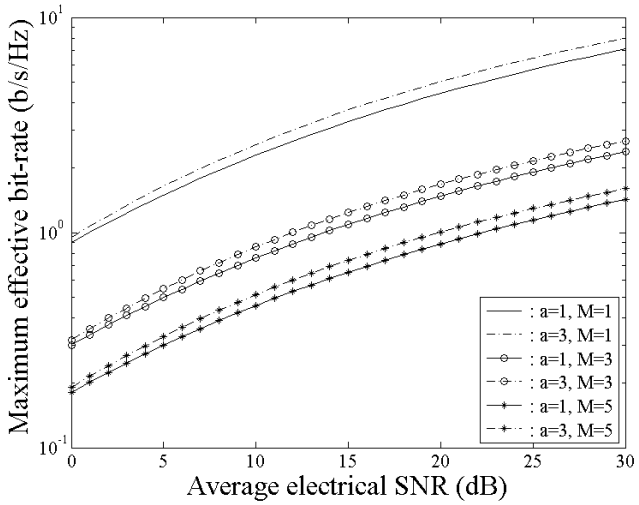

FIGURE 1. Normalized maximum effective bit rate, R_{av}/B, of an FSO link with time diversity versus the average electrical SNR, μ, for various values of M and α.

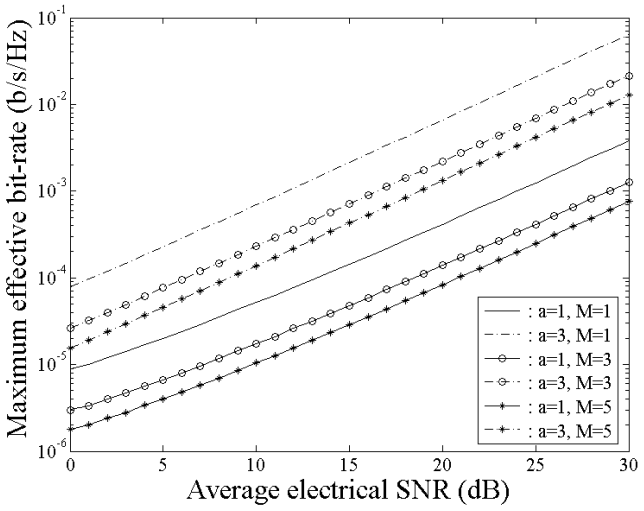

FIGURE 2. Maximum effective bit rate, R_{out}/B, of an FSO link with time diversity versus the average electrical SNR, μ, for various values of M and α.

In Fig. (1), we present the results for the maximum effective bit rate. We can see that as the parameter α increases, the bit-rate of the channel increases too, as it was expected. Moreover, in Fig. (1) it is clear that the use of time diversity technique decreases the maximum effective bit rate of the channel of the FSO link. This result in the time diversity scheme is due to the fact that the same information signal must be sent multiple times at different time slots.

In Fig. (2), we present the corresponding results for the maximum effective bit – rate, obtained from the outage capacity with r=0.01 (i.e. percentage rate 1%) which is a typical value in order to estimate the outage capacity.

CONCLUSIONS

In this work we estimated the maximum effective bit rate that an FSO communication link with time diversity, can achieve, under strong atmospheric turbulence conditions, modeled with the K distribution. This bit rate represents the practical maximum bit rate that such a system can attain due the fact that these systems are using one and only trans-receiver pair and the channel's capacity is finite. We derive closed form mathematical expressions for the estimation of this metric for both cases of fading statistics, i.e. fast and slow. Through the obtained expressions, we presented various numerical results for the maximum effective bit rate, for different values of SNR arriving at the receiver and the time diversity parameter. These results clearly demonstrate that although time diversity techniques, achieve improved availability and performance (BER) of an FSO link, they lead to a decrease of the maximum bit rate.

REFERENCES

1. D. Keddar, and S. Arnon, "Urban Optical Wireless Communication Networks: the Main Challenges and Possible Solutions," *IEEE Opt. Com.,* pp. S1-S7, 2004.
2. S. Arnon, "Optical Wireless Communications," *Encycl. Opt. Eng.*, Marcel Dekker Inc. New York, pp. 1866-1886, 2003.

3. H. Henniger, and O. Wilfert, “An Introduction to Free-Space Optical Communications,” *Radioengineering*, vol. 19, iss. 2, pp. 203-212, 2010.
4. A.K. Majumdar, “Free-Space Laser Communication Performance in the Atmospheric Channel,” *J. Opt. Fiber Commun. Rep.*, vol. 2, pp. 345-396, 2005.
5. W.O. Popoola, and Z. Ghassemlooy, “BPSK Subcarrier Intensity Modulated Free-Space Optical Communications in Atmospheric Turbulence,” *IEEE/OSA Journal of Lightwave Technology*, vol. 27, iss. 5-8, pp. 967-973, 2009.
6. L.C. Andrews, R.L. Phillips, C.Y. Hopen, Laser Beam Scintillation with Applications, SPIE Optical Engineering Press, (2001).
7. L.C. Andrews, M.A. Al-Habash, C.Y. Hopen, and R.L. Phillips, Theory of Optical Scintillation: Gaussian Beam Wave Model, Waves in Random Media, 11 (2001) 271-291.
8. Z. Ghassemlooy and W.O. Popoola, "Terrestrial Free-Space Optical Communications", book chapter in "Mobile and Wireless Communications: Network Layer and Circuit Level Design", Salma Ait Fares and Fumiyuki Adachi (Ed.), ISBN: 978-953-307-042-1, InTech, 2010.
9. M.H. Mahdieh and M. Pournoury, Atmospheric Turbulence and Numerical Evaluation of Bit Error Rate (BER) in Free-Space Communication, Optics and Laser Technology, 42, 1 (2010) 55-60.
10. W.O. Popoola, Z. Ghassemlooy, C.G. Lee and A.C. Boucouvalas, “Scintillation effect on intensity modulated laser communication systems - a laboratory demonstration”, *Optics & Laser Technology*, vol. 42, pp. 682–692, 2010.
11. R. Rachmani, and S. Arnon, “Wavelength Diversity in Turbulence Channels for Sensor Networks,” *IEEE 26th Convention of Electrical and Electronics Engineers in Israel, IEEEI 2010*, art. no. 5661946, pp. 915-918, 2010.
12. H.E. Nistazakis and G.S. Tombras, “On the use of Wavelength and Time Diversity in Optical Wireless Communication Systems over Gamma-Gamma Turbulence Channels”, *Elsevier, Journal of Optics & Laser Technology*, Vol. 44, Iss. 7, pp. 2088-2094, 2012.
13. S.M. Navidpour, M. Uysal, and M. Kavehrad, “BER Performance of Free Space Optical Transmission with Spatial Diversity,” *IEEE Trans. Wireless Commun.*, vol. 6, iss. 8, pp. 2813-2819, 2007.
14. T.A. Tsiftsis, H.G. Sandalidis, G.K. Karagiannidis, and M. Uysal, “Optical Wireless Links with Spatial Diversity Over Strong Atmospheric Turbulence Channels,” *IEEE Transactions on Wireless Communications*, vol. 8, iss. 2, art. no. 4786457, pp. 951-957, 2009.
15. A.N. Stassinakis, H.E. Nistazakis, and G.S. Tombras, “Comparative Performance Study of One or Multiple Receivers Schemes for FSO Links Over Gamma Gamma Turbulence Channels”, *Taylor & Francis Group, Journal of Modern Optics*, Vol. 59, Iss. 11, pp. 1023-1031, 2012.
16. F. Xu, A. Khalighi, P. Caussé, and S. Bourennane, “Channel Coding and Time-Diversity for Optical Wireless Links,” *Optics Express*, vol. 17, iss. 2, pp. 872-887, 2009.
17. E. Wainright, H.H. Refai, and J.J. Sluss Jr., “Wavelength Diversity in Free-Space Optics to Alleviate Fog Effects”, *Proceedings of SPIE - The International Society for Optical Engineering*, vol. 5712, art. no. 16, pp. 110-118, 2005.
18. E.J. Shin, V.W.S. Chan, Optical Communication Over the Turbulent Atmospheric Channel using Spatial Diversity, Conference Record / IEEE Global Telecommunications Conference 3, (2002) 2055-2060.
19. H.E. Nistazakis, “A Time-Diversity Scheme for Wireless Optical Links Over Exponentially Modeled Turbulence Channels”, *Elsevier, Optik -International Journal for Light and Electron Optics*, in press.
20. M. Uysal, S.M. Navidpour and J. Li, “Error Rate Performance of Coded Free Space Optical Links Over Strong Turbulence Channels", IEEE Communications Letters, Vol. 8, no 10, 2004.
21. H.G. Sandalidis, T.A. Tsiftsis, “Outage probability and ergodic capacity of free-space optical links over strong turbulence”, *Electronics Lett*ers, Vol. 44, no. 1, p.p. 46 – 47, 2008.
22. H.E. Nistazakis, A.D. Tsigopoulos, M.P. Hanias, C.D. Psychogios, D. Marinos, C. Aidinis, and G.S. Tombras, Estimation of Outage Capacity for Free Space Optical Links Over I-K and K Turbulent Channels, Radioengineering, 20, 2 (2011) 493-498.
23. R. Purvinskis, D. Giggenbach, H. Henniger, N. Perlot, and F. David, “Multiple Wavelength Free-Space Laser Communications,” *Proceedings of SPIE - The International Society for Optical Engineering*, vol. 4975, pp. 12-19, 2003.
24. H.E. Nistazakis, V.D. Assimakopoulos, and G.S. Tombras, “Performance Estimation of Free Space Optical Links Over Negative Exponential Atmospheric Turbulence Channels,” *Elsevier OPTIK*, vol. 122, pp. 2191-2194, 2011.

25. A. Katsis, H.E. Nistazakis, and G.S. Tombras, “Bayesian and frequentist estimation of the performance of free space optical channels under weak turbulence conditions”, *Journal of the Franklin Institute*, vol. 346, pp. 315-327, 2009.
26. X. Zhu, and J.M. Kahn, “Free-Space Optical Communications Through Atmospheric Turbulence Channels,” *IEEE Trans. on Communications*, vol. 50, iss. 8, pp.1293-1300, 2002.
27. V.S. Adamchik, O.I. and Marichev, “The Algorithm for Calculating Integrals of Hypergeometric Type Function and its Realization in Reduce System,” *Proc. International Conference on Symbolic and Algebraic Computation*, pp. 212-224, Tokyo, Japan, 1990.
28. H.E. Nistazakis, E.A. Karagianni, A.D. Tsigopoulos, M.E. Fafalios, and G.S. Tombras, “Average capacity of optical wireless communication systems over atmospheric turbulence channels”, *IEEE/OSA Journal of Lightwave Technology*, Vol. 27, no. 8, pp. 974-979, (2009).
29. H.E. Nistazakis, G.S. Tombras, A.D. Tsigopoulos, E.A. Karagianni, and M.E. Fafalios, “Capacity estimation of optical wireless communication systems over moderate to strong turbulence channels”, *Journal of Communications and Networks*, Vol. **11**, Iss. 4, pp. 387-392, (2009).
30. F. Lazarakis, G.S. Tombras, and K. Dangakis, Average Channel Capacity in a Mobile Radio Environment with Rician Statistics, IEICE Trans. Commun., E77-B, 7 (1994) 971-977.
31. C. Liu, Y. Yao, Y.X. Sun, J.J. Xiao and X.H. Zhao, Average Capacity Optimization in Free-Space Optical Communication System Over Atmospheric Turbulence Channels with Pointing Errors, Optics Letters, 35, 19 (2010) 3171-3173.
32. S. Furrer, P. Coronel and D. Dahlhaus, Simple Ergodic and Outage Capacity Expressions for Correlated Diversity Ricean Fading Channels, IEEE Transaction on Wireless Communications, 5, 7 (2006) 1606-1609.
33. A. Belmonte and J.M. Kahn, Capacity of coherent free-space optical links using atmospheric compensation techniques, Optics Express, 17, 4 (2009) 2763-2773.
34. A.N. Stassinakis, G.G. Chronopoulos and H.E. Nistazakis, " Availability Investigation of Free Space Optical Links with Time Diversity for Turbulence Channels Modeled with the K-Distribution ", Nausivios Chora 2012, submitted.

Σύγκριση Απλοποιημένης Μεθόδου Πραγματικής Συχνότητας με Μεθόδους Κατανεμημένης Ενίσχυσης στη Σχεδίαση Ενισχυτή Χαμηλού Θορύβου για Εφαρμογές Ευρείας Ζώνης 3.1-10.6 GHz

Νικόλαος Χατζηαθανασίου[α] και Ευαγγελία Καραγιάννη[β]

[α]Εθνικό Μετσόβιο Πολυτεχνείο, Τμήμα Ηλεκτρολόγων Μηχανικών, Τομέας Συστημάτων Μετάδοσης Πληροφορίας και Τεχνολογίας Υλικών
[β]Σχολή Ναυτικών Δοκίμων, Τομέας Συστημάτων Μάχης, Ναυτικών Επιχειρήσεων, Θαλασσίων Επιστημών, Ναυτιλίας, Ηλεκτρονικών και Τηλεπικοινωνιών

Abstract. A Simplified Real Frequency Technique (SRFT) is being implemented with MATLAB in order to design a Low Noise Amplifier (LNA) for UWB (Ulta Wide Band) applications, working in the 3.1-10.6 GHz frequency zone. Additionally two other designs are being examined based on the distributed amplification method, in order to compare the techniques and highlight the advantages of the new SRFT technique.

Keywords: Low Noise Amplifier, Ultra-Wide Band, Simplified Real Frequency Technique, Distributed Systems, Microwave Integrated Circuits, Design, Optimization.
PACS: 85.40.Qx, 84.30.Le, 06.20.fb, 06.30.Ft, 84.40.Xb, 84.30.Vn, 84.40.Dc, 89.20.Ff, 02.50.Ng

ΤΟ ΠΡΟΤΥΠΟ ULTRA WIDE BAND

Ο ενισχυτής που σχεδιάζεται στην παρούσα εργασία προορίζεται για συσκευές που υποστηρίζουν την τεχνολογία Ευρείας Ζώνης Ultra-Wide Band (UWB). Πρόκειται για μια ασύρματη τεχνολογία που έχει σαν στόχο να υποστηρίζει υπηρεσίες μεταφοράς δεδομένων σε πάρα πολύ υψηλούς ρυθμούς. Γι' αυτό και το διατιθέμενο φάσμα συχνοτήτων είναι πολύ μεγάλο.

Σύμφωνα με την Ομοσπονδιακή Επιτροπή Επικοινωνιών των Ηνωμένων Πολιτειών Αμερικής (FCC) το UWB αναφέρεται σε κάθε τεχνολογία με εύρος ζώνης που είτε υπερβαίνει τα 500 MHz ή το 20% της κεντρικής συχνότητας λειτουργίας. Το Φεβρουάριο 2002 η FCC κατοχυρώνει για την τεχνολογία UWB το διάστημα συχνοτήτων 3.1 -10.6 GHz και το Νοέμβριο 2005 η Ένωση Εθνικών Τηλεπικοινωνιών Αμερικής (ITU) εκδίδει έκθεση συστάσεων γι' αυτήν την τεχνολογία. Η FCC όρισε ως μέγιστο όριο εκπομπής ισχύος από τους πομπούς UWB την τιμή -41.3 dBm/MHz [1]. Πρόκειται για πολύ χαμηλή τιμή που είναι της τάξης του θορύβου που προκαλούν διάφορες οικιακές συσκευές.

Το UWB εμφανίζεται σε δύο εκδοχές [2]: Το παλμικό (pulsed UWB) και το UWB με χρήση OFDM (Ορθογωνική Πολύπλεξη με Διαίρεση Συχνότητας) ή άλλες συναφείς τεχνολογίες παράλληλων φερόντων. Η πρώτη εκδοχή είναι η πλέον διαδεδομένη. Εδώ, το εκπεμπόμενο σήμα αποτελείται από πολύ στενούς παλμούς. Μερικά ελκυστικά χαρακτηριστικά του pulsed

UWB είναι τα εξής: Ανοχή σε φαινόμενα multipath, διότι η διάρκεια του παλμού UWB είναι πολύ μικρότερη από την εξάπλωση χρονοκαθυστέρησης. Αυτό σημαίνει ότι τα αντίγραφα του σήματος λόγω πολυδιαδρομικής διάδοσης θα φτάσουν στο δέκτη πολύ μετά την άφιξη του κανονικού σήματος [3]. Όμως, ακριβώς γι' αυτό το λόγο, θα υπάρξουν προβλήματα διασυμβολικής παρεμβολής. Ένα άλλο πλεονέκτημα είναι ότι στην περίπτωση των παραδοσιακών τεχνικών μετάδοσης, απαιτούνται τοπικοί ταλαντωτές και μίκτες για τη διαμόρφωση του φέροντος για την εκπομπή και για την αποδιαμόρφωση στη λήψη, κάτι που δε συμβαίνει στο UWB. Επίσης, υπάρχει η δυνατότητα πολύ υψηλού ρυθμού μετάδοσης και τέλος λόγω της χαμηλής ισχύος εκπομπής, δεν απαιτείται ενισχυτής ισχύος για τη μετάδοση όπως συμβαίνει με άλλες τεχνικές μετάδοσης.

Γενικά, πρόκειται για τεχνολογία που προορίζεται για επικοινωνίες και προσωπικά δίκτυα κλειστού χώρου. Χαρακτηριστική εφαρμογή της τεχνολογίας αυτής είναι η ασύρματη μεταφορά δεδομένων Video μεταξύ συσκευών που υποστηρίζουν το εν λόγω πρότυπο. Άλλες εφαρμογές του UWB είναι η απεικόνιση μέσω ραντάρ, συλλογή δεδομένων από αισθητήρες, εφαρμογές εντοπισμού και παρακολούθησης ακριβείας κ.α.

ΜΕΘΟΔΟΣ ΚΑΤΑΝΕΜΗΜΕΝΗΣ ΕΝΙΣΧΥΣΗΣ

Στους συμβατικούς ενισχυτές που βασίζονται σε τρανζίστορ (αλλά και παλιότερα στους ενισχυτές λυχνιών κενού) υπάρχει ένας εγγενής περιορισμός στο γινόμενο κέρδος επί εύρος συχνοτήτων που μπορεί να επιτευχθεί. Αυτό σημαίνει ότι δεν μπορεί κανείς να σχεδιάσει ένα ενισχυτή που να λειτουργεί και σε πολύ υψηλές συχνότητες και σε πολύ υψηλό κέρδος. Έτσι κάνουμε πάντοτε ένα συμβιβασμό στις απαιτήσεις μας. Ανάλογα με την εφαρμογή μπορούμε να σχεδιάσουμε ένα ενισχυτή μεγάλου κέρδους σε σχετικά μικρό εύρος ζώνης ή ένα ενισχυτή που επιτυγχάνει μέτριο κέρδος σε μεγαλύτερο εύρος συχνοτήτων. Ο εγγενής αυτός περιορισμός έγκειται στις παρασιτικές χωρητικότητες που έχουν τα τρανζίστορ στην είσοδο και την έξοδό τους [4]. Έτσι αν βάλουμε στη σειρά δύο ενισχυτικές βαθμίδες, με τη δεύτερη να ενισχύει το σήμα από την έξοδο της πρώτης, τότε φυσικά το κέρδος θα αυξηθεί στις χαμηλές συχνότητες, αλλά θα μειώνεται στις υψηλές λόγω της συνολικής αυξημένης χωρητικότητας.

Ο παραπάνω περιορισμός αίρεται με την εφαρμογή της κατανεμημένης ενίσχυσης. Στους κατανεμημένους ενισχυτές οι χωρητικότητες εισόδου και εξόδου που περιορίζουν το εύρος ζώνης των τρανζίστορ, απορροφούνται σε γραμμές μεταφοράς που συνδέουν τα τρανζίστορ μεταξύ τους. Η γραμμή μεταφοράς (ιδανική) δεν παραμορφώνει με κανένα τρόπο ένα σήμα και έχει απεριόριστο εύρος ζώνης. Μία όψη αυτού είναι το γεγονός ότι η αντίσταση Z που παρουσιάζει η γραμμή (η χαρακτηριστική αντίσταση της γραμμής) έχει μία σταθερή (θετική) τιμή σε όλες τις συχνότητες. Επομένως σύμφωνα με τη σχέση

$$A_V(f) = \frac{V_{out}}{V_{in}} = g \cdot Z(f) \qquad (1)$$

όπου g η διαγωγιμότητα ($I_{out} = g \cdot V_{in}$), το κέρδος του ενισχυτή είναι επίσης σταθερό με τη συχνότητα. Τώρα η σχέση (1) μας λέει ότι μπορούμε να αυξήσουμε το κέρδος του ενισχυτή αν αυξήσουμε το g. Αυτό μπορεί να γίνει για παράδειγμα αν οδηγήσουμε το σήμα εισόδου σε πολλά ίδια τρανζίστορ και μετά "συλλέξουμε" το ρεύμα που δίνει το καθένα και το οδηγήσουμε στο φορτίο μας. Με αυτόν τον τρόπο η ισοδύναμη διαγωγιμότητα του ενισχυτή πολλαπλασιάζεται κατά το πλήθος των τρανζίστορ. Αυτή η οδήγηση του σήματος εισόδου στα τρανζίστορ, καθώς και η οδήγηση του ρεύματος εξόδου των στο φορτίο γίνονται με τη χρήση των γραμμών μεταφοράς που απορροφούν τις χωρητικότητες των τρανζίστορ. Το τίμημα που πληρώνει κανείς για την επέκταση της λειτουργίας του ενισχυτή σε μεγάλες συχνότητες είναι η χρονική καθυστέρηση που υφίσταται το σήμα εξόδου κατά τη διέλευσή του από την γραμμή

μεταφοράς μέχρι να φθάσει στο φορτίο. Σε εφαρμογές που αυτή η καθυστέρηση δεν διαδραματίζει σπουδαίο ρόλο, η χρησιμοποίηση του κατανεμημένου ενισχυτή είναι εφικτή. Το κυκλωματικό διάγραμμα ενός κατανεμημένου ενισχυτή φαίνεται παρακάτω.

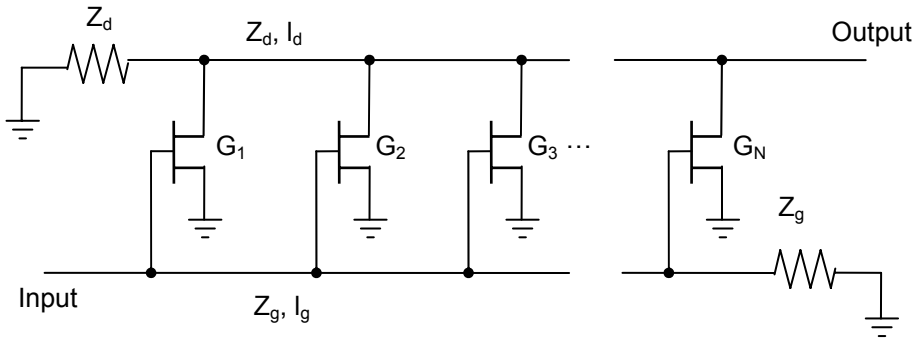

ΣΧΗΜΑ 2. Κατανεμημένος Ενισχυτής

Βλέπουμε ότι υπάρχουν δύο γραμμές μεταφοράς. Η μία από αυτές χρησιμοποιείται για να μεταφέρει το σήμα προς ενίσχυση στον ακροδέκτη της πύλης Gate των τρανζίστορ και η δεύτερη παραλαμβάνει το ενισχυμένο από κάθε τρανζίστορ σήμα στον ακροδέκτη εξόδου Drain και το οδηγεί προς το φορτίο. Από τις ονομασίες των δύο αυτών ακροδεκτών η γραμμή εισόδου ονομάζεται Gate line και η γραμμή εξόδου Drain line. Η Gate line έχει χαρακτηριστική αντίσταση Z_g και η Drain line Z_d.

Η ενίσχυση έγκειται στο μηχανισμό λειτουργίας του τρανζίστορ και μοντελοποιείται ως μία πηγή ρεύματος εξαρτώμενη από την τάση εισόδου. Το ρεύμα που δίνει το κάθε τρανζίστορ προστίθεται με το ρεύμα των υπολοίπων με αποτέλεσμα να έχουμε στο φορτίο μεγάλο ρεύμα. Στην ουσία πρόκειται για μία διάταξη παράλληλων μονοπατιών ρεύματος, τα οποία συναντούνται για να δώσουν το επιθυμητό μεγάλο ρεύμα στην έξοδο. Προκειμένου τα ρεύματα αυτά να προστίθεται εν φάση θα πρέπει το χρονικό διάστημα που απαιτείται για να διανύσει το σήμα την απόσταση ανάμεσα σε δύο τρανζίστορ στις δύο γραμμές μεταφοράς να είναι το ίδιο. Αυτό επιτυγχάνεται με κατάλληλη επιλογή των μηκών l_g, l_d και των παραγόντων διάδοσης φάσης (phase propagation factor) β_g, β_d στις δύο γραμμές μεταφοράς, ώστε να ισχύει $\beta_g{*}l_g=\beta_d{*}l_d$. Τερματίζουμε τις δύο γραμμές μεταφοράς στο ένα άκρο τους με αντιστάσεις ίσες με την χαρακτηριστική αντίσταση των δύο γραμμών, προκειμένου να μην έχουμε ανακλάσεις. Επίσης τερματίζουμε τη γραμμή εξόδου με ένα φορτίο που έχει αντίσταση ίση με τη χαρακτηριστική αντίσταση Z_d της γραμμής για να έχουμε μέγιστη μεταφορά ισχύος. Από την παραπάνω περιγραφή συμπεραίνουμε ότι το κέρδος ενίσχυσης είναι ανάλογο με το πλήθος των τρανζίστορ. Σε ένα κατανεμημένο ενισχυτή με N το πλήθος τρανζίστορ που έχουν διαγωγιμότητα g_m, το κέρδος τάσης A_v στο φορτίο Z_d είναι $A_v = \frac{N \cdot g_m \cdot Z_d}{2}$. Ο παράγοντας ½ οφείλεται στο γεγονός ότι το ρεύμα στη θύρα εξόδου σε κάθε τρανζίστορ έχει δύο συνιστώσες. Η μία κατευθύνεται προς το φορτίο και η άλλη απορροφάται χωρίς ανακλάσεις στην άλλη άκρη της γραμμής εξόδου. Η παραπάνω σχέση μας δείχνει ότι μπορούμε να μεγαλώνουμε το κέρδος απεριόριστα με τη χρησιμοποίηση ολοένα και περισσότερων τρανζίστορ. Επίσης από την ανάλυση αυτή προκύπτει ότι κέρδος είναι ομοιόμορφο.

Αντί των γραμμών μεταφοράς που στην επίπεδη (planar) τεχνολογία είναι συνήθως μικροταινίες μπορούμε να χρησιμοποιήσουμε και τεχνητές γραμμές μεταφοράς αποτελούμενες από συγκεντρωμένα (lumped) στοιχεία, όπως πυκνωτές και πηνία. Αυτό γινόταν σε περασμένες δεκαετίες όταν οι δυνατότητες της επίπεδης τεχνολογίας ήταν περιορισμένες και δεν μας επέτρεπαν να έχουμε κυκλώματα με τα ενεργά στοιχεία (τρανζίστορ) αλλά και τα παθητικά (γραμμές μεταφοράς, πηνία, πυκνωτές) ολοκληρωμένα πάνω στο ίδιο υπόστρωμα. Μία

τεχνητή γραμμή μεταφοράς για τη gate line και τη drain line μπορεί να έχει τη μορφή του σχήματος 2.

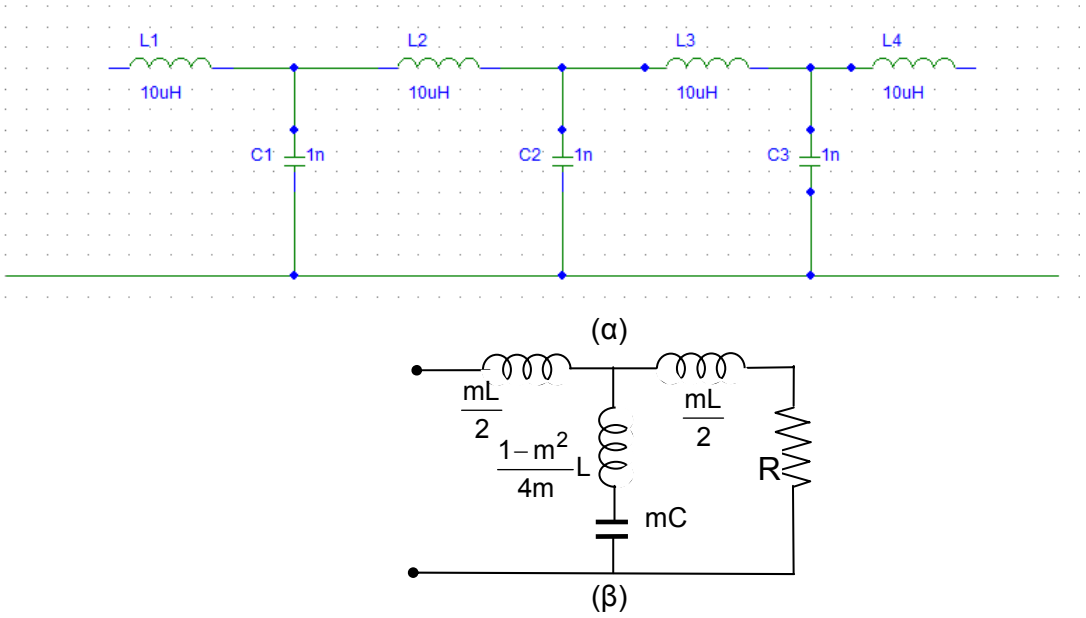

ΣΧΗΜΑ 2. (α) Τεχνητή γραμμή μεταφοράς (β) m-παραγώμενο φίλτρο (m-derived filter) ως τερματισμός της γραμμής

Μία παραλλαγή του κατανεμημένου ενισχυτή είναι ο ενισχυτής μήτρας (matrix amplifier) στον οποίο χρησιμοποιούνται περισσότερα του ενός τρανζίστορ ανά βαθμίδα ώστε κάθε βαθμίδα να δίνει μεγαλύτερο κέρδος ή να έχει καλύτερη συμπεριφορά στις υψηλότερες συχνότητες. Έτσι για παράδειγμα μπορεί να χρησιμοποιηθεί σαν ενισχυτικό κύτταρο η σειριακή τοπολογία (cascode) [5].

Μία συνήθης τακτική για την αύξηση του εύρους ζώνης του κατανεμημένου ενισχυτή μέσω της μείωσης της ανά μέτρο χωρητικότητας της γραμμής μεταφοράς στην πύλη και την αύξηση της ισχύος εξόδου, είναι η σύνδεση ενός πυκνωτή κατάλληλης χωρητικότητας $q \cdot C_{gs}$ στην πύλη των τρανζίστορ [6], [7], [8], [9].

Όσον αφορά την επίδοση των κατανεμημένων ενισχυτών ως προς το θόρυβο, στο [10] περιγράφεται το γεγονός ότι για σχετικά μεγάλο αριθμό τρανζίστορ η εικόνα θορύβου μειώνεται. Στον θόρυβο των κατανεμημένων ενισχυτών συμβάλλουν οι αντιστάσεις τερματισμού και ο εσωτερικός θόρυβος των FETs.

1η Σχεδίαση: Κατανεμημένος Ενισχυτής Χαμηλού Θορύβου

Το τρανζίστορ που χρησιμοποιήσαμε για τον κατανεμημένο ενισχυτή είναι το PHEMT ATF-36077 από την AVAGO TECHNOLOGIES. Είναι ένα ψευδομορφικό High Electron Mobility Transistor που βασίζεται σε GaAs και λειτουργεί με εξαιρετικά μικρό θόρυβο. Όταν είναι κατάλληλα προσαρμοσμένο στην είσοδό του επιτυγχάνει εικόνα θορύβου που κυμαίνεται μεταξύ 0.3 dB στο 1GHz μέχρι 0.65 dB στα 18GHz. Το δε κέρδος ισχύος πέφτει από τα 25 dB σε DC λειτουργία στα 15 dB σε συχνότητα 16 GHz.

Στο σχήμα 5, από τις γραφικές παραστάσεις (α), (β) και (γ), παρατηρούμε ότι το κέρδος είναι μέτριο, η εικόνα θορύβου εφάμιλλη με αυτήν που παρουσιάζεται στο [10] και ο συντελεστής ανάκλασης εισόδου είναι μέτριος.

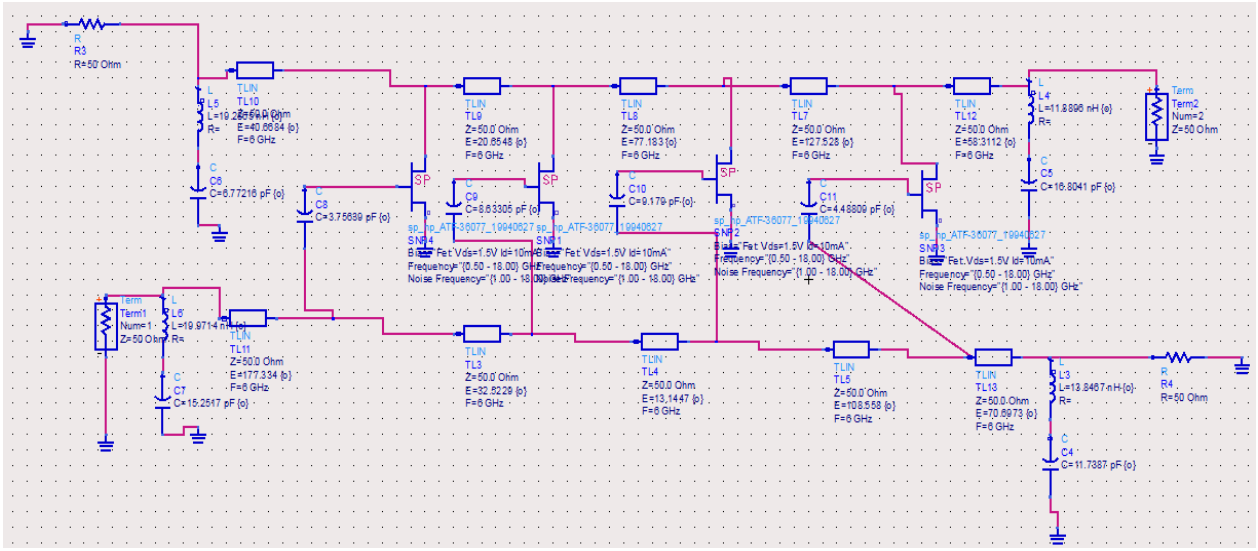

ΣΧΗΜΑ 3. Η σχεδίαση του LNA

2η Σχεδίαση: Matrix Amplifier

Μπορούμε να βελτιώσουμε το παραπάνω φτωχό κέρδος του ενισχυτή χρησιμοποιώντας ένα matrix amplifier, όπως παρουσιάζεται στο [11].

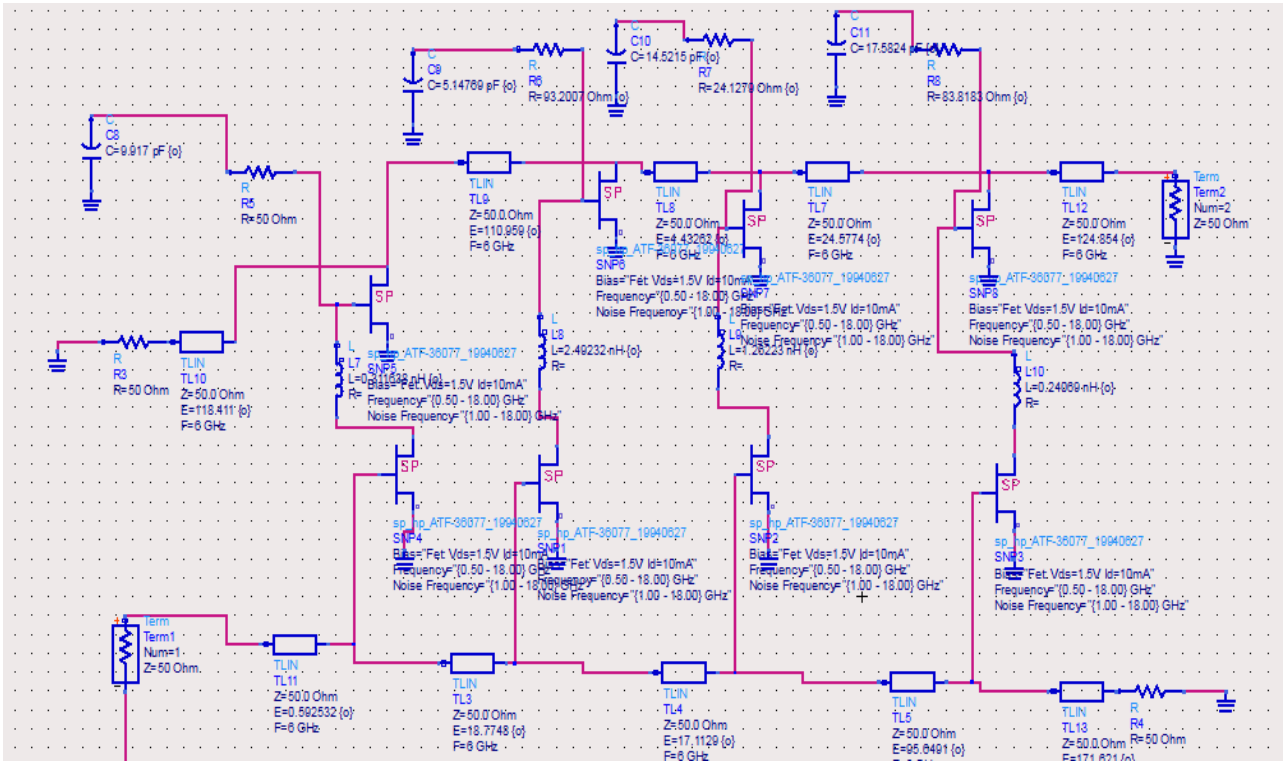

ΣΧΗΜΑ 4. Matrix Amplifier

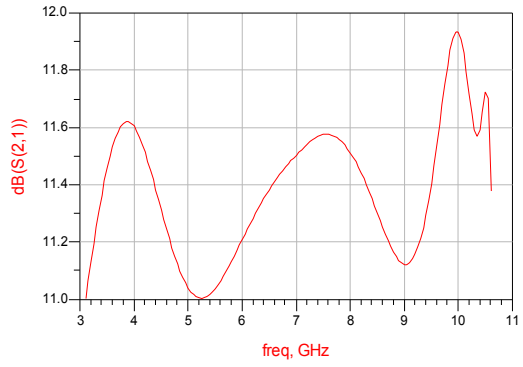

(α)

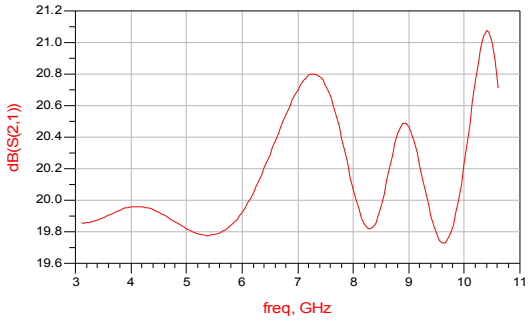

(δ)

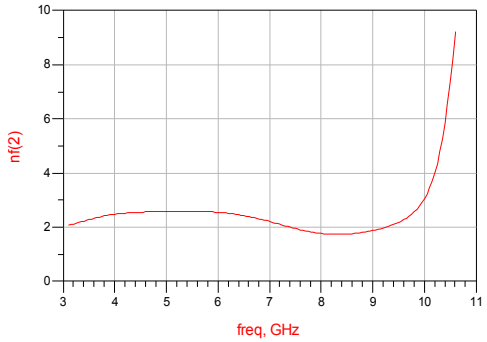

(β)

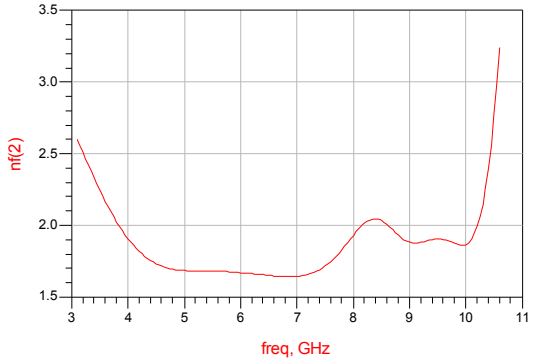

(ε)

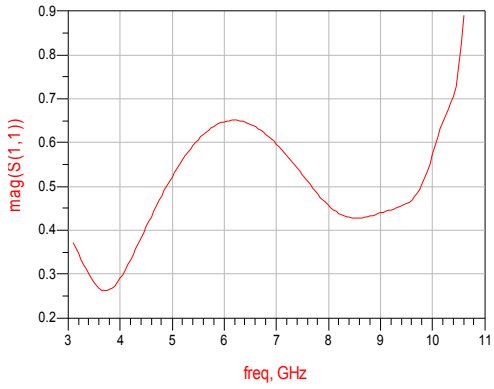

(γ)

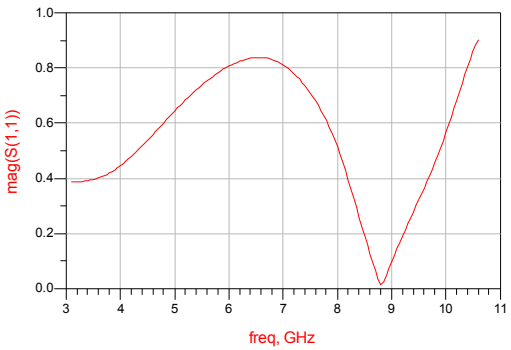

(στ)

ΣΧΗΜΑ 5. Η επίδοση των ενισχυτών όσον αφορά το κέρδος (α), (δ), την εικόνα θορύβου (β), (ε) και το συντελεστή ανάκλασης εισόδου (γ), (στ). Η πρώτη στήλη (α), (β) και (γ) είναι τα αποτελέσματα της προσομοίωσης του κατανεμημένου ενισχυτή του σχήματος 1, ενώ η δεύτερη στήλη (δ), (ε) και (στ) είναι τα αποτελέσματα της προσομοίωσης του matrix amplifier του σχήματος 2.

Κάθε ενισχυτικό κύτταρο στον παραπάνω κατανεμημένο ενισχυτή αποτελείται από δύο FETs συνδεδεμένα σε σειρά σε συνδεσμολογία κοινής πηγής. Με το κύκλωμα αυτό αυξάνεται κατά πολύ η ισοδύναμη διαγωγιμότητα του ενισχυτικού κυττάρου σε σχέση με τη διαγωγιμότητα του καθενός τρανζίστορ ξεχωριστά. Το πηνίο L (peaking inductor) χρησιμοποιείται για τη βελτίωση της απόκρισης συχνότητας στις υψηλές συχνότητες.

Χρησιμοποιώντας κατάλληλες τιμές για την αντίσταση R και τον πυκνωτή C, καθώς και για το πηνίο L μπορούμε να κάνουμε την ισοδύναμη διαγωγιμότητα περίπου σταθερή στο διάστημα συχνοτήτων που μας ενδιαφέρει. Για το σκοπό αυτό χρησιμοποιήσαμε τη βελτιστοποίηση του ADS από την οποία φάνηκε ότι ο ενισχυτής έχει πολύ καλή επίδοση χωρίς τη χρήση των πυκνωτών $q \cdot C_{GS}$ και των m-derived filter τερματισμών.

Το σχηματικό στο ADS παρουσιάζεται στο σχήμα 4.

Παρατηρούμε ότι το κέρδος είναι περίπου 20-21 dB, δηλαδή σχεδόν διπλάσιο σε σχέση με τον προηγούμενο κατανεμημένο ενισχυτή. Επίσης τόσο ο συντελεστής ανάκλασης εισόδου όσο και η εικόνα θορύβου είναι σαφώς καλύτεροι.

ΑΠΛΟΠΟΙΗΜΕΝΗ ΜΕΘΟΔΟΣ ΠΡΑΓΜΑΤΙΚΗΣ ΣΥΧΝΟΤΗΤΑΣ

Η απλοποιημένη μέθοδος πραγματικής συχνότητας (Simplified Real Frequency Technique - SRFT)[12] αποτελεί μία παραλλαγή της μεθόδου που εισήγαγε το 1979 ο Carlin [13]. Πρόκειται για μία αριθμητική μέθοδο βελτιστοποίησης που χρησιμοποιείται κατά κόρο για τη σχεδίαση κυκλωμάτων προσαρμογής ενός τρανζίστορ σε εφαρμογές μεγάλου εύρους συχνοτήτων. Οι περισσότερες αριθμητικές μέθοδοι που χρησιμοποιούνται στα διάφορα σχεδιαστικά πακέτα CAD προϋποθέτουν καταρχήν από το χρήστη να επιλέξει μία λογική κυκλωματική τοπολογία με κάποιες αρχικές τιμές. Στη συνέχεια η επίδοση του κυκλώματος βελτιστοποιείται με την κατάλληλη αλλαγή των τιμών των παθητικών στοιχείων που συνθέτουν το κύκλωμα. Η βελτιστοποίηση αυτή γίνεται βάσει μίας αντικειμενικής συνάρτησης (objective function) που θέτει ο χρήστης και στην οποία αποτυπώνεται η επιθυμητή απόκριση του κυκλώματος που θέλει να σχεδιάσει. Πρόκειται για μία συνάρτηση των τιμών των παθητικών στοιχείων X $\{X_1, X_2, \ldots, X_n\}$ του κυκλώματος προσαρμογής, καθώς και των δεδομένων αντίστασης $Z_L=R_L+jX_L$ (ή αγωγιμότητας ή παραμέτρων σκέδασης) του φορτίου (Load) κεραίας ή ενισχυτή που θέλουμε να προσαρμόσουμε σε μία ζώνη συχνοτήτων ω. Ένα παράδειγμα αντικειμενικής συνάρτησης προς βελτιστοποίηση είναι το Κέρδος Ισχύος Μεταφοράς (Transducer Power Gain) TPG που ορίζεται ως ο λόγος της ισχύος στο φορτίο προς τη διαθέσιμη ισχύ που δίνει μία γεννήτρια στην είσοδο. Επιθυμούμε να είναι όσο γίνεται πιο μεγάλο και σταθερό στη ζώνη συχνοτήτων που μας ενδιαφέρει. Σε μαθηματικούς όρους, θέλουμε το $T=T(\omega, Z_L, X_1, X_2, \ldots, X_n)$ να προσεγγίζει την τιμή T_0 που επιλέγει ο χρήστης. Έτσι, σχηματίζουμε μία συνάρτηση σφάλματος $\varepsilon(\omega) = T(\omega, R_L(\omega), X_L(\omega), X_1, X_2, \ldots X_n) - T_0$, την οποία θέλουμε να ελαχιστοποιήσουμε. Στην τεχνική βιβλιογραφία υπάρχουν πολλά αριθμητικά πακέτα ελαχιστοποίησης της παραπάνω συνάρτησης, αλλά είναι συνήθως κατάλληλα μόνο για κυκλώματα στενού εύρους ζώνης με συνήθως δύο μόνο άεργα στοιχεία (πυκνωτές/πηνία).

Επιπλέον, το πρόβλημα ελαχιστοποίησης της συνάρτησης σφάλματος ε(ω) καθίσταται έντονα μη γραμμικό. Η απλοποιημένη μέθοδος πραγματικής συχνότητας παρακάμπτει την παραπάνω δυσκολία με το να εκφράζει τους συντελεστές σκέδασης του στη μορφή:

$$Sij = \frac{h(p)}{g(p)} = \frac{h_n p^n + h_{n-1} p^{n-1} + \ldots + h_1 p + h_0}{g_k p^k + \ldots + g_1 p + g_0} \qquad (2)$$

Στη συνέχεια κατασκευάζουμε τη συνάρτηση σφάλματος συναρτήσει των συντελεστών σκέδασης της παραπάνω μορφής και η ελαχιστοποίηση γίνεται πλέον ως προς τους

συντελεστές h_i του πολυωνύμου h(p) πράγμα που όπως αποδεικνύεται καθιστά το πρόβλημα μη γραμμικό, αλλά με μη γραμμικότητα τάξης δύο, ανεξάρτητα από το πλήθος των στοιχείων του κυκλώματος. Στη θεωρία της βελτιστοποίησης είναι γνωστό ότι, αν η μη γραμμικότητα της αντικειμενικής συνάρτησης είναι τάξης μεγαλύτερης του δύο, τότε κάποιος μπορεί να παγιδευτεί σε τοπικά ελάχιστα και η ίδια η σύγκλιση της αριθμητικής μεθόδου είναι αμφίβολη. Επιπλέον, σε αυτές τις περιπτώσεις το τελικό αποτέλεσμα είναι πολύ εξαρτώμενο από τις αρχικές αυθαίρετες τιμές των μεταβλητών που υπεισέρχονται στη βελτιστοποίηση. Από την άλλη μεριά στην SRFT η μη γραμμικότητα είναι τάξης δύο - και η σύγκλιση είναι σχεδόν βέβαιη. Η κυκλωματική τοπολογία είναι αυτή ενός βαθυπερατού L-C φίλτρου όπως φαίνεται στο σχήμα 6.

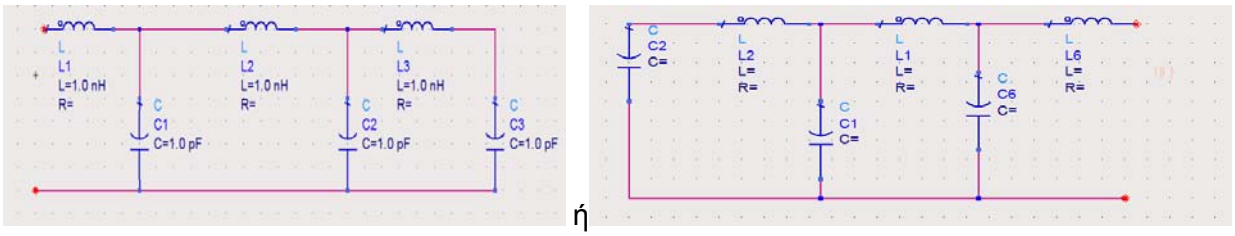

ΣΧΗΜΑ 6. Προσομοίωση γραμμής μεταφοράς

Το αν φίλτρο αυτό θα ξεκινά με ένα παράλληλο πυκνωτή ή με ένα εν σειρά πηνίο, προκύπτει από τη σύνθεση της αντίστασης εισόδου του, όπως θα δούμε παρακάτω.

Στην SRFT, είναι δυνατόν το κύκλωμα προσαρμογής να αποτελείται και από γραμμές μεταφοράς. Σε αυτήν την περίπτωση θεωρούμε ότι όλες οι γραμμές έχουν το ίδιο ηλεκτρικό μήκος και η βελτιστοποίηση γίνεται ως προς τη χαρακτηριστική αντίσταση τους. Υπάρχει η δυνατότητα το κύκλωμα να περιέχει και μετασχηματιστές που ως γνωστόν μπορούν ιδανικά να μετασχηματίζουν και αντιστάσεις σε άπειρο εύρος ζώνης. Η χρήση μετασχηματιστών δίνει περισσότερους βαθμούς ελευθερίας, αλλά στην πράξη είναι δύσκολο να χρησιμοποιηθούν σε ένα κύκλωμα.

Επιπλέον, ο χρήστης έχει τη δυνατότητα να χρησιμοποιήσει στην παραπάνω βασική L-C τοπολογία και εν σειρά πυκνωτές ή πηνία εν παραλλήλω που κάνουν τη διάταξη μας ζωνοπερατή.

Τα βασικά βήματα στην υλοποίηση ενός αλγορίθμου βασισμένου στην SRFT είναι τα εξής:

1) Αρχικοποίηση των συντελεστών h_i του πολυωνύμου $h(p) = h_n p^n + h_{n-1} p^{n-1} + ... + h_0$ που εμφανίζεται στον αριθμητή του συντελεστή ανάκλασης (κανονικοποιημένο ως προς τη μοναδιαία αντίσταση) S=h(p)/g(p) της σχέσης (2) του κυκλώματος προσαρμογής (equalizer). Η αρχικοποίηση αυτή είναι αυθαίρετη αν και μπορείς κανείς να κάνει μία αρχικοποίηση που να έχει νόημα για το πρόβλημά μας [14].

2) Με βάση την επιλογή του αριθμού k της σχέσης (2) είναι δυνατό να βρεθούν οι συντελεστές g_i του πολυώνυμου g(p) που εμφανίζεται στον παρανομαστή του συντελεστή ανάκλασης (κανονικοποιημένο ως προς τη μοναδιαία αντίσταση) S=h(p)/g(p) του προσαρμοστικού κυκλώματος (equalizer). Τα βήματα για την κατασκευή του πολυωνύμου αυτού περιγράφονται στο [16] και βασίζονται στο γεγονός ότι το προσαρμοστικό κύκλωμα είναι χωρίς απώλειες.

3) Έχοντας πλέον κατασκευάσει (αρχικοποιήσει) το συντελεστή ανάκλασης S εκφράζουμε τη συνάρτηση σφάλματος συναρτήσει του S και των παραμέτρων σκέδασης του φορτίου που θέλουμε να προσαρμόσουμε (οι παράμετροι σκέδασης για το φορτίο πρέπει να είναι φυσικά γνωστοί εκ των προτέρων). Το φορτίο αυτό μπορεί να είναι είτε παθητικό, όπως μία κεραία, είτε ενεργό όπως ένα FET.

4) Ελαχιστοποιούμε τη συνάρτηση σφάλματος με τον αλγόριθμο ελαχίστων τετραγώνων. Έτσι βρίσκουμε το βελτιστοποιημένο πολυώνυμο h(p).

5) Επαναλαμβάνουμε το βήμα 2) για να βρούμε το βέλτιστο πολυώνυμο g(p).

6) Κατασκευάζουμε το συντελεστή ανάκλασης S=h(p)/g(p) και από αυτόν την αντίσταση εισόδου $Z_{in}=\frac{1-S}{1+S}=\frac{g(p)-h(p)}{g(p)+h(p)}$ που είναι ένα ρητό πολυώνυμο ως προς p.

7) Η διαδικασία που οδήγησε στα πολυώνυμο g από το πολυώνυμο h στο βήμα 5) εξασφαλίζει ότι η αντίσταση εισόδου $Z_{in}=\frac{1-S}{1+S}=\frac{g(p)-h(p)}{g(p)+h(p)}$ είναι συνθέσιμη [15] με ένα δίκτυο L-C. Σε μαθηματική ορολογία το πολυώνυμο $g(p)=g_k p^k+g_{k-1}p^{k-1}+...+g_0$ είναι Hurwitz, δηλαδή με ρίζες μόνο στο τρίτο και τέταρτο τεταρτημόριο του μιγαδικού επιπέδου και θετικούς πραγματικούς συντελεστές. Εκφράζοντας το Z_{in} στην μορφή μερικών κλασμάτων είναι δυνατή η εξαγωγή των τιμών των χωρητικοτήτων και των αυτεπαγωγών του δικτύου L-C τερματισμένου σε μοναδιαία αντίσταση.

3η Σχεδίαση: Μέθοδος SRFT

Ακολουθώντας το [16] υλοποιήσαμε ρουτίνες στο Matlab για τη σχεδίαση προσαρμοστικών κυκλωμάτων στην είσοδο και έξοδο και του P-HEMT ATF-36007 της AVAGO στη ζώνη 3-11 GHz. Η συχνότητα κανονικοποίησης ήταν f_{norm}=11 GHz. Η υλοποίηση αυτή δεν περιλαμβάνει μετασχηματιστές, ούτε εν σειρά πυκνωτές ή εν παραλλήλω πηνία. Η σχεδίαση έγινε σε δύο βήματα. Στο πρώτο βήμα σχεδιάστηκε το προσαρμοστικό κύκλωμα εισόδου έχοντας το FET τερματισμένο από τη μεριά εξόδου σε χαρακτηριστική αντίσταση 50 Ohm.

Ο στόχος τον οποίο θέσαμε στη συνάρτηση σφάλματος προέκυψε μετά από εύρεση του μέγιστου κέρδους ισχύος μεταφοράς TPG (Transducer Power Gain) που μπορεί να δώσει ένα μονόδρομο τρανζίστορ, όταν είναι βέλτιστα προσαρμοσμένο στην είσοδο από κάποιο ιδεατό κύκλωμα, στο διάστημα συχνοτήτων που μας ενδιαφέρει. Το TPG αυτό δίνεται από την σχέση (3).

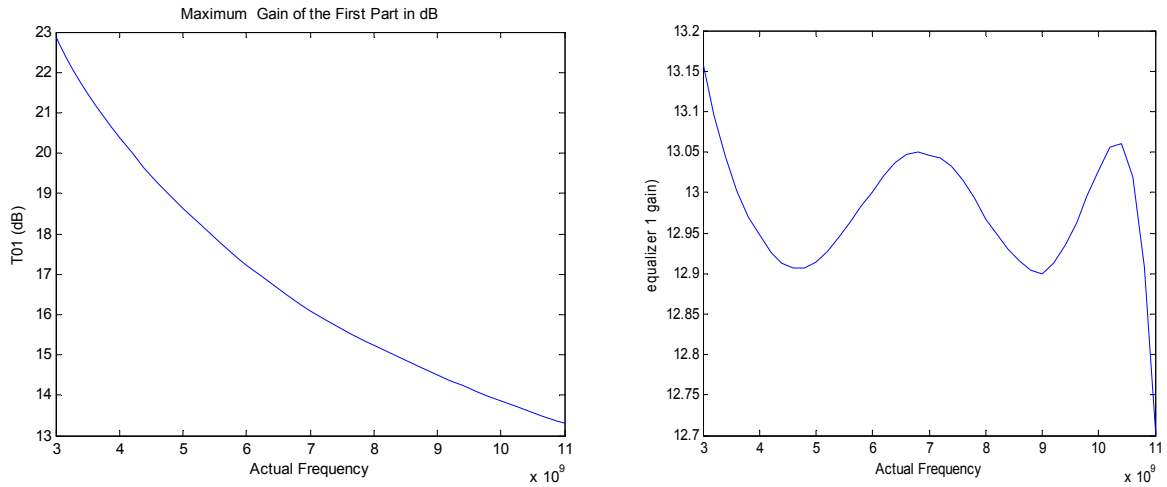

(α) (β)

ΣΧΗΜΑ 7. (α) Μέγιστο κέρδος με προσαρμοσμένη την είσοδο και (β) Βελτιστοποιημένο κέρδος με κύκλωμα προσαρμογής εισόδου.

$$T_{01}=\frac{|S_{21}(\omega)|^2}{1-|S_{11}(\omega)|^2} \qquad (3)$$

Η σχέση αυτή ισχύει σαν μία πρώτη εκτίμηση για το τρανζίστορ μας, αφού αυτό δεν είναι μονόδρομο. Η γραφική παράσταση της σχέσης αυτής ως προς τη συχνότητα φαίνεται στο σχήμα 7(α).

Το TPG έχοντας ένα προσαρμοστικό κύκλωμα στην είσοδο του FET δίνεται από τη σχέση:

$$T_1(\omega) = \frac{|S_{21F}|^2 |S_{21}|^2}{|1 - S_{22F}S_{11}|^2} \tag{4}$$

όπου S_{21F} και S_{22F} είναι οι παράμετροι σκέδασης που αναφέρονται στο κύκλωμα προσαρμογής. Το S_{21F} αναφέρεται στη μεταφορά ισχύος από αριστερά προς τα δεξιά και το S_{22} στο συντελεστή ανάκλασης της ισχύος που προσπίπτει από το FET προς τα αριστερά στο προσαρμοστικό κύκλωμα. Είναι $S_{22F}=h_F/g_F$ και $S_{21F}=1/g_F$. Ο στόχος που θέσαμε είναι το TPG να είναι ίσο με 13 dB, δηλαδή το ελάχιστο στην παραπάνω γραφική παράσταση του σχήματος 7(α).

Έτσι η συνάρτηση σφάλματος error1 είναι η εξής :

$$\text{error1} = 10\log\left(\frac{|S_{21F}|^2 \cdot |S_{21}|^2}{|1 - S_{22F}S_{11}|^2}\right) - 13 \tag{5}$$

Χρησιμοποιήσαμε μία τυχαία αρχικοποίηση για το διάνυσμα h, με h=[-1 1 -1 1 -1]. Το h έχει 5 στοιχεία με αποτέλεσμα το τελικό κύκλωμα να έχει 5 παθητικά στοιχεία. Η βελτιστοποίηση είχε ως αποτέλεσμα το TPG που φαίνεται στο σχήμα 7(β). Όπως παρατηρούμε πρόκειται για μία πολύ καλή προσέγγιση.

Στο δεύτερο στάδιο προσθέτουμε και το κύκλωμα προσαρμογής εξόδου του τρανζίστορ και βελτιστοποιούμε το ολικό TPG. Επειδή όμως το τρανζίστορ που χρησιμοποιούμε είναι εκ κατασκευής καλά προσαρμοσμένο στην αντίσταση των 50 Ohms, το προσαρμοστικό κύκλωμα εξόδου μπορεί να προσφέρει μία μικρή μόνο βελτίωση. Ας προσπαθήσουμε λοιπόν το κύκλωμα αυτό να προσφέρει μια σταθερή ενίσχυση 0.7 dB. Οπότε θέτουμε ως στόχο το τελικό TPG να είναι 13 + 0.7 =13.7 dB (τα 13 dB προκύπτουν από το TPG του προηγούμενου σταδίου).

Το κύκλωμά μας θα έχει τη μορφή [17] του σχήματος 9.

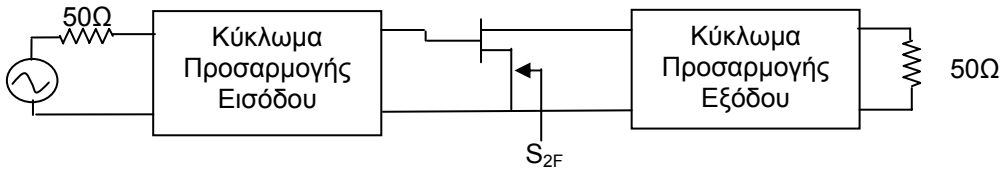

ΣΧΗΜΑ 9. Ενισχυτής με κυκλώματα προσαρμογής στην είσοδο και την έξοδο

Το τελικό TPG που βελτιστοποιείται στο βήμα αυτό δίνεται από την εξής σχέση :

$$T_2(\omega) = T_1(\omega) \cdot \frac{|S_{21B}|^2}{|1 - S_{2F}S_{11B}|^2} \tag{6}$$

όπου $T_1(\omega)$ είναι το TPG που επιτεύχθηκε στο προηγούμενο στάδιο, $S_{21B}=1/g_B$ είναι η παράμετρος μεταφοράς ισχύος στο δεύτερο κύκλωμα προσαρμογής – κύκλωμα προσαρμογής

εξόδου (back end matching network) από αριστερά προς δεξιά, και S_{2F} είναι η παράμετρος σκέδασης που φαίνεται στο παραπάνω σχήμα και ισούται με

$$S_{2F} = S_{22} + \frac{S_{12}S_{21}S_{22F}}{1 - S_{11}S_{22F}} \qquad (7)$$

Το S_{22F} στην παραπάνω σχέση ισούται με h_F/g_F όπου h_F ,g_F είναι τα πολυώνυμα που περιγράφουν το πρώτο κύκλωμα προσαρμογής (εισόδου) και προέκυψαν από τη βελτιστοποίηση του πρώτου σταδίου.

Η συνάρτηση σφάλματος (error function) αυτού του σταδίου δίνεται από τη σχέση:

$\text{error}_2 = 10 \cdot \log(T_2(\omega)) - 13.7$

Χρησιμοποιώντας και πάλι μία αυθαίρετη αρχικοποίηση h=[-1 1 -1 1 -1 1] (το κύκλωμα προσαρμογής θα περιέχει 6 στοιχεία) το TPG που επιτυγχάνεται παρουσιάζεται στο σχήμα 10(α).

Αυτή η γραφική παράσταση δεν προέκυψε από προσομοίωση στο ADS αλλά από υπολογισμό του TPG (στο MATLAB) συναρτήσει των παραμέτρων σκέδασης του τρανζίστορ και των συντελεστών ανάκλασης των κυκλωμάτων προσαρμογής εισόδου και εξόδου (equalizers) που προέκυψαν μετά από τη βελτιστοποίηση. Βλέπουμε ότι στο διάστημα 3-11 GHz έχουμε μία απόκλιση από το στόχο των 13.7 dB της τάξης του $-0.22\text{dB} < \Delta T < 0.07\text{dB}$. Ο στόχος επετεύχθη με άριστη προσέγγιση.

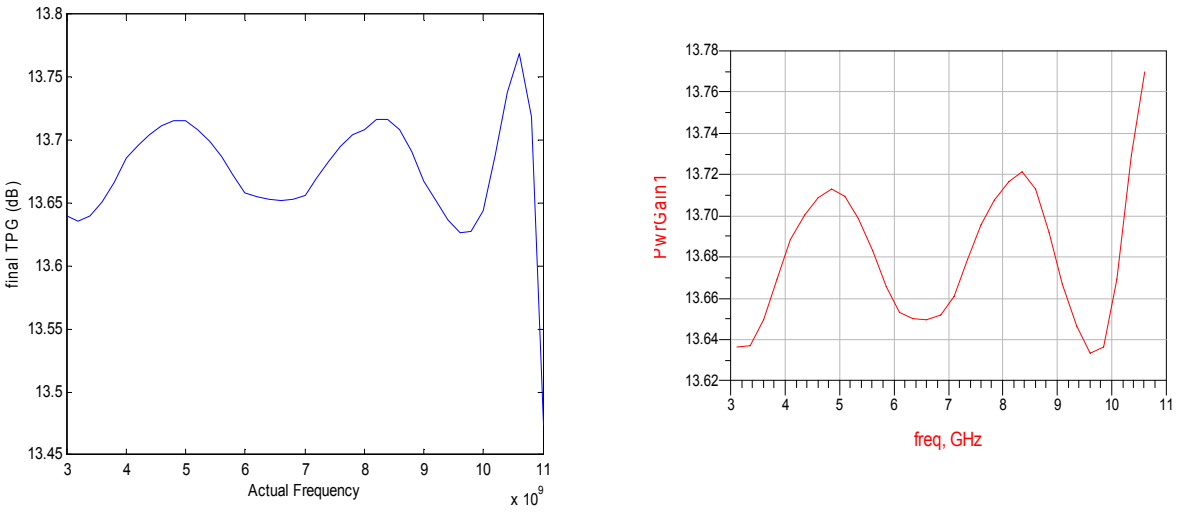

ΣΧΗΜΑ 10. (α) Τελικό κέρδος με τη SRFT (β) Κέρδος ισχύος μεταφοράς μετά την προσομοίωση

Τα πολυώνυμα που προέκυψαν από τη βελτιστοποίηση είναι τα εξής :

Για το κύκλωμα προσαρμογής εισόδου είναι:
h_F = [0.7706 1.2850 0.7948 0.6418 -0.1236 0]
g_F = [0.7706 2.6921 4.4258 4.7448 3.0830 1.0000]

Για το δεύτερο προσαρμοστικό κύκλωμα είναι :
h_B = [4.4353 2.8273 6.5209 2.8844 2.0559 0.4783 0]
g_B = [4.4353 8.6576 14.0695 13.9405 9.9071 4.4769 1.0000]

Για τη σύνθεση των κυκλωμάτων χρησιμοποιούμε μία ρουτίνα synthesis.m η οποία δέχεται στην είσοδό της τα αντεστραμμένα διανύσματα h,g και δίνει στην έξοδο τις τιμές των πυκνωτών και πηνίων που θα πρέπει να χρησιμοποιήσουμε. Έτσι έχουμε τις εξής τιμές:

L_1=0.7924 nH C_2=0.561 pF L_3=1.0682 nH C_4=0.367 pF L_5=0.2803 nH

Για το κύκλωμα προσαρμογής εξόδου, η ρουτίνα synthesis.m μας δίνει :

L_1= 1.1007 nH C_2= 0.4477 pF L_3= 1.3901 nH C_4= 0.4859 pF L_5= 1.0939nH C_6= 0.2235 pF.

Αν χρησιμοποιήσουμε τώρα το κύκλωμα αυτό στο ADS θα προκύψει η σχεδίαση, όπως παρουσιάζεται στο σχήμα 11.

Κάνοντας προσομοίωση στο κύκλωμα αυτό στο διάστημα 3.1-10.6 GHz, προκύπτει το κέρδος ισχύος μεταφοράς που φαίνεται στο σχήμα 10(β).

Η προσομοίωση αυτή με το ADS συμφωνεί απολύτως με το TPG του σχήματος 10(α) που υπολογίσαμε θεωρητικά μέσω των βελτιστοποιημένων παραμέτρων σκέδασης των δύο κυκλωμάτων προσαρμογής. Αυτό σημαίνει ότι η σύνθεση των κυκλωμάτων είναι επιτυχής.

Θα πρέπει όμως να εξετάσουμε και την ευστάθεια του ενισχυτή. Θα θεωρήσουμε ότι στην είσοδο και έξοδό του συνδέονται φορτία 50Ω. Η συνθήκη για να είναι ευσταθής ο ενισχυτής στην είσοδο και έξοδο είναι οι συντελεστές ανάκλασης εισόδου και εξόδου να έχουν μέτρο μικρότερο του ένα. Βλέπουμε ότι και τα δύο μέτρα είναι μικρότερα του ένα σε όλο το διάστημα συχνοτήτων (σχήμα 12). Επομένως ο ενισχυτής είναι ευσταθής στην τυπική περίπτωση που στην είσοδο και έξοδό του συνδέονται φορτία των 50 Ω.

Τέλος πρέπει να δούμε και την εικόνα θορύβου στην έξοδο του ενισχυτή. Βλέπουμε ότι η μέγιστη εικόνα θορύβου είναι 1.04 dB (σχήμα 13) που είναι μία αποδεκτή τιμή.

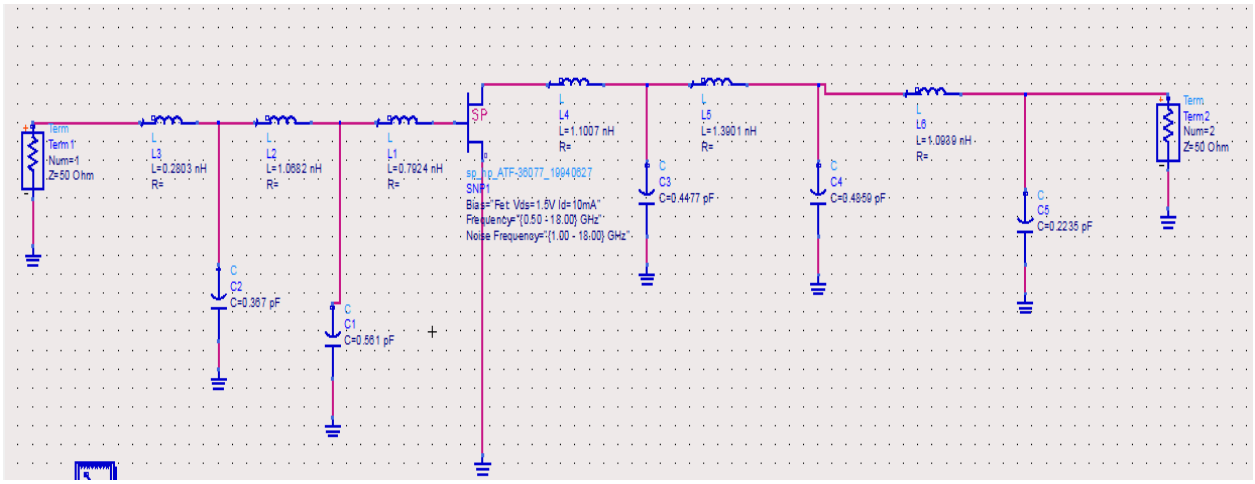

ΣΧΗΜΑ 11. Κύκλωμα Ενισχυτή υπό την SRFT

Θα πρέπει να σημειώσουμε ότι σύμφωνα με το φύλλο δεδομένων του κατασκευαστή του PHEMT που χρησιμοποιούμε, το τρανζίστορ παρουσιάζει το φαινόμενο της σχετικά μικρής μόνο επιδείνωσης της εικόνας θορύβου όταν στην είσοδό του παρουσιάζεται σύνθετη αντίσταση λίγο ή πολύ διαφορετική από τη σύνθετη αντίσταση που καθιστά την εικόνα θορύβου τη μικρότερη δυνατή. Το φαινόμενο αυτό καθιστά δυνατή τη λειτουργία του τρανζίστορ ως ενισχυτή μικρού θορύβου σε μεγάλο εύρος ζώνης (broadband LNA). Η σύνθετη αντίσταση στην είσοδο μπορεί να έχει μεγάλες διακυμάνσεις σε ένα τόσο μεγάλο εύρος συχνοτήτων, αλλά αυτό επηρεάζει

ελάχιστα το θόρυβο στην έξοδο του ενισχυτή. Έτσι παρόλο που η παραπάνω βελτιστοποίηση με την SRFT που πραγματοποιήσαμε δεν έλαβε υπόψη την απαίτηση για μικρό θόρυβο η εικόνα θορύβου εξόδου είναι ανεκτή. Παρόλα αυτά οι Gunes και Bilgin ενσωμάτωσαν επιτυχώς στην Απλοποιημένη Μέθοδο Πραγματικής Συχνότητας και την απαίτηση για μικρό θόρυβο, αλλά και μικρό λόγο στασίμων κυμάτων [18]. Επίσης, όπως περιγράφεται στο [12], η SRFT μπορεί εύκολα να επεκταθεί και για την σύνδεση σε σειρά ενισχυτικών βαθμίδων με ενεργά στοιχεία.

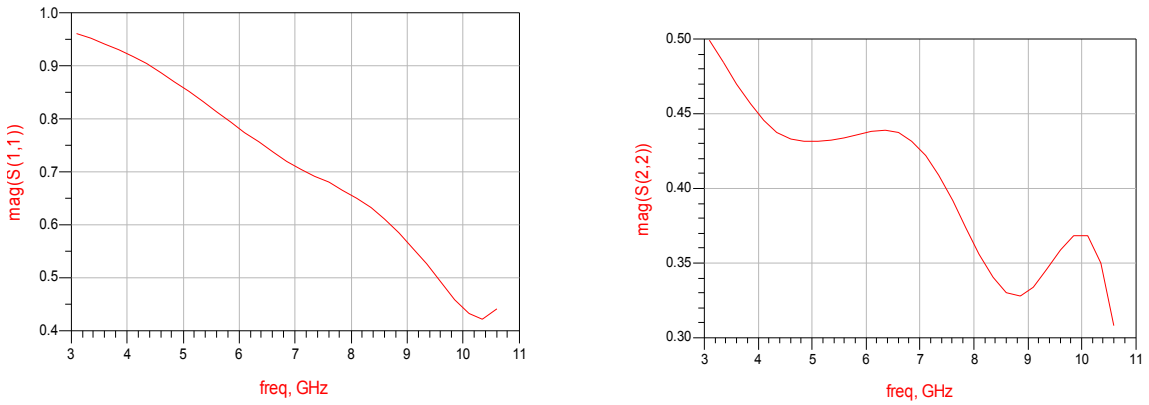

ΣΧΗΜΑ 12. Απόκριση των (α) S_{11} και (β) S_{22}

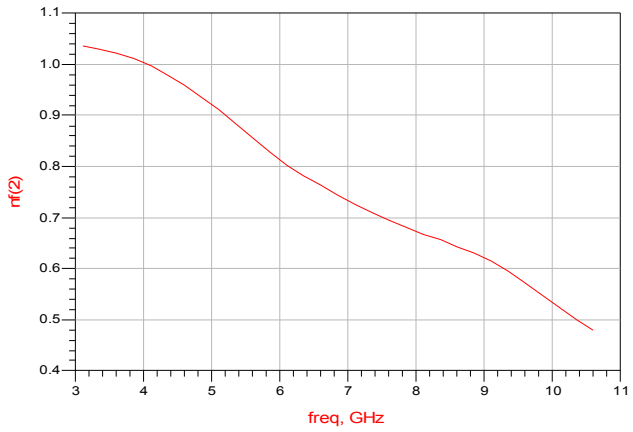

ΣΧΗΜΑ 13. Εικόνα θορύβου

ΣΥΜΠΕΡΑΣΜΑΤΑ

Γενικά η απλοποιημένη μέθοδος πραγματικής συχνότητας (SRFT) είναι η πιο πολλά υποσχόμενη μέθοδος, όπως άλλωστε περιγράφεται στο [18]. Στην εργασία τους αυτή, οι Gunes και Bilgin κατάφεραν με συστηματικό τρόπο χρησιμοποιώντας τη SRFT να επιτύχουν τα καλύτερα δυνατά αποτελέσματα ως προς το σταθεροποιημένο κέρδος, την εικόνα θορύβου, και το λόγο στάσιμων κυμάτων. Συγκεκριμένα χρησιμοποίησαν τα δεδομένα από το datasheet του ενεργού στοιχείου για να βρουν τον καλύτερο δυνατό συνδυασμό για τα παραπάνω μεγέθη σε μία σειρά από συχνότητες για τις οποίες οι κατασκευάστριες εταιρίες έδιναν δεδομένα για τα

τρανζίστορ. Οι συνδυασμοί αυτοί αποτέλεσαν και τους στόχους προς επίτευξη μέσω της σύνθεσης των προσαρμοστικών κυκλωμάτων εισόδου και εξόδου με τη SRFT.

Στη δική μας εργασία δείξαμε ένα μόνο μέρος των δυνατοτήτων της SRFT υλοποιώντας κατάλληλες ρουτίνες στο MATLAB. Πραγματικά, με την SRFT πετύχαμε την καλύτερη δυνατή σταθεροποίηση του κέρδους του ενισχυτή (στην τιμή 14 dB) σε όλο το UWB φάσμα, πράγμα που είναι βασική απαίτηση στις τεχνολογίες UWB. Η εικόνα θορύβου επίσης ήταν πάρα πολύ καλή (0.7 db), όπως και ο συντελεστής ανάκλασης εξόδου (0.3 σε απόλυτους αριθμούς). Το μόνο μειονέκτημα στην υλοποίησή μας ήταν ο συντελεστής ανάκλασης στην είσοδο με μέση τιμή 0.75.

Στη σχεδίαση που αναπτύχθηκε στην παρούσα εργασία, χρησιμοποιήθηκε μόνο μία ενισχυτική βαθμίδα, με αποτέλεσμα το κέρδος να είναι μικρό, όμως ανεκτό για ένα ενισχυτή χαμηλού θορύβου. Μεγαλύτερο κέρδος επιτυγχάνουμε όταν χρησιμοποιούμε περισσότερα ενισχυτικά κύτταρα σε σειρά. Πράγματι, στη μέθοδο της κατανεμημένης ενίσχυσης, και μάλιστα στην περίπτωση του κατανεμημένου ενισχυτή μήτρας (matrix distributed amplifier) έχουν επιτευχθεί πολύ καλά αποτελέσματα, δεδομένης ιδιαιτέρως της χαμηλής εικόνας θορύβου, πράγμα όχι συνηθισμένο για ένα κατανεμημένο ενισχυτή. Πιο συγκεκριμένα, πετύχαμε κέρδος γύρω στο 20.4 dB, εικόνα θορύβου 2 dB και μέτριο συντελεστή ανάκλασης εισόδου με τιμή 0.4.

Η απλοποιημένη μέθοδος πραγματικής συχνότητας έδωσε εξαιρετικά αποτελέσματα όσον αφορά στο κέρδος και στο θόρυβο, συγκρινόμενη με τις μεθόδους κατανεμημένης ενίσχυσης.

REFERENCES

1. FCC 02-48, Federal Communications Commission, April 22, 2002.
2. Stephen Wood, Roberto Aiello, *Essentials of UWB*, Cambridge University Press, 2008, pp.12-16.
3. Win, Scholtz, “On the Robustness of Ultra-Wide Bandwidth Signals in Dense Multipath Environments” IEEE COMMUNICATIONS LETTERS 2, 51-53 (1998).
4. Wong, *Fundamentals of distributed amplification*, Artech House, 1993, pp. 10-20.
5. Lee, The design of CMOS radio-frequency integrated circuits, second edition, Cambridge University press, 2004, pp. 248.
6. E. A. Karagianni, N. K. Uzunoglu, A Distributed Transmission Line Amplifier with Constant Gain Operating DC up to 40 GHz for Wideband Telecommunication Applications, 8th International Conference on Advances in Communications and Control, pp. 501-504,2001.
7. Bahl, Fundamentals of RF and Microwave Transistor Amplifiers, Wiley, 2009, pp. 72.
8. Kim, B, Tserng, H.Q, *Electronic Letters* 20, pp. 288-289 (1984)
9. Ayasli, Miller, Mozzi, Hanes,”Capacitively Coupled Traveling-Wave Power Amplifier”, IEEE TRANSACTIONS ON MICROWAVE THEORY AND TECHNIQUES 32, 1704-1709 (1984)
10. Aitchison, “The Intrinsic Noise Figure of the MESFET Distributed Amplifier”, *IEEE TRANSACTIONS ON MICROWAVE THEORY AND TECHNIQUES* 33, pp. 460-466 (1985).
11. Guan, Nguyen, “Low-power-consumption and high-gain CMOS distributed amplifiers using cascade of inductively coupled common-source gain cells for UWB systems”, IEEE TRANSACTIONS ON MICROWAVE THEORY AND TECHNIQUES 54 pp. 3278-3283 (2006).
12. Yarman, Carlin, “A Simplified Real Frequency Technique Applied to Broadband Multistage Microwave Amplifiers”, IEEE TRANSACTIONS ON MICROWAVE THEORY AND TECHNIQUES 30 pp. 2216-2222 (1982).
13. Carlin, Komiak, "A new method of broad-band equalization applied to microwave amplifiers", *IEEE TRANSACTIONS ON MICROWAVE THEORY AND TECHNIQUES* 24, pp. 170-175 (1977).
14. Σχεδίαση Ενισχυτή Χαμηλού Θορύβου για Εφαρμογές Ευρείας Ζώνης 3.1-10.6GHz, Διπλωματική Εργασία, Νικόλαος Χατζηαθανασίου, ΕΚΠΑ, 2011.
15. Yarman, Design *of Ultra Wideband Antenna Matching Networks*, Springer, 2008, pp. 190-197.
16. Yarman, *DESIGN OF ULTRA WIDEBAND POWER TRANSFER NETWORK*, Wiley, 2010, pp.634-686
17. Yarman, *DESIGN OF ULTRA WIDEBAND POWER TRANSFER NETWORK*, Wiley, 2010, pp. 636
18. F. Gune¸s, C. Bilgin, “A GENERALIZED DESIGN PROCEDURE FOR A MICROWAVE AMPLIFIER: A TYPICAL APPLICATION EXAMPLE”, *Progress In Electromagnetics Research* B10, pp. 1–19 (2008).

Implementation Limitations of STANAG 1008 Design Constraints for Pulsed Loads

George J. Tsekouras[a], Fotis D. Kanellos[b], John M. Prousalidis[c] and Ioannis K. Hatzilau[a]

[a] *Hellenic Naval Academy, Department of Electrical Engineering and Computer Science, Terma Hatzikiriaku, 18539, Piraeus, Greece*
[b] *Technical University of Crete, Production Engineering & Management Department, Chania, 73100, Greece*
[c] *National Technical University of Athens, School of Naval Architecture and Marine Engineering, 9, Iroon Polytecheniou Street, 157 80, Zografou Campus, Athens, Greece*

Abstract. Crucial power quality problems in ship electric power systems, known as "voltage/frequency modulation", are usually caused by specific type of loads known as "pulsed loads". Pulsed loads require regularly or randomly repeated high power consumption in short time intervals. NATO standard, STANAG 1008, imposes two design inequalities involving the power factor of the pulsed load and the ratio between the apparent power of the pulsed load and the full rated apparent power of the supply at the occurrence of the pulse. If these two inequalities are satisfied for a low voltage ship service power supply system, the voltage and frequency modulation will not exceed 2% and 0,5%, respectively. However, no well-based theoretical analysis of the phenomenon is used. The mathematical analysis of voltage/frequency phenomenon was presented in a series of two companion past papers proving that the phenomenon is depends on several parameters such as pulsed load period and duty cycle, the technical characteristics of the generators and their frequency and voltage controllers, the technical characteristics of the cable between the pulsed load and the generator etc. In this paper, the impact of the aforementioned parameters to STANAG 1008 design constraints for voltage and frequency modulation will be examined based on the theoretical analysis already developed by the authors. The effects of the respective parameters on STANAG 1008 pulsed load limit curves are presented and commented highlighting some of the issues to be addressed by future standards.

Keywords: Ship electric power system, STANAG 1008, pulsed loads, voltage and frequency modulation, modeling.
PACS: 84.70.+p

INTRODUCTION

In recent years Power Supply Quality (PSQ) for ship power systems has become a significant issue as the equipment installed on board is increasingly electrified. One of the most critical PSQ problems is "voltage and frequency modulation". Generally, "modulation" is defined as "voltage and frequency periodic or quasi-periodic variations such as might be caused by

regularly or randomly repeated loading with frequency less than nominal" [1-3]. Pulsed loads provoke modulation, as they require high power for a very short time interval (in the order of a few seconds or even up to some milliseconds). This operation is often repeated on a regular or almost regular basis introducing a periodicity on the entire phenomenon.

The primary effects of pulse loading have been already studied in the context of voltage flicker, dynamic and transient stability, excitation of torsional frequencies in generators etc according to previous experience from continental power systems [4]. Pulse loading may also affect the operation of several subsystems of the ship such as radarscopes, communication and navigation equipment etc.

Voltage and frequency modulations are calculated as the difference between maximum and minimum values expressed as a percentage of the double of the nominal value as shown in (1) and (2):

$$M_V = \frac{V_{\max} - V_{\min}}{2V_n} \tag{1}$$

$$M_f = \frac{f_{\max} - f_{\min}}{2f_n} \tag{2}$$

Voltages in (1) may be used in rms, peak or mean values.

In Fig. 1, voltage and frequency modulation caused by a rectangular pulsed load is shown.

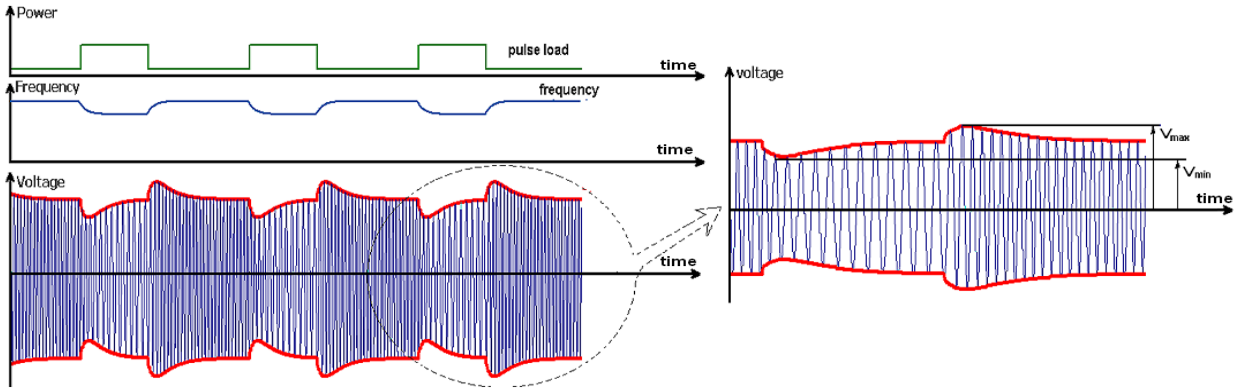

FIGURE 1. Frequency and voltage modulation caused by a rectangular pulsed load.

Up to now, few standards have dealt with this issue and have released relevant rules. Especially, in IEEE-45 the respective parameters have not been quantified [1], while USA-MIL-1399 [3] is overlapped with STANAG-1008 [2]. The following analysis will be based on STANAG 1008 (edition 9) [2], which is the NATO naval standard dealing with PSQ issues. It sets the limits of voltage and frequency modulation for the low voltage shipboard electrical power systems (440 V, 115 V, 60 Hz, 400 Hz) to 2% and 0.5%, respectively. STANAG 1008 deals only with the Ship Service Power Supply System excluding ship electric propulsion systems.

According to the design constraints of STANAG 1008 [8: Annex B § 9.d], in order voltage and frequency modulation not to exceed the aforementioned limits, reactive and active power of the pulsed load should satisfy the following inequalities:

$$\text{Voltage modulation: } \Delta Q < 0.065 \cdot S_S \tag{3}$$

$$\text{Frequency modulation: } \Delta P < 0.25 \cdot S_S \tag{4}$$

where ΔP and ΔQ are the active and the reactive power of the pulsed load respectively, S_S is

the full rated apparent power of the supply at the occurrence of the pulsed load. Considering the apparent power of the pulsed load ΔS and the power factor of the pulsed load $\cos\phi$, the inequalities (3) and (4) can be written as:

$$\text{Voltage modulation:}\quad \cos\phi > \sqrt{1-\left(a\cdot\frac{1}{\Delta S}\right)^2}\ :\quad a=0.065 \tag{5}$$

$$\text{Frequency modulation:}\quad \Delta S\cdot\cos\phi < \beta\ :\quad \beta=0.25 \tag{6}$$

where α and β are the two parameters affecting the dimension of acceptable and unacceptable areas of operation. STANAG α, β parameters are fixed at 0.25 and 0.065, respectively. The respective graphical representation of inequalities (5), (6) is shown in Fig.2.

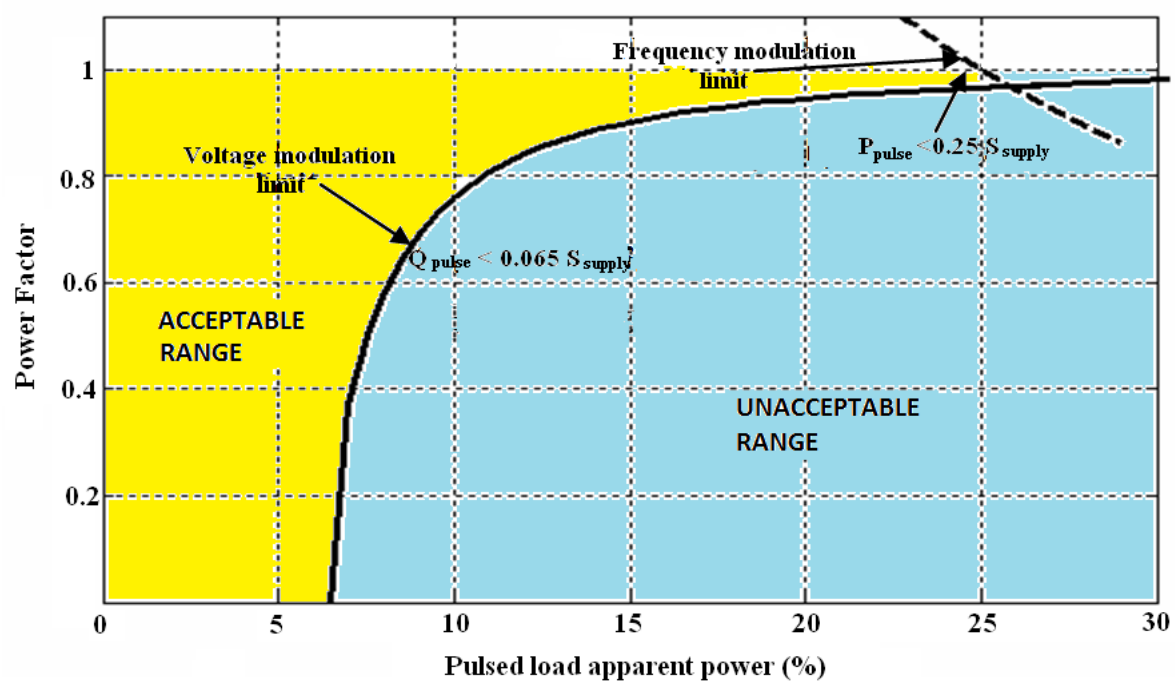

FIGURE 2. Limit curves for pulsed load operation according inequalities (5) and (6), where the acceptable and unacceptable range of pulsed load installed capacity is highlighted.

In previous papers of the authors [5-7], the electric power system of conventional ship and of All-Electric Ship has been examined proving that STANAG 1008 guideline seems to be a method leading to a rather rough estimation of pulsed loads limits, as it considers only the pulsed load relative apparent power ΔS and the power factor of the pulsed load $\cos\phi$. However, additional parameters such as the pulse load period and duty cycle, the time-profile and the point of the connection of the pulsed load, the technical characteristics of the generators (like sub-transient reactance, intertia) and their associated frequency and voltage controllers (like governor and automatic voltage regulator (AVR) gains etc), the loading factor of the generator at the time of the pulsed load occurrence, the equivalent length of the cable between the pulsed load and the generator etc, should be taken into account

Later, in a series of two companion papers [8-9] the theoretical analysis of the frequency and voltage modulation has been presented for a simplified ship power system respectively leading to more complex inequalities including all the above mentioned affecting parameters.

In this paper, the STANAG 1008 design constraints for voltage and frequency modulation will be examined based on the respective theoretical analysis of ship's simplified power system [8-9]. Emphasis will be placed on the effects of the respective parameters on the pulsed load limit curves of STANAG 1008 and the respective deviations caused by the variation of the parameters affecting voltage/frequency modulation will be demonstrated.

THEORETICAL ANALYSIS OF FREQUENCY & VOLTAGE MODULATION IN A SIMPLIFIED SHIP'S ELECTRIC POWER SYSTEM

Simplified Electrical Circuit of Ship Power System

The electric power system of a ship is considered as simplified as possible, as shown in Fig. 3 and proposed in [5]. The proposed simplified configuration can lead to the equivalent model of a conventional ship or an All Electric Ship. According to this approach, the bulk power produced by the equivalent synchronous generator is transferred to the load via a major electrical path with complex impedance $R+j\cdot X_C$. Automatic voltage and frequency regulators control the AC voltage and its frequency, respectively.

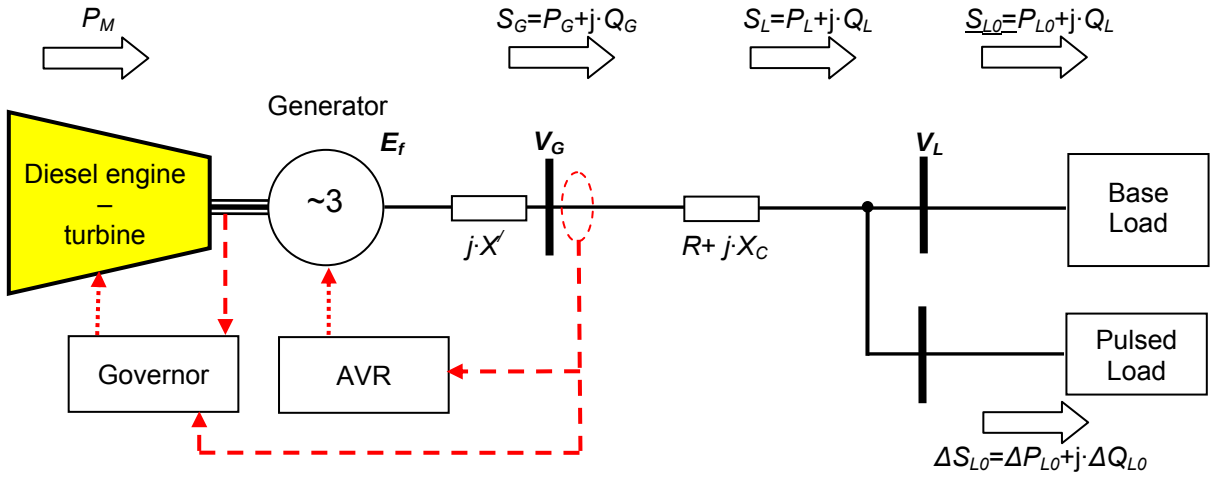

FIGURE 3. Equivalent topology of a ship electric power system.

For the following analysis the electric and mechanical parameters with the respective measurement units used, are listed next:

- E_F is the generator excitation voltage (V [volts] or p.u. [per unit]),
- V_G is the voltage at the generator ends (V or p.u.),
- V_L is the voltage at the load connection point (V or p.u.),
- E_{F0} is the generator excitation voltage (p.u.) before the occurrence of the pulsed load,
- V_{G0} is the voltage at the generator ends (p.u.) before the occurrence of the pulsed load,
- V_{L0} is the voltage at the load connection point (p.u.) before the occurrence of the pulsed load,
- T_M is the accelerating mechanical torque on generator shaft (Nm),
- T_G is the electromechanical torque on generator gap (Nm),
- P_M is the accelerating mechanical power on generator shaft (W or p.u.),

- S_G, P_G, Q_G are the apparent, the active and the reactive power produced by the generator respectively (VA or p.u., W or p.u., var or p.u.),
- S_S is the full rated apparent power of the supply at the occurrence of the pulsed load, which is the nominal base apparent power of the electric power system (VA),
- X' is the equivalent sub-transient reactance of the generator (Ω or p.u.),
- R, X_C are the equivalent resistance and the equivalent reactance of the cables between generator output and load bus respectively (Ω or p.u., Ω or p.u.),
- S_L, P_L, Q_L are the apparent, the active and the reactive power of the system load respectively (VA or p.u., W or p.u., var or p.u.),
- S_{L0}, P_{L0}, Q_{L0} are the apparent, the active and the reactive power of the system base load (without the pulsed load) respectively (VA or p.u., W or p.u., var or p.u.),
- ΔS, ΔP, ΔQ are the apparent, the active and the reactive power of the system pulsed load respectively (VA or p.u., W or p.u., var or p.u.),
- ω, f are the ship electric power system cyclic frequency and the respective frequency (rad/s or p.u., Hz or p.u.),
- ω_0, f_0 is the ship electric power system base cyclic frequency and the respective base frequency (rad/s or p.u., Hz or p.u.),
- Δf is the frequency deviation from its nominal value and is equal to 1-f (p.u.),
- J is the generator rotor inertia constant (kg·m^2),
- J' is the generator rotor inertia constant (s), which is equal to $J \cdot \omega_0^2 / S_S$,
- T is the pulsed load period (s),
- dc is the pulsed load duty cycle (-),
- cosφ is the pulsed load power factor (-),
- I_L, I_{Ld}, I_{Lq} are the system load current and the respective d-axis, q-axis components (A or p.u.),
- R_f, K_f are the frequency droop and the integral gain of the frequency regulator,
- K, K_V are the proportional and the integral gain of automatic voltage regulator respectively,
- $M_f^{\lim}$ is the frequency modulation limit (-),
- $M_V^{\lim}$ is the voltage modulation limit (-).

The supplied load consists of a base load (including electric propulsion in the case of All Electric Ship) and a pulsed load. A typical pulsed load profile as that shown in Fig. 4a is used for the analysis that follows. System pulsed load is modeled by the following expressions:

$$\Delta S(t) = \Delta S \cdot \sum_{n=0}^{\infty} \left[u(t - n \cdot T) - u(t - (n + dc) \cdot T) \right] \tag{7}$$

$$\Rightarrow \Delta P(t) = \Delta S \cdot \cos\varphi \cdot \sum_{n=0}^{\infty} \left[u(t - n \cdot T) - u(t - (n + dc) \cdot T) \right] \tag{8}$$

where $u(t)$ is the unit step-function.

Constant power load modeling approach is fairly accurate for the examined range of frequency and voltage deviation, provided that that loads in modern ship configurations are often interfaced with the grid via power electronic converters, which provide fast dynamic reactions. So the respective profile of the total load demand is presented in Fig. 4b.

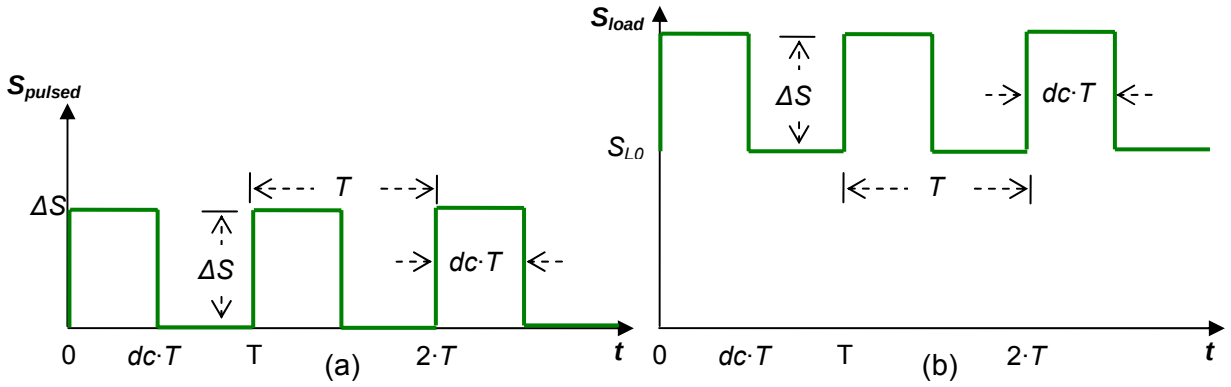

FIGURE 4. a) Pulsed load typical profile, b) total load typical profile.

Frequency Modulation Estimation

Here, the mathematical base of frequency modulation in the presence of pulsed load is presented. The detailed mathematical nalysis can be found in [8].

If friction losses are neglected, then the motion equation of the generator rotor is:

$$J \cdot \frac{d\omega}{dt} = T_M - T_G \tag{9}$$

Taking into consideration that P_M is the accelerating mechanical power, P_G the active power produced by the generator, ω is the rotor rotating speed, which is equal to frequency f in p.u., and Δf=1-f, equation (8) can be rewritten:

$$J' \cdot f \cdot \frac{d\Delta \mathrm{f}}{\mathrm{dt}} = \Delta P_G - \Delta P_M (p.u.) \tag{10}$$

If both primary and secondary frequency adjustment is taken into account, the frequency droop equation of the generator is:

$$\Delta P_M = R_f \cdot \Delta f + K_f \cdot \int_o^t \Delta f \cdot d\tau \tag{11}$$

Where, R_f is the frequency droop of the combination of the generator and its associated speed governor, K_{fl} the integral gain of the speed controller.

Assuming that frequency is close to its nominal value ($f \approx 1$ p.u.) and taking into consideration the set of equations (8), (10) and (11) the following equation is obtained:

$$J' \cdot \frac{d\Delta f}{dt} = \Delta S \cdot \cos\varphi \cdot \sum_{n=0}^{\infty} \Big[u(t - n \cdot T) - u(t - (n + dc) \cdot T) \Big] - R_f \cdot \Delta f - K_f \cdot \int_o^t \Delta f \cdot d\tau \tag{12}$$

If

$$R_f^2 > 4 \cdot J^{/} \cdot K_f \tag{13}$$

then by applying Laplace and inverse Laplace transformation to equation (12) frequency in time domain is equal to:

$$\Delta f(t)=\frac{\Delta S\cdot\cos\phi}{J'\cdot(p_2-p_1)}\cdot\sum_{n=0}^{\infty}\left[\begin{array}{l}\left(e^{-p_1(t-nT)}-e^{-p_2(t-nT)}\right)\cdot u(t-nT)\\-\left(e^{-p_1(t-(n+dc)\cdot T)}-e^{-p_2(t-(n+dc)\cdot T)}\right)\cdot u(t-(n+dc)\cdot T)\end{array}\right] \tag{14}$$

Where

$$p_1=\frac{R_f-\sqrt{R_f^2-4\cdot J'\cdot K_f}}{2\cdot J'}\qquad p_2=\frac{R_f+\sqrt{R_f^2-4\cdot J'\cdot K_f}}{2\cdot J'} \tag{15}$$

According to (2) and taking into account the frequency function of eq. (14), frequency modulation becomes:

$$M_{\mathrm{f}}=\frac{f_{\max}-f_{\min}}{2f_n}=\frac{\Delta\mathrm{S}\cdot\cos\phi\cdot c}{2\cdot f_n\cdot\sqrt{R_f^2-4\cdot J'\cdot K_f}} \tag{16}$$

with the parameter *c* calculated as follows:

$$c=c'\left(p_1,dc,T,t_{\max 1},t'_{\max 2}\right)-c'\left(p_2,dc,T,t_{\max 1},t'_{\max 2}\right) \tag{17}$$

where,

$$t_{\max 1}=\max\left(\frac{1}{p_2-p_1}\cdot\ln\left[\frac{p_2}{p_1}\cdot\frac{\left(e^{p_2dcT}-1\right)}{\left(e^{p_1dcT}-1\right)}\cdot\frac{\left(e^{p_1T}-1\right)}{\left(e^{p_2T}-1\right)}\right],\ 0\right) \tag{18}$$

$$t'_{\max 2}=\min\left(\frac{1}{p_2-p_1}\cdot\ln\left[\frac{p_2}{p_1}\cdot\frac{\left(e^{p_2T}-e^{p_2dcT}\right)}{\left(e^{p_1T}-e^{p_1dcT}\right)}\cdot\frac{\left(e^{p_1T}-1\right)}{\left(e^{p_2T}-1\right)}\right];dc\cdot T\right) \tag{19}$$

$$c'\left(p,dc,T,t_{\max 1},t'_{\max 2}\right)=\frac{\left(e^{pdcT}-1\right)\cdot e^{-p\cdot t_{\max 1}}+\left(e^{pT}-e^{pdcT}\right)\cdot e^{-p\cdot t'_{\max 2}}-e^{pT}+e^{pdcT}}{e^{pT}-1} \tag{20}$$

Taking into consideration STANAG-1008 constraint for frequency modulation, (M_f should be smaller than $M_f^{\lim}$ = 0.5%), then the following inequality is obtained:

$$\Delta S\cdot\cos\varphi<\frac{2\cdot M_f^{\lim}\cdot f_n\cdot J'\cdot(p_2-p_1)}{c} \tag{21}$$

Inequality (21) defines a parabolic curve on the *S-cosφ* plane, as it is also foreseen by STANAG-1008 (as shown in Fig. 2 and defined by inequality (4)) involving several parameters of ship electric power system model such as *dc*, *T*, R_f, *J'*, K_f which must be taken into account during the design of the electric power system. Moreover, it appears that the *S-cosφ* limitation curve for frequency deviation is not unique as assumed in standards like STANAG-1008, but it depends on the system model parameters mentioned above. Inequality (21) has been

developed within time interval $t\in[0,\infty)$, while standards, like STANAG-1008, do not define the respective study time period of the frequency modulation.

R_f should not lie into the region defined by $R_f^2=4\cdot J'\cdot K_f$ and $R_f^2<4\cdot J'\cdot K_f$ as it might provoke significant frequency oscillations.

In general the respective upper limit for frequency modulation can be expressed by a general function of the following form for this simplified ship power system:

$$F_f(T,dc,J',K_f,R_f,\Delta S,\cos\varphi)\le M_f^{\lim} \tag{22}$$

Voltage Modulation Estimation

Here, the mathematical basis for the estimation of voltage modulation caused by pulsed loads is presented. The detailed mathematical analysis can be found in [9].

More specifically the electric behavior of the system shown in Fig. 3 is similar to the behavior of an RL circuit, where the RL circuit consists of the equivalent sub-transient reactance of the generator X', the equivalent reactance X_C of the cables between generator output and load bus and the equivalent resistance R. The voltages at the ends of the RL branch, namely, the electromagnetic force E_F of synchronous generator and the load voltage V_L, are related with the current flowing through it by the following set of differential equations (all AC quantities are expressed to a rotating reference frame attached to voltage, V_L).

$$E_{Fd}=V_{Ld}+R\cdot I_{Ld}-\left(X'+X_C\right)\cdot I_{Lq}+\frac{X'+X_C}{\omega_0}\cdot\frac{dI_{Ld}}{dt} \tag{23}$$

$$E_{Fq}=\underbrace{V_{Lq}}_{0}+R\cdot I_{Lq}+\left(X'+X_C\right)\cdot I_{Ld}+\frac{X'+X_C}{\omega_0}\cdot\frac{dI_{Lq}}{dt} \tag{24}$$

It is noted that the generator saturation has been ignored in this study.

The respective vector diagram is presented in Fig. 5, where phase angle θ is the load current phase angle with respect to load voltage vector V_L.

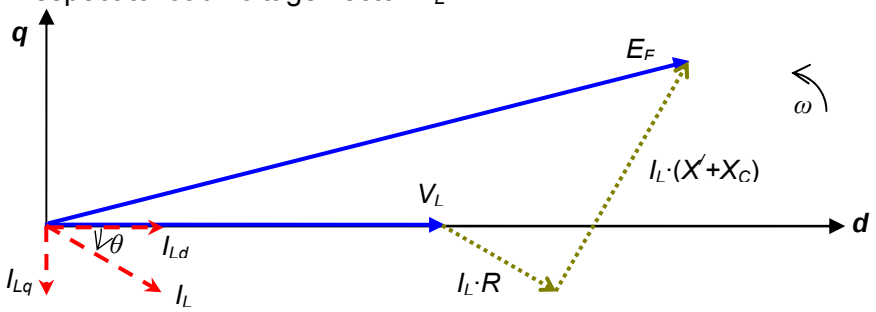

FIGURE 5. Vector diagram of simplified electrical circuit of ship power system.

For the operating conditions of the ship electric system studied in this paper, the so-called induction voltage terms (including current derivatives) in equations (23) and (24) can be neglected without affecting significantly the accuracy of the results [10, 11] and the following set of equations is formed:

$$E_{Fd} = V_{Ld} + R \cdot I_{Ld} - \left(X^{/} + X_C \right) \cdot I_{Lq} \tag{25}$$

$$E_{Fq} = R \cdot I_{Lq} + \left(X^{/} + X_C \right) \cdot I_{Ld} \tag{26}$$

The electromagnetic force E_F of synchronous generator is adjusted by the Automatic Voltage Regulator (AVR). For simplification purposes and without loss of generalization, a simple proportional – integral (PI) controller is assumed, while the generator bus is considered as the voltage control point. Thus, AVR can be modeled as following:

$$E_f = E_{f0} + K \cdot \Delta V_G + K_V \cdot \int_0^t \Delta V_G \cdot d\tau \tag{27}$$

with

$$\Delta V_G = V_{G0} - V_G = 1 - V_G \tag{28}$$

While

$$\Delta V_L = V_{L0} - V_L \tag{29}$$

$$\Delta S_L \cong S_L - S_{L0} \tag{30}$$

$$S_L = V_L \cdot I_L \text{ (root mean values)} \tag{31}$$

Where E_{F0}, V_{G0}, V_{L0}, S_{L0} are the synchronous generator electromagnetic force, the generator bus voltage, the load bus voltage and the system base load apparent power before the occurrence of the pulsed load, respectively.

Applying Laplace transformation, Taylor series expansion of E_F with respect to V_L and S_L approximated by 1st order terms and inverse Laplace transformation, load bus voltage variance is given by:

$$\Delta V_L(t) = \begin{cases} \Gamma_1 \cdot \Delta S \cdot \sum_{n=0}^{\infty} \left(u(t - n \cdot T) - \left(u(t - n \cdot T - dc \cdot T) \right) \right) \\ + \Gamma_2 \cdot \Delta S \cdot \sum_{n=0}^{\infty} \left(e^{-\gamma \cdot (t - n \cdot T)} \cdot u(t - n \cdot T) - e^{-\gamma (t - n \cdot T - dc \cdot T)} \cdot \left(u(t - n \cdot T - dc \cdot T) \right) \right) \end{cases} \tag{32}$$

where

$$V_{G0}^2 = 1 = V_{L0}^2 + \frac{R^2 + X_C^2}{V_{L0}^2} \cdot S_{L0}^2 + 2 \cdot (R \cdot \cos\varphi + X_C \cdot \sin\varphi) \cdot S_{L0} \tag{33}$$

$$V_{L0} = \sqrt{\frac{1 - 2 \cdot (R \cdot \cos\varphi + X_C \cdot \sin\varphi) \cdot S_{L0} + \left(\left(2 \cdot (R \cdot \cos\varphi + X_C \cdot \sin\varphi) \cdot S_{L0} - 1 \right)^2 - 4 \cdot (R^2 + X_C^2) \cdot S_{L0}^2 \right)^{1/2}}{2}} \tag{34}$$

$$E_{F0} = \left(V_{L0}^2 + \frac{R^2 + X^2}{V_{L0}^2} \cdot S_{L0}^2 + 2 \cdot (R \cdot \cos\varphi + X \cdot \sin\varphi) \cdot S_{L0} \right)^{1/2} \tag{35}$$

$$\mathrm{A}_1 = \frac{R \cdot \cos\varphi + X \cdot \sin\varphi + \dfrac{R^2 + X^2}{V_{L0}^2} \cdot S_{L0}}{E_{f0}} \tag{36}$$

$$\mathrm{A}_2 = \frac{V_{L0} - \dfrac{R^2 + X^2}{V_{L0}^3} \cdot S_{L0}^2}{E_{f0}} \tag{37}$$

$$\mathrm{B}_1 = \frac{R \cdot \cos\varphi + X_C \cdot \sin\varphi + \dfrac{R^2 + X_C^2}{V_{L0}^2} \cdot S_{L0}}{V_{G0}} \tag{38}$$

$$\mathrm{B}_2 = \frac{V_{L0} - \dfrac{R^2 + X_C^2}{V_{L0}^3} \cdot S_{L0}^2}{V_{G0}} \tag{39}$$

$$\Gamma_1 = \frac{\mathrm{B}_1}{\mathrm{B}_2} > 0 \tag{40}$$

$$\Gamma_2 = \frac{\mathrm{B}_2 \cdot \mathrm{A}_1 - \mathrm{B}_1 \cdot \mathrm{A}_2}{\mathrm{B}_2 \cdot (\mathrm{A}_2 + \mathrm{B}_2 \cdot \mathrm{K})} > 0 \tag{41}$$

$$\gamma = \frac{\mathrm{B}_2 \cdot K_V}{\mathrm{A}_2 + \mathrm{B}_2 \cdot \mathrm{K}} \tag{42}$$

According to (1) and taking into account the voltage variance function of eq. (32), voltage modulation becomes:

$$M_V = \frac{V_{\max} - V_{\min}}{2 \cdot V_n} = \frac{\max \Delta V_L - \min \Delta V_L}{2 \cdot V_n} = \frac{\Gamma_1 + \Gamma_2 \cdot \dfrac{2 \cdot e^{\gamma \cdot T} - e^{\gamma \cdot T \cdot (1-dc)} - 1}{e^{\gamma \cdot T} - 1} \cdot \Delta S}{2 \cdot V_n} \tag{43}$$

Taking into consideration STANAG-1008 constraint for voltage modulation, (M_V should be smaller than $M_V^{\lim}$ = 2%), the following inequality is obtained:

$$M_V < M_V^{\lim} \tag{44}$$

If it is assumed that $R \approx 0$, $V_n \approx 1$ p.u., $E_F \approx 1$ p.u., $X \approx X_C$, $X + X_C \approx 2 \cdot X$ and $1 - X^2 \cdot S_{L0}^2 \approx 1 - X_C^2 \cdot S_{L0}^2$, then (43) turns into,

$$M_V = \frac{\Delta S}{2} \cdot \left[Z_1 + Z_2 \sin\varphi \right] \tag{45}$$

with

$$Z_1 = \frac{\mathrm{X}^2 \cdot S_{L0}}{1 - \mathrm{X}^2 \cdot S_{L0}^2} + \frac{2 \cdot \mathrm{X}' \cdot \mathrm{X} \cdot S_{L0}}{(K+1) \cdot (1 - \mathrm{X}^2 \cdot S_{L0}^2)^2} \cdot \frac{2 \cdot e^{\gamma \cdot T} - e^{\gamma \cdot T \cdot (1-dc)} - 1}{e^{\gamma \cdot T} - 1} \tag{46}$$

$$Z_2 = \frac{\mathrm{X}}{1-\mathrm{X}^2 \cdot S_{L0}^2} + \frac{\mathrm{X}' \cdot (1+\mathrm{X}^2 \cdot S_{L0}^2)}{(K+1) \cdot (1-\mathrm{X}^2 \cdot S_{L0}^2)^2} \cdot \frac{2 \cdot e^{\gamma \cdot T} - e^{\gamma \cdot T \cdot (1-dc)} - 1}{e^{\gamma \cdot T} - 1} \tag{47}$$

Then the following inequality is obtained:

$$\cos\varphi > \sqrt{1 - \left(\frac{Z_1}{Z_2}\right)^2 + \frac{4 \cdot \mathrm{M}_V^{\lim} \cdot Z_1}{Z_2^2} \cdot \frac{1}{\Delta S} - \frac{4 \cdot \left(\mathrm{M}_V^{\lim}\right)^2}{Z_2^2} \cdot \frac{1}{\Delta S^2}} \tag{48}$$

Considering that the products $X^2 \cdot S_{L0}^2$, $X_C^2 \cdot S_{L0}^2$ and $X \cdot X_C \cdot S_{L0}$ are negligible, then (48) becomes,

$$\cos\varphi > \sqrt{1 - \left(\frac{a}{\Delta S}\right)^2} \tag{49}$$

with

$$\alpha = \frac{2 \cdot \mathrm{M}_V^{\lim}}{\mathrm{X} + \frac{\mathrm{X}'}{(K+1)} \cdot \frac{2 \cdot e^{\gamma \cdot T} - e^{\gamma \cdot T \cdot (1-dc)} - 1}{e^{\gamma \cdot T} - 1}} \tag{50}$$

that is of the same form with the inequality proposed in STANAG 1008 (see eq. (5)).

Inequalities (44), (48) and (49) define limitation curves on the S-cosφ plane similar to the one foreseen by STANAG-1008, ehich however, include several parameters of ship electric power system model such as *dc*, *T*, *K*, K_I, X_C, X', S_{L0}. Therefore, it can be concluded that *S*-cosφ limitation curve for voltage deviation is not unique as assumed in standards like STANAG-1008, but it depends on the system model parameters mentioned above which must be taken into account during the design of the ship electric power system. Inequalities (48) and (49) have been also developed within time interval $t \in [0,\infty)$, while standards, like STANAG-1008, do not define the respective study time period of the voltage modulation.

In general the respective upper limit for voltage modulation can be expressed by a general function of the following form:

$$F_V(T, dc, X_C, R, X', K, K_I, S_{L0}, \Delta\mathrm{S}, \cos\varphi) \le M_V^{\lim} \tag{51}$$

NUMERICAL ANALYSIS OF FREQUENCY & VOLTAGE MODULATION IN A SIMPLIFIED SHIP'S ELECTRIC POWER SYSTEM

Simplified Electrical Circuit of a S Frigate Power System

The electric power system of a Hellenic Naval's S frigate consists of 4 generators Smit/Slikkerver DG 77/48/60 with nominal line to line voltage 450 V, nominal frequency 60 Hz, nominal apparent power 937,5 kVA, nominal active power 750 kW, nominal power factor 0,80 (ind.) and direct axis transient reactance 0,225 p.u. (for base power equal to the nominal power of one generator). The load demand of the frigate is usually between 500 to 1500 kVA with a typical average load of 750 kVA approximately, which is equal to 80% of the nominal apparent power of one generator. For reliability reasons two generators operate in parallel, while the other

two can be started in few seconds, if any of the two main generators is shut down or the demand load exceed a predifened limit.

For the rest of the analysis, the base voltage of the power system is 450 V and the system base apparent power is 1875 kVA (=2·937,5 kVA/generator). The respective direct axis transient reactance of the equivalent generator is obtained as 0,225 p.u. according to Millman's theorem. If the electromagnetic force, E_f , of each generator are of the same value then the equivalent E_F is also the same. The typical average load of 750 kVA corresponds to 0,4 p.u. of the system base apparent power. The generator rotor inertia constant (s) J' of the equivalent generator is the same with that of a single generator, with a typical value of 4 s.

Taking into consideration that the maximum voltage drop is 6% then the respective equivalent impedance of the cable can not exceed 0,15 p.u. for a typical average load of 750 kVA, and 0,075 p.u. for a maximum load of 1500 kVA. A typical value of impedance is considered of 0,0375 p.u.. It is noted that the ratio of impedance / resistance of a E1VV cable varies from 9,5 for cross-section of 1,5mm^2 to 1232 for cross-section of 300 mm^2. In this analysis, this ratio is assumed 50 corresponding to the cross-section of 10 mm^2, and the respective resistance 50 times smaller of the respective impedance, that is 0,00075 p.u..

Based on the respective theoretical analysis pulsed load period, T, can take any value with usual values between 1 ms to 10 s, while the duty cycle, *d.c.,* varies between 0% to 100%. The respective typical values of pulsed period and duty cycle are 1 s and 50%.

The parameters of the frequency regulator (frequency drop R_f and integral gain K_f) and automatic voltage regulator (proportional K and integral gain K_V) can be selected properly so that no operation problems occur. Respective typical values are: R_f =20, K_f = 10, K=5, K_V = 5.

Modulation Limitations for the Simplified Electrical Circuit of a S Frigate Power System: Basic Scenario

Based on the theoretical analysis the frequency modulation limit is estimated by ineq. (21) with $M_f^{\lim}$ = 0.5% (the STANAG-1008 limit) and the respective curve is presented together with the respective curves of STANAG 1008 for frequency and voltage modulation in Fig. 6. It is obvious that the unacceptable operating area due to frequency modulation increases, but large part of it is cancelled by the operating area determined by the STANAG 1008 voltage modulation (green dotted line). This means that there is an area of S-cosφ which is allowed by the STANAG-1008 curves, while it is not allowed by the theoretically obtained frequency modulation limit curve.

According to the analytical theoretical analysis the voltage modulation limit is estimated by ineq. (44) with $M_V^{\lim}$ = 2.0% (the STANAG-1008 limit) and the respective curve is presented together with the curves of STANAG 1008 for frequency and voltage modulation in Fig. 7. The respective unacceptable operating area due voltage modulation limit violation decreases significantly for big values of power factor (cosφ>0,4). While for small values of power factor (cosφ<0,4) the opposite behaviour occurs. This means that there is an area of S-cosφ which is allowed by the STANAG-1008 curves, while it is not allowed by the theoretically obtained voltage modulation limit curve.

If inequality (49) is used with $M_V^{\lim}$ = 2.0% (the STANAG-1008 limit), then Fig. 8 is obtained, where the unacceptable operating area due to voltage modulation limit violation has decreased more than the previous one for small values of power factor. However, in this case study it can not be used, as the equivalent impedance of the cables X_C is smaller than the equivalent direct axis transient reactance of the equivalent generator X', while in inequality (49) $X_C >> X'$ is assumed .

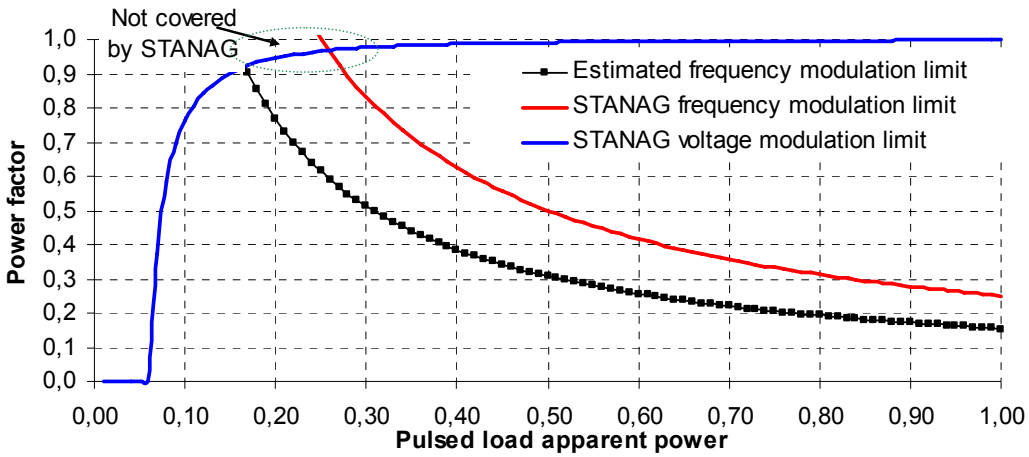

FIGURE 6. Power factor vs pulse load apparent power of the frequency modulation for the basic scenario of the simplified power system of an S frigate.

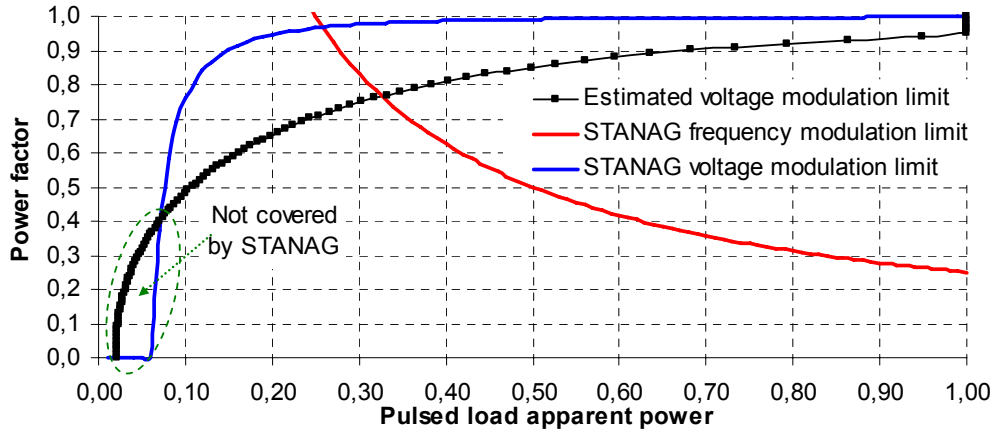

FIGURE 7. Power factor vs pulse load apparent power of the voltage modulation for the basic scenario of the simplified power system of an S frigate.

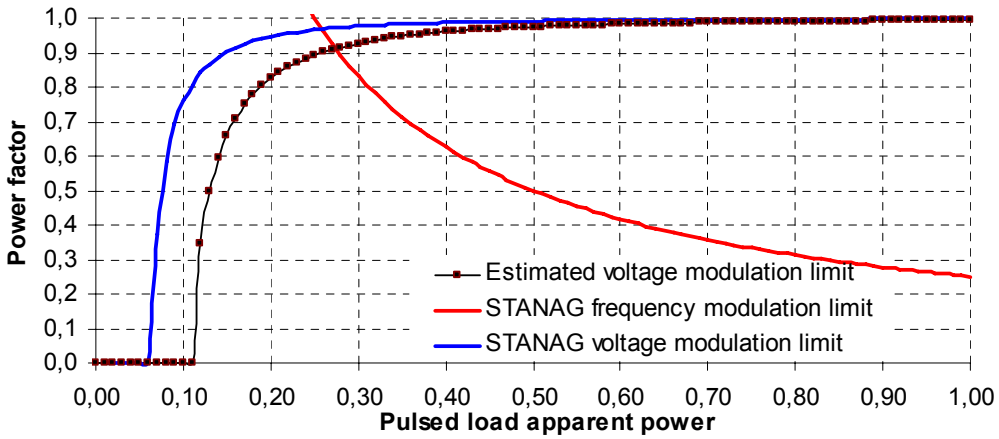

FIGURE 8. Power factor vs pulse load apparent power of the approximated voltage modulation for the basic scenario of the simplified power system of an S frigate.

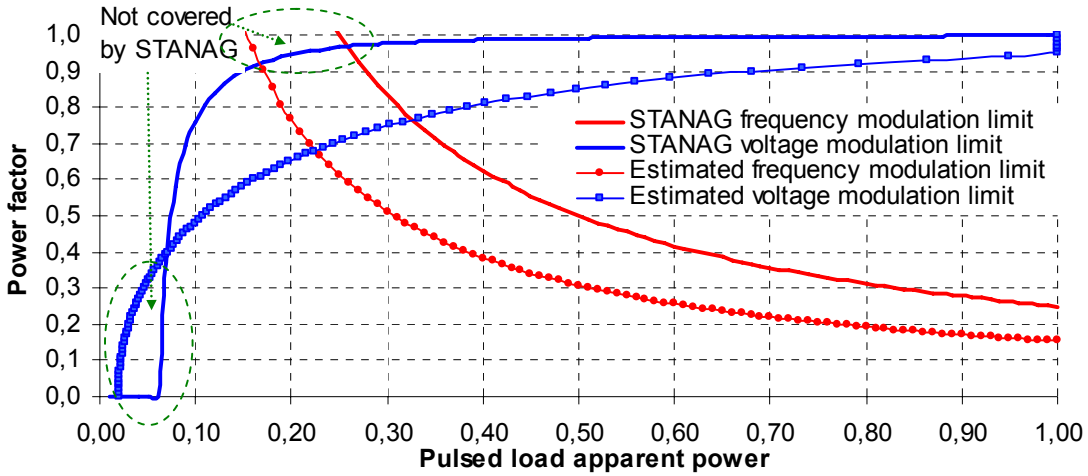

FIGURE 9. Power factor vs pulse load apparent power of the frequency modulation and the voltage modulation of the theoretical analysis for the basic scenario of the simplified power system of an S frigate.

In Fig. 9 the limit curves for the voltage and the frequency modulation are presented together with the respective ones of STANAG 1008, where the difference between the unacceptable operating areas between the theoretical analysis and STANAG 1008 becomes aparent. STANAG 1008 happens to be stricter than the theretically obtained model in case of voltage modulation, especially for power factor larger than 0.4 in case of frequency modulation is more optimistic.

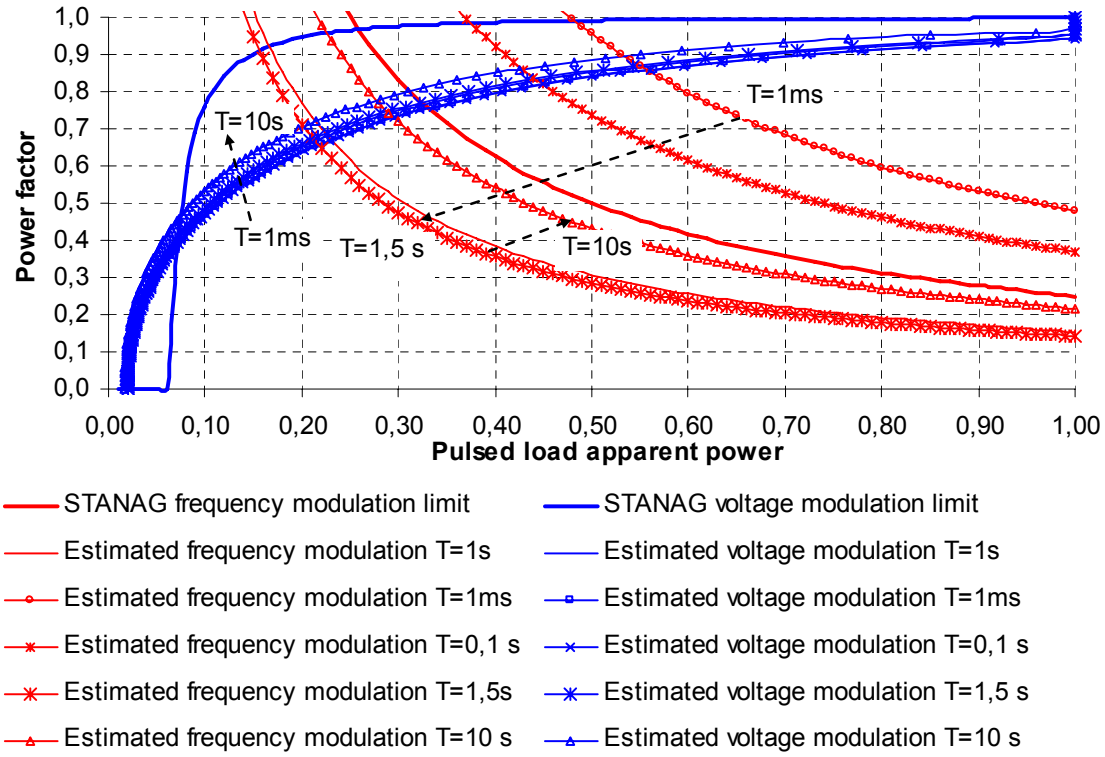

FIGURE 10. Power factor vs pulse load apparent power of the frequency modulation and the voltage modulation of the theoretical analysis for different values of the time period for the pulsed load of the simplified power system of an S frigate.

Modulation Limitations for the Simplified Electrical Circuit of a S Frigate Power System: Time Period of Pulsed Load

Pulsed load period affects both frequency and voltage modulation. The respective analysis has been developed for a range of values from 1 ms up to 10 s as following: from 1 ms up to 20 ms with a time step of 1 ms,fro 20 ms up to 100 ms with a time step of 10 ms, from 200 ms up to 2 s with a step of 100 ms, from 2 s up to 10 s with a step of 1 s.

In Fig. 10 the respective results are presented. The unacceptable operating area due to frequency modulation limit violation increases for pulsed load period less than 1,5 s, while it decreases for larger values. The theoretical curve coincides to STANAG curve for T=0,32s, approximately. The unacceptable operating area of the theoretical analysis for pulsed load period greater than 0,32s is larger than the respective one of STANAG 1008.

The unacceptable operating area due to voltage modulation increases for pulsed load period ranging from 1 ms to 10 s. However, the impact is not significant while the unacceptable operating area obtained by the theoretical analysis is smaller than the respective one of STANAG 1008; especially for power factor values greater than 0,5.

Modulation Limitations for the Simplified Electrical Circuit of a S Frigate Power System: Duty Cycle of Pulsed Load

Pulsed load duty cycle *d.c.* of affects both frequency and voltage modulation. The respective analysis has been developed for a range of values from 1% up to 99% with a step of 1%.

In Fig. 11 the respective results for pulsed load duty cycle are presented. The unacceptable operating area due to frequency modulation limit violation increases until pulsed load duty cycle becomes equal to 65% ~ 70%; while it decreases for larger values. The theoretical curve coincides to STANAG's one for *d.c.*= 20%, approximately. The unacceptable operating area as obtained by the theoretical analysis for pulsed load duty cycle greater than 20% is larger than the respective one as obtained by STANAG 1008.

The unacceptable operating area due to voltage modulation limit violation increases with pulsed load duty cycle, but the observed increse is small while the unacceptable operating area obtained by the theoretical analysis is smaller than STANAG's respective one for power factor larger than 0,5.

Modulation Limitations for the Simplified Electrical Circuit of a S Frigate Power System: Generation Rotor Inertia

Generator rotor inertia constant J' affects only frequency modulation. The values of this parameter should satisfy the following inequality according to the respective theoretical analysis (see inequality (13)):

$$R_f^2 > 4 \cdot J' \cdot K_f \Rightarrow J' < \frac{R_f^2}{4 \cdot K_f} \tag{52}$$

Taking into consideration that in the basic scenario, R_f =20, K_f = 10 Hz, then J' should be smaller than 10 s. The respective analysis has been developed for J' values ranging from 0 s up to 10 s as following: from 0 ms up to 30 ms with a step of 1 ms, from 30 ms up to 200 ms with a step of 10 ms, from 200 ms up to 9,9 s with a step of 100 ms, from 9,9 s up to 9,99 s with a step of 10 ms.

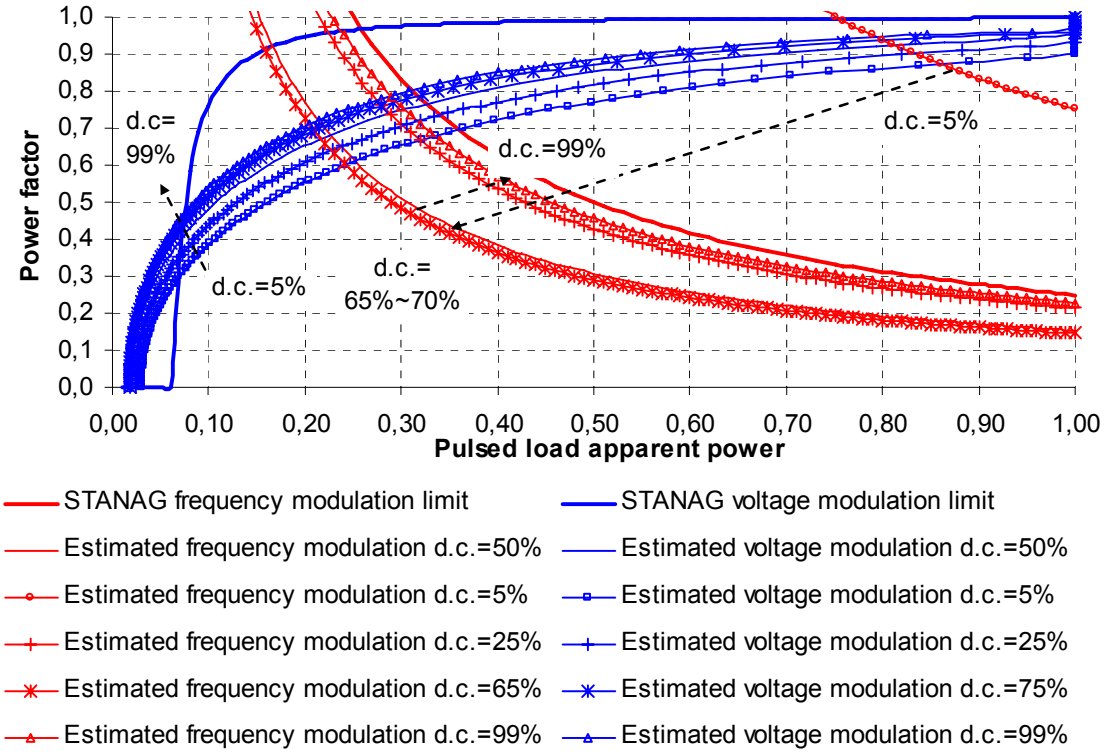

FIGURE 11. Power factor vs pulse load apparent power of the frequency modulation and the voltage modulation of the theoretical analysis for different values of the duty cycle for the pulsed load of the simplified power system of an S frigate.

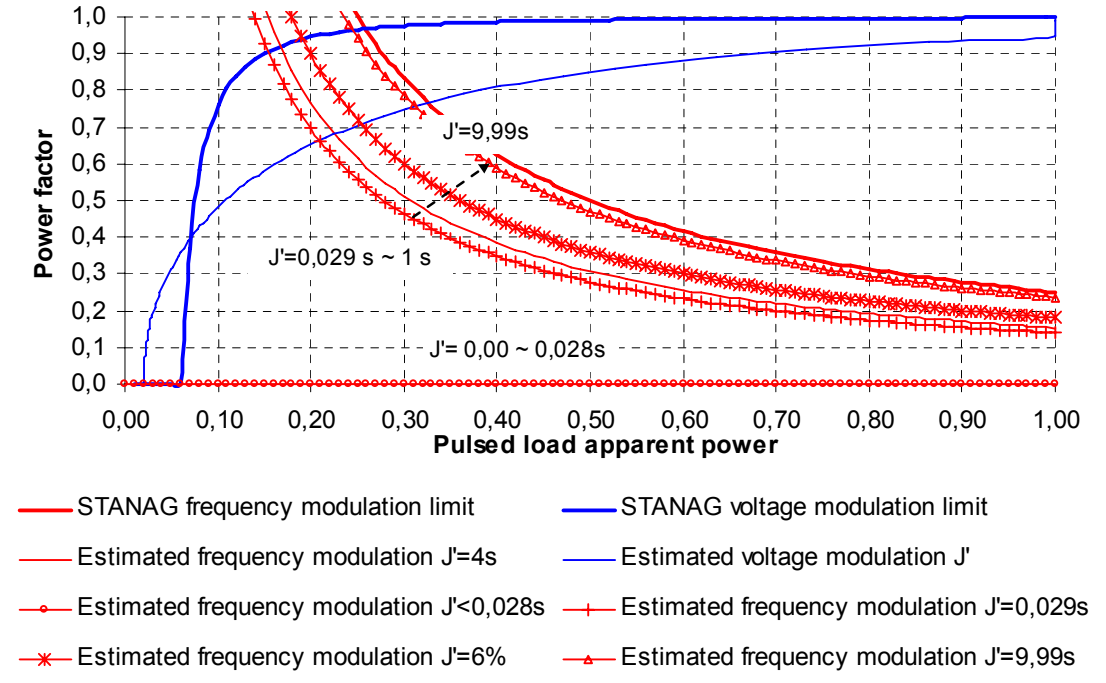

FIGURE 12. Power factor vs pulse load apparent power of the frequency modulation and the voltage modulation of the theoretical analysis for different values of the generator rotor inertia constant of the simplified power system of an S frigate (0≤J'<10 s).

In Fig. 12, the respective results considering different values of generator rotor inertia constant are presented. The unacceptable operating area due frequency modulation violation decreases in a non-linear fashion, as generator rotor inertia increases. For extremely small values (not met in practice) the respective curve becomes horizontal. The theoretically obtained limit curve tends to coincide wirth STANAG's one for large values of J/ . Values larger than 10 s lead to frequency oscillations and they should be avoided [8]. The unacceptable operating area as obtained by the theoretical analysis is larger than the respective one obtained by STANAG 1008. The effect of J/ is limited practically, as J/ can be calculated easily and it has not significant variations throughout generator life.

Modulation Limitations for the Simplified Electrical Circuit of a S Frigate Power System: Frequency Drop of Frequency Regulator

Frequency droop R_f applied to the generator frequency regulator affects only frequency modulation. The values of this parameter should satisfy the following inequality according to the respective theoretical analysis (see inequality (13)):

$$R_f^2 > 4 \cdot J' \cdot K_f \Rightarrow R_f > \sqrt{4 \cdot J' \cdot K_f} \tag{53}$$

Taking into consideration that in the basic scenario, J' = 4 s, K_f = 10 Hz , then the R_f should be larger than 12,649. The usual values of R_f lie between 20 and 100. The respective analysis has been developed for R_f ranging from 12,65 up to 150 as following: from 12,65 up to 13 with a a step of 0,05, from 13 up to 20 with a step of 1, from 20 up to 150 with a step of 5.

In Fig. 13, the respective results are presented. The unacceptable operating area due frequency modulation limit violation decreases in a nonlinear fashion as R_f increases. The theoretically obtained curve coincides to STANAG's one for R_f = 36, approximately. R_f practically should be large enough so that the respective unacceptable operation area due to frequency modulation limit violation be suppressed. However, large values of R_f can lead to significant active power generation variations even for small variations of frequency, which is not desirable for system stability reasons.

Modulation Limitations for the Simplified Electrical Circuit of a S Frigate Power System: Integral Gain of Frequency Regulator

The integral gain of generator frequency regulator affects only frequency modulation. K_f should satisfy the following inequality according to the respective theoretical analysis (see inequality (13)):

$$R_f^2 > 4 \cdot J' \cdot K_f \Rightarrow K_f < \frac{R_f^2}{4 \cdot J'} \tag{54}$$

Taking into consideration that, R_f =20 and J' = 4 s for the the basic scenario then K_f should be smaller than 25 Hz. It should also be positive, because, if K_f=0 then no secondary frequency is possible leading to a permanent, "steady-state", frequency error [8]. The folowing analysis has been developed for K_f ranging from 1 mHz up to 25 Hz as following: from 1 mHz up to 20 mHz with a step of 1 mHz, from 20 mHz up to 100 mHz with a step of 10 mHz, from 100 mHz up to 1 Hz with a step of 100 mHz, from 1 Hz up up to 24 Hz with a step of 1 Hz, from 24,1 Hz up to 24,9 Hz with a step of 100 mHz.

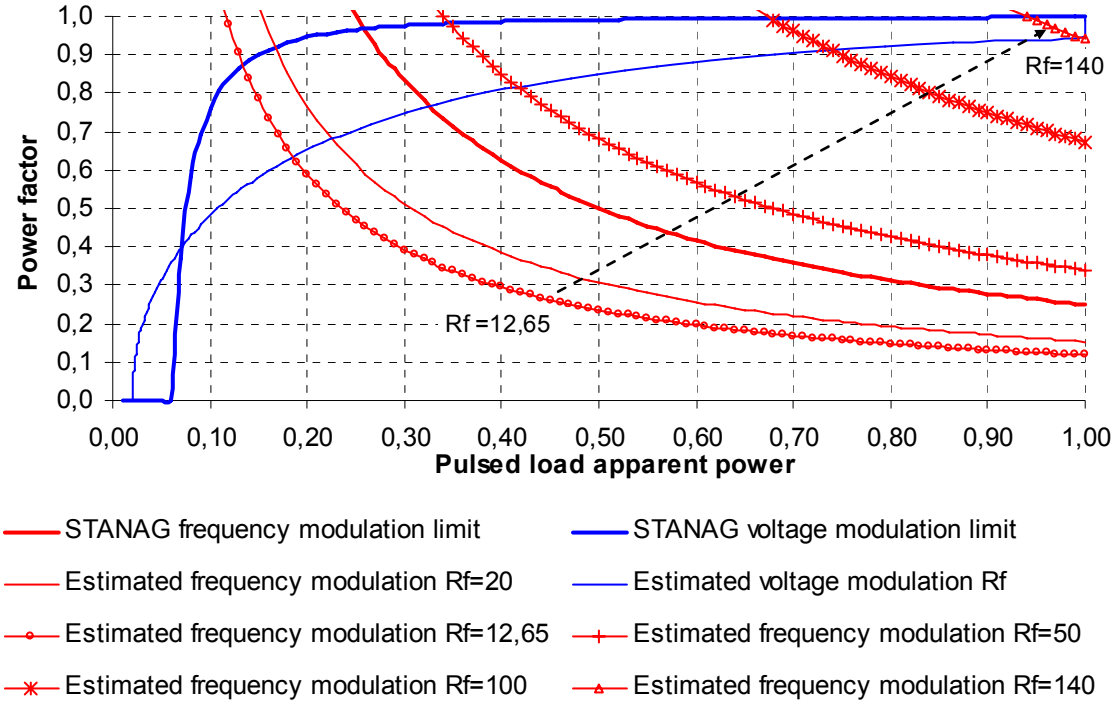

FIGURE 13. Power factor vs pulse load apparent power of the frequency modulation and the voltage modulation of the theoretical analysis for different values of the frequency drop of the frequency regulator of the simplified power system of an S frigate (Rf≥12,65).

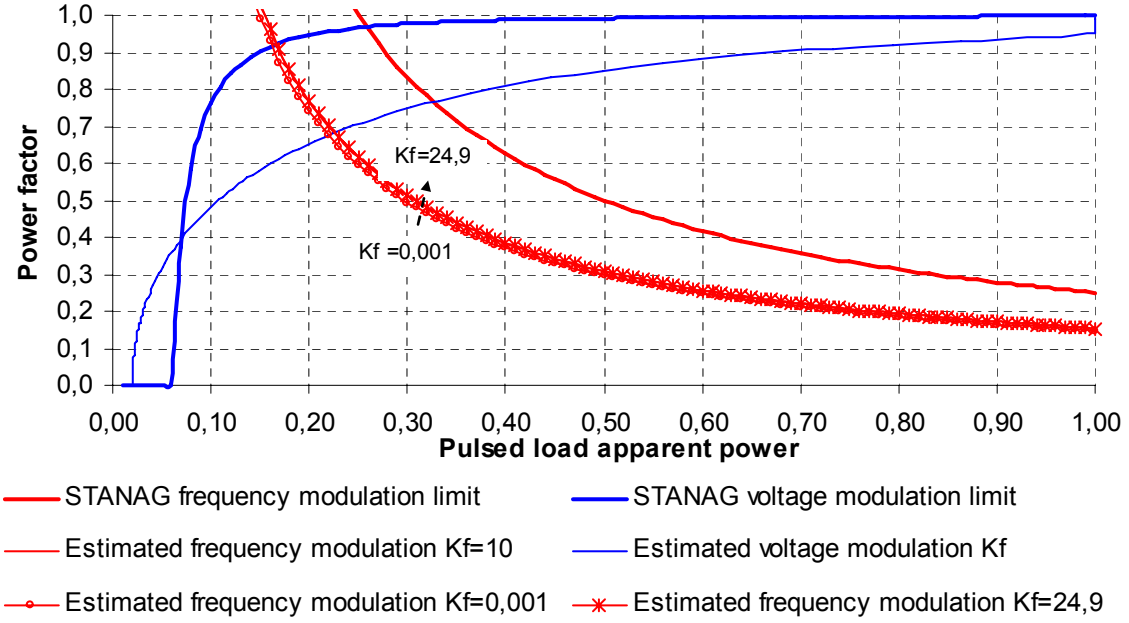

FIGURE 14. Power factor vs pulse load apparent power of the frequency modulation and the voltage modulation of the theoretical analysis for different values of the integral gain of the frequency regulator of the simplified power system of an S frigate (0<Kf<25 Hz).

In Fig. 14, the respective results are presented. The unacceptable operating area due to frequency modulation limit violation decreases extremely slightly, as K_f increases. Practically, the effect of K_f is very limited.

Modulation Limitations for the Simplified Electrical Circuit of a S Frigate Power System: Equivalent Reactance of Cables

The equivalent reactance of the cables X_C affects only voltage modulation. Taking into consideration maximum allowable voltage drop the following analysis has been developed for X_c ranging from 0 up to 0,075 p.u. with a step of 0,005 p.u..

In Fig. 15, the respective results are presented. The unacceptable operating area due to voltage modulation limit violation increases significantly as X_C increases. The unacceptable operating area as obtained by the theoretical analysis is smaller than the respective one of STANAG 1008 for all power factor values if X_C is smaller than 0,035 p.u.. However, if X_C is larger than 0,0385 p.u. then voltage modulation limit would not be satisfied for small pulsed load power factor, as it is obtained by the respective curves.

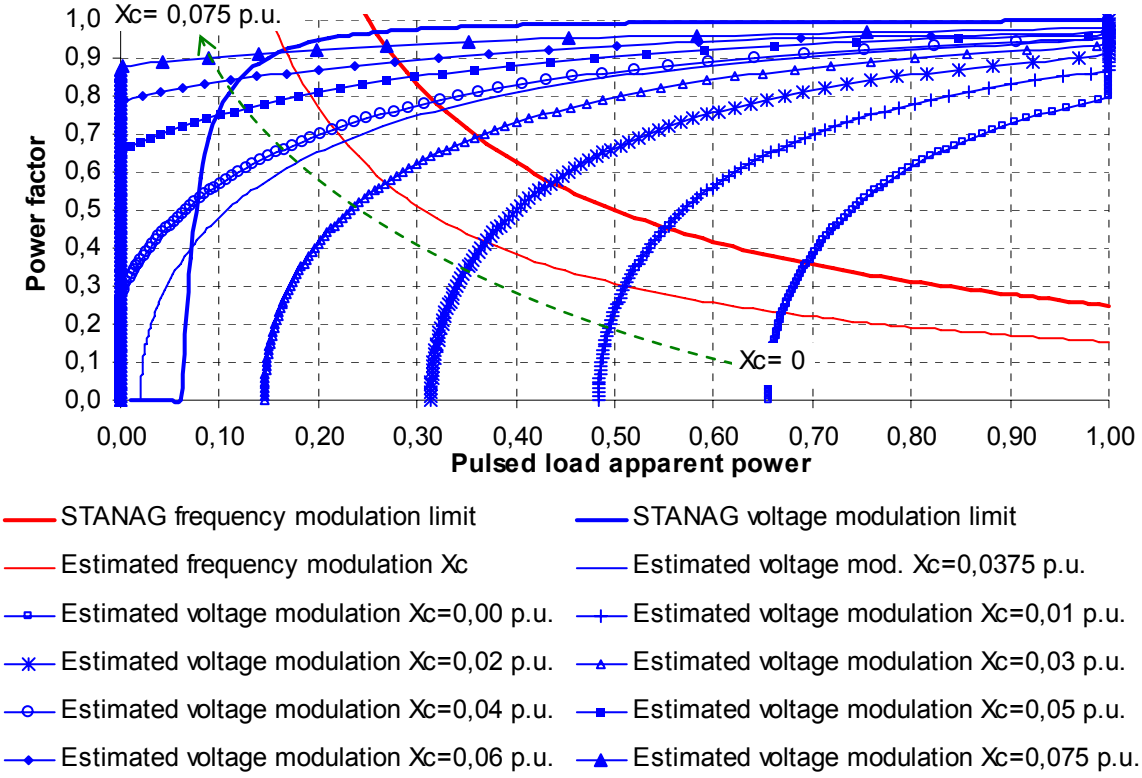

FIGURE 15. Power factor vs pulse load apparent power of the frequency modulation and the voltage modulation of the theoretical analysis for different values of the equivalent reactance of cables of the simplified power system of an S frigate ($0 \leq X_C \leq 0,075$ p.u.).

Modulation Limitations for the Simplified Electrical Circuit of a S Frigate Power System: Equivalent Resistance of Cables

The equivalent resistance of the cables, *R,* affects only voltage modulation. Taking into consideration the maximum allowable voltage drop and the proportion between cable reactance

and resistance the resistance can be 5 to 1500 times smaller than the respective reactance of usual cable types. Next, the effet of ratio *r* is investigated, where:

$$r < \frac{X_C}{R} \tag{55}$$

In Fig. 16, the respective results for different values of *r* are presented. The unacceptable operating area due to voltage modulation limit violation decreases slightly as *r* increases (cable resistance decreases). However, it should be noted that the critical affecting factor is the cable reactance.

Modulation Limitations for the Simplified Electrical Circuit of a S Frigate Power System: Equivalent Sub-transient Reactance of Generator

The equivalent sub-transient reactance of the generator, X'' , affects only voltage modulation. Taking into consideration the practical limitations for the reactance of a synchronous machine it should vary from 9% up to 22% p.u. for turbo-generators, from 12% up to 30% for salient-pole generators with damper winding and from 20% up to 40% for salient-pole generators without damper winding [12]. The respective analysis has been developed for a range of values from 0,09 p.u. up to 0,040 p.u. with a step of 0,01 p.u..

In Fig. 17 the respective results are presented for variable X''. The unacceptable operating area due to voltage modulation limit violation increases slightly as X'' increases. The effects of X'' are practically limited as it can be calculated and it constitutes a technical characteristic throughout generator lifetime.

Modulation Limitations for the Simplified Electrical Circuit of a S Frigate Power System: Apparent Power of System Base Load without Pulsed Load

The apparent power of system base load S_{L0} affects voltage modulation only. S_{L0} varies from 0 p.u. up to 1 p.u. theoretically, although in a power system of two generators S_{L0} is limited to 0,5 p.u., so that, if one generator is shut down the other generator can take over all the remaining load. Here, the respective analysis has been developed for S_{L0} ranging from 0,00 p.u. up to 1,00 p.u. with a step of 0,01 p.u.. In Fig. 18, the respective results for different values of system base load apparent power are presented.

The unacceptable operating area due to voltage modulation limit violation increases slightly as S_{L0} increases. This is expected under the assumption the system remains stable and reliable. S_{L0} becomes a crucial affecting factor as it varies during ship power system operation. If S_{L0} is larger than 0,7 p.u. then voltage modulation limitation criterion would not be satisfied for small pulsed load power factor values according to the obtained limitation curves.

Modulation Limitations for the Simplified Electrical Circuit of a S Frigate Power System: Proportional Gain of Automatic Voltage Regulator of Generator

The proportional gain of generator automatic voltage regulator, *K,* affects only voltage modulation. Theoretically, *K* could take any positive value; however it can not be arbitrarily large as the ratio K/K_V should be small enough to ensure fast response of the Proportional-Integral Controller (PID).

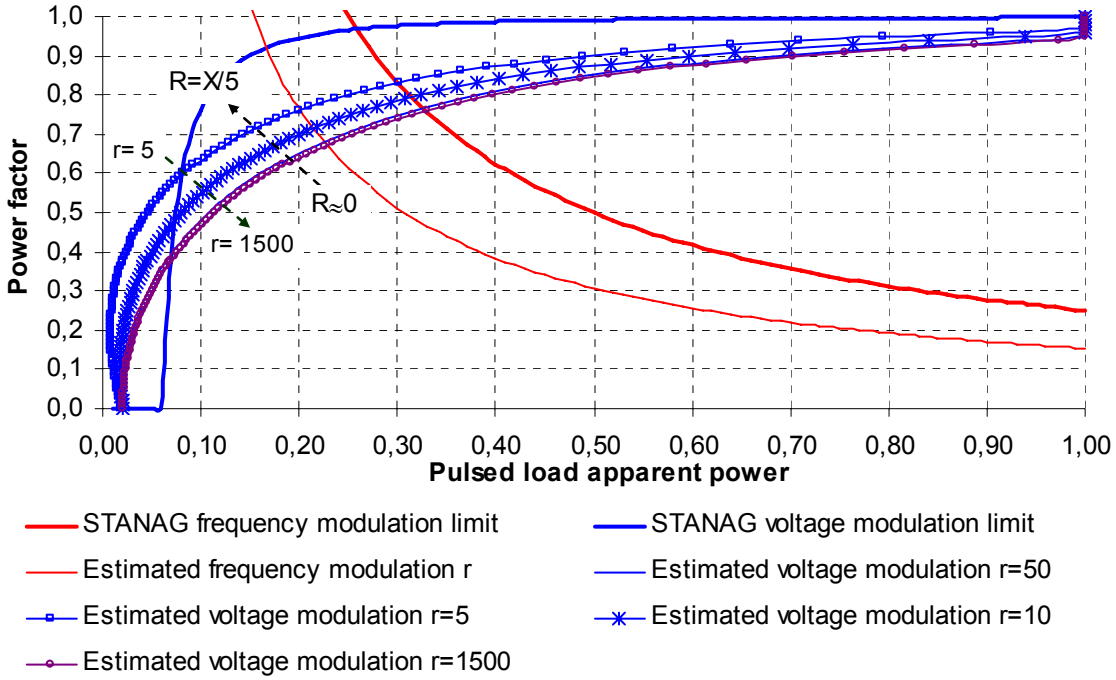

FIGURE 16. Power factor vs pulse load apparent power of the frequency modulation and the voltage modulation of the theoretical analysis for different values of the respective ratio between equivalent reactance to equivalent resistance of cables of the simplified power system of an S frigate ($5 \leq r \leq 1500$).

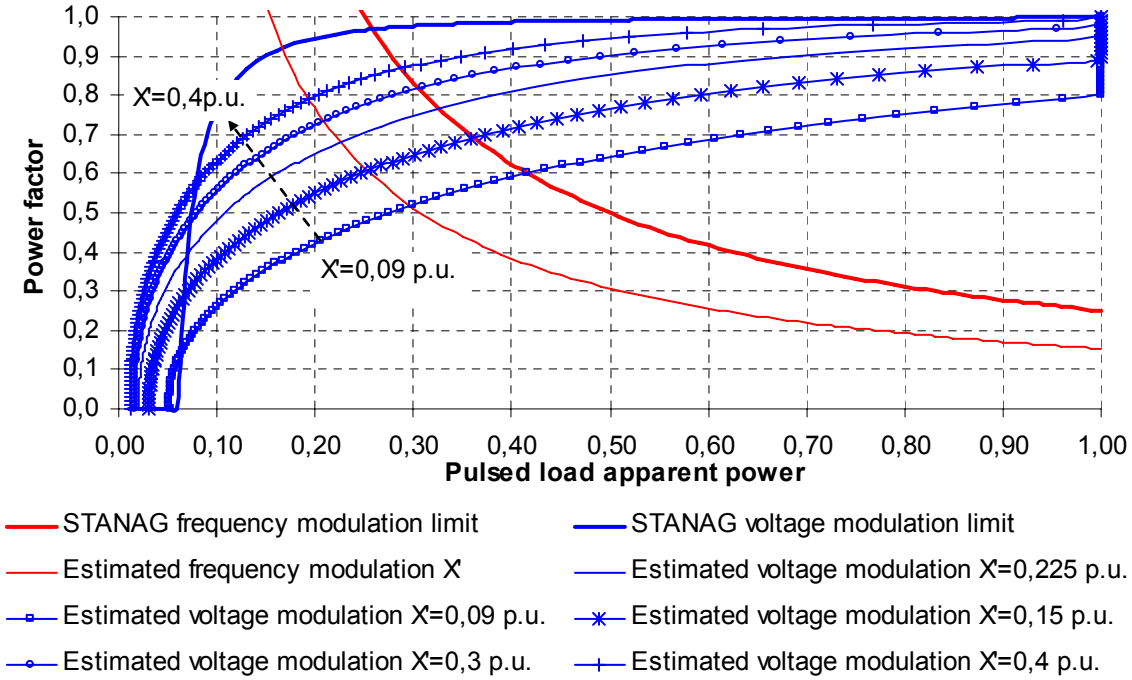

FIGURE 17. Power factor vs pulse load apparent power of the frequency modulation and the voltage modulation of the theoretical analysis for different values of the equivalent sub-transient reactance of generator of the simplified power system of an S frigate (0,09 p.u. $\leq X' \leq$ 0,40 p.u.).

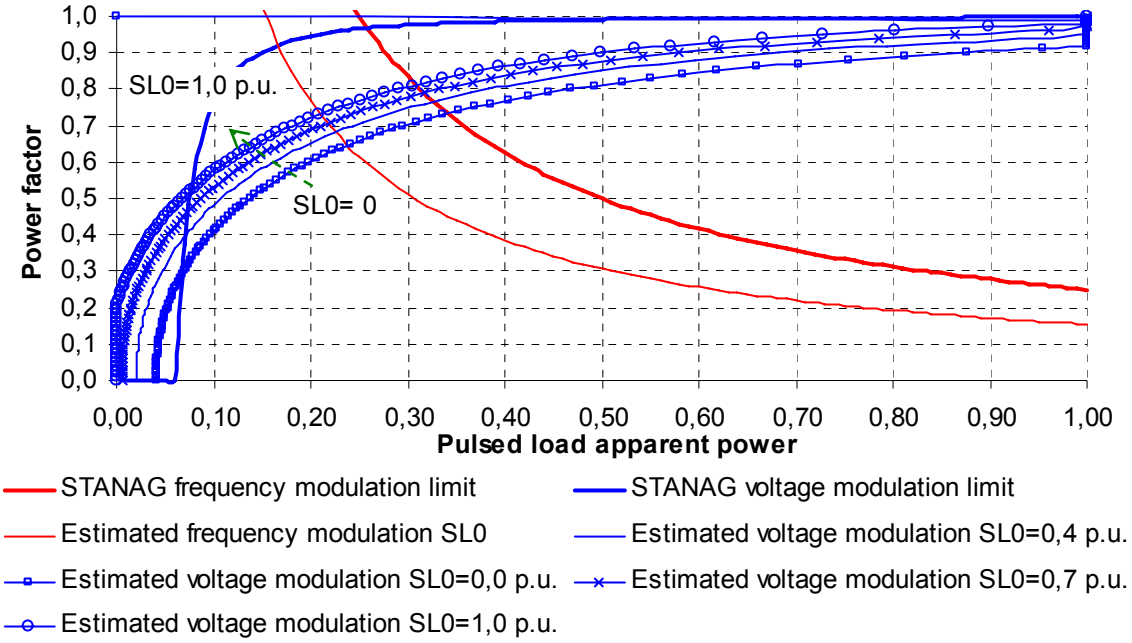

FIGURE 18. Power factor vs pulse load apparent power of the frequency modulation and the voltage modulation of the theoretical analysis for different values of the apparent power of the system base load of the simplified power system of an S frigate (0,00 p.u. ≤ S_{L0} ≤ 1,00 p.u.).

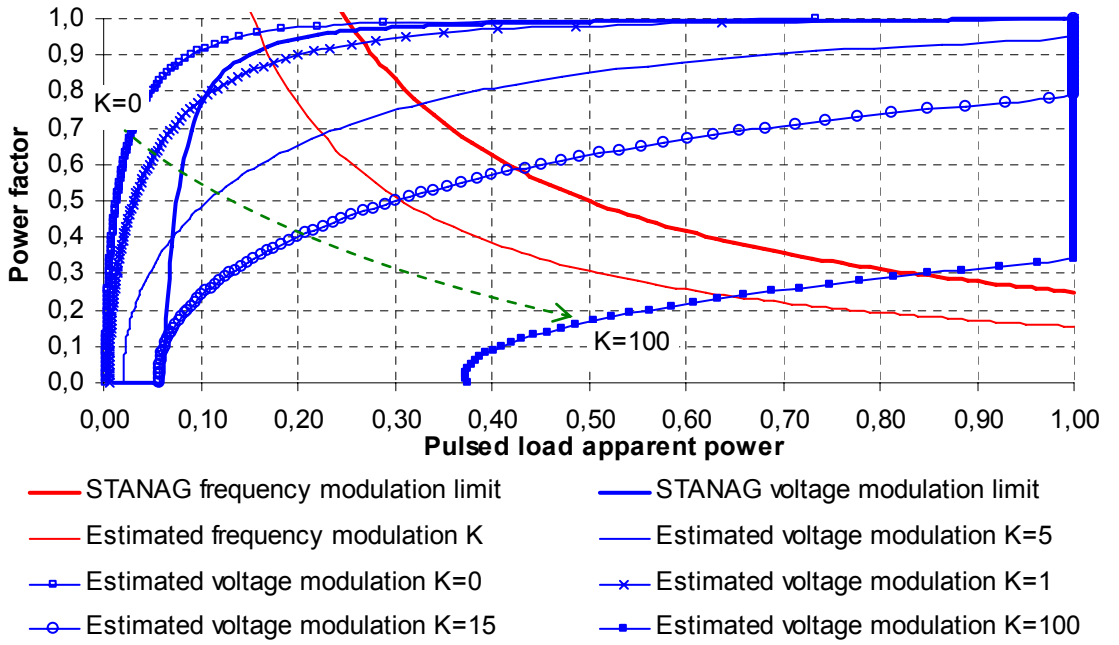

FIGURE 19. Power factor vs pulse load apparent power of the frequency modulation and the voltage modulation of the theoretical analysis for different values of the proportional gain of the automatic voltage regulator of the simplified power system of an S frigate.

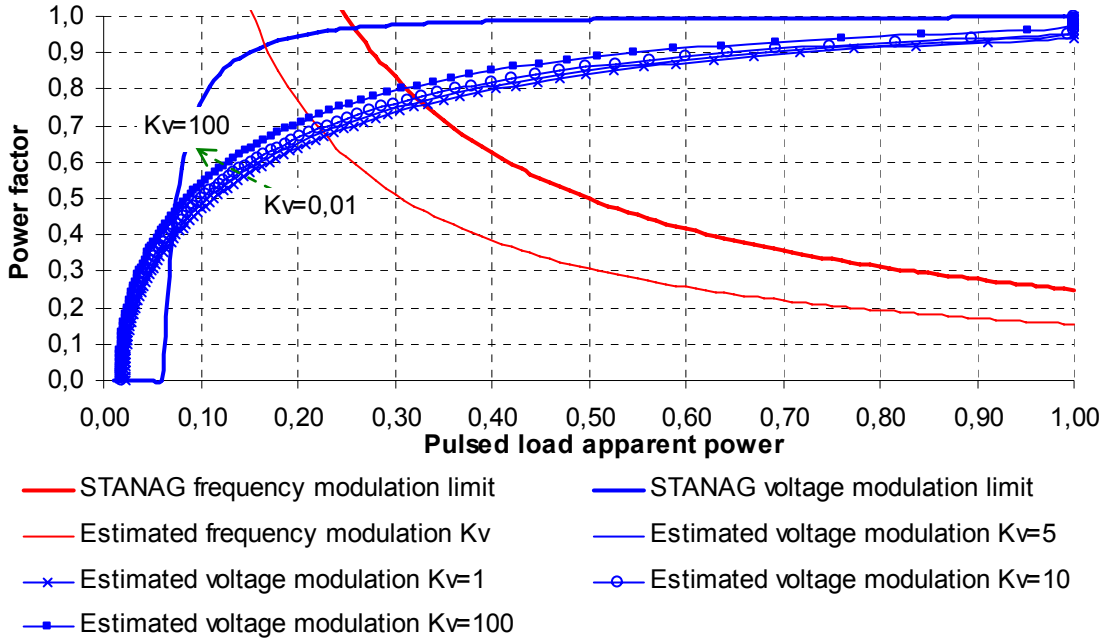

FIGURE 20. Power factor vs pulse load apparent power of the frequency modulation and the voltage modulation of the theoretical analysis for different values of the integral gain of the automatic voltage regulator of the simplified power system of an S frigate.

Here, the following analysis has been developed for K ranging from 0 up to 100 with a step of 1. In Fig. 19, the results for different values of K are presented. The unacceptable operating area due to voltage modulation decreases fast and in a nonlinear fashion as K increases. If K is larger than 16 then STANAG's voltage modulation constraint is satisfied for any pulsed load.

Modulation Limitations for the Simplified Electrical Circuit of a S Frigate Power System: Integral Gain of Automatic Voltage Regulator of Generator

The integral gain K_V of generator automatic voltage regulator affects only voltage modulation. Theoretically, K_V could take any positive value; however as noted above the response time of the PID Controller depends on the ratio K/K_V. Here, the following analysis has been developed for K_V ranging from 0 up to 100, as following: from 0,01 up to 2 with a step of 0,01 and from 2 up to 100 with a step of 1.

In Fig. 20, the respective results for different values of K_V are presented. The unacceptable operating area due to voltage modulation limit violation increases slightly and in a nonlinear fashion as K_V increases. K_V should be positive as for zero value a non-zero voltage "steady-state" error would occur. It should also be large enough in order to obtain large K/K_V ratio, ensuring, in this way, fast response of PID controller.

The proper selection of the values of the PID controller parameters is a complex issue higly related with the dynamics of the of the power system and the generator itself.

CONCLUSIONS

In this paper, STANAG 1008 design constraints for frequency and voltage modulation have been examined applying the proper theoretical analysis in a simplified ship power system. The effects of several parameters such as pulsed load period and duty cycle, the technical characteristics of the generators and their frequency and voltage controllers, the technical characteristics of the cables connecting the pulsed load and generator etc, were examined. The conclusions drawn by the above analysis regarding the significance of the consequent effects are synoptically presented in Table 1.

TABLE (1). Significance of the effects of various parameters and STANAG shortcomings in the frequency/voltage modulation for the simplified ship power system.

Modulation	**Frequency**		**Voltage**	
Parameter	**Significance**	**STANAG shortcoming**	**Significance**	**STANAG shortcoming**
Pulsed load period	Very significant	Yes	Average	Yes ($\cos\varphi$<0,5)
Pulsed load duty cycle	Very significant	Yes	Significant	Yes ($\cos\varphi$<0,5)
Generator rotor inertia constant	Average	~	No	-
Frequency drop of frequency regulator	Very significant	Yes (R_f<36)	No	-
Integral gain of frequency regulator	Extremely small	Yes, special cases (K_f=0, etc.)	No	-
Equivalent reactance of cables	No	-	Extremely significant	Yes
Equivalent resistance of cables	No	-	Average	~
Equivalent sub-transient reactance of the generator	No	-	Significant	Yes
Apparent power of system base load without pulsed load	No	-	Significant	Yes
Proportional gain of the automatic voltage regulator	No	-	Very significant	Yes
Integral gain of the automatic voltage regulator	No	-	Small	~

In more detail, the effect of each studied parameter is analyzed next:

- **Pulsed load period, *T*:** It affects significantly frequency modulation, as the unacceptable operating area varies non-monotonically within the region of values studied, [1 ms, 10 s], with a critical value of *T* being being equal to 1,5s for the case studied (see Fig. 10). Voltage modulation practicaly is not affected.
- **Pulsed load duty cycle, *d.c.*:** It affects significantly frequency modulation, as the unacceptable operating area varies non-monotonically within the region of values studied, [0%, 100%], with a critical value of d.c. lying between 65%~70% (see Fig. 11). It also affects voltage modulation but not to the extent in case of frequency modulation.
- **Generator rotor inertia constant, *J'*:** It affects frequency modulation to a limited extent for practical values. This parameter could not be a design variable as it is a technical characteristic of generators.
- **Freqeuncy drop of frequency regulator, R_f:** It affects frequency modulation. Especially, for small values of R_f the effect becomes very significant as the

unacceptable operating area increases considerably. Large values can be chosen for R_f while power system stability issues should be taken into consideration.

- **Integral gain of frequency regulator, K_f:** It affects frequency modulation to a limited extent as this parameter is determined mainly by the other parameters of the generator: rotor inertia *J'* and frequency droop, R_f.
- **Equivalent reactance of cables, X_c:** It affects only voltage modulation. The respective effect becomes extremely significant, as the increase of this parameter enlarges the unacceptable operating area. X_c could vary into a wide range of values, as it depends on the connection point of the different electric consumers and the equivalent reactance of each consumer which varies with time.
- **Equivalent resistance of cables, *R*:** It affects voltage modulation to a limited extent, as it is usually equal to 1/100 up to 1/50 of the respective cable reactance. Its effect is rather degraded by cable reactance effect.
- **Sub-transient reactance of generators, *X'*:** It affects voltage modulation to a significant extent as the increase of *X'* enlarges the unacceptable operating area. This parameter could not be a design variable as it is a technical characteristic of the generators.
- **System base load apparent power, S_{L0}:** It affects voltage modulation to a significant extent as the increase of S_{L0} enlarges the unacceptable operating area in a nonlinear and monotonical fashion. It varies significantly with time as it depends on the variation of the demand of the electric consumers.
- **Proportional gain of equivalent generator automatic voltage regulator, *K*:** It affects voltage modulation to a significant extent as the increase of *K* reduces considerably the unacceptable operating area. This parameter is a technical characteristic of generator controller.
- **Integral gain of generator automatic voltage regulator, K_v:** It affects voltage modulation to a rather limited extent. This parameter is a technical characteristic of generator controller and its value is selected taking into consideration the technical characteristics of the generators, voltage variation limit and the controller response.

The above analysis has proved that the *S-cosf* limitation curve proposed in STANAG 1008 is not unique. Furthermore, it is observed that the examined parameters of the power system model display in a non-linear fashion the *S-cosf* limitation curve. Under these circumstances it seems necessary that the aforementioned parameters (Table 1) affecting voltage and frequency modulation should be taken into consideration in future standards dealing with power quality issues in ship electric power systems.

The theoretical analysis which has been synoptically presented above aims to provide an answer to this problem. Alternatively, the whole power system should be simulated for different operation conditions so that the respective limits for frequency/voltage modulation be obtained. The presented work aims to be the motivation for further research on the topic and to provide general directions to follow for ship electric systems design issues dealing with pulse load integration.

REFERENCES

1. IEEE Std 45-1998, "IEEE Recommended Practice for Electrical Installations on Shipboard".
2. STANAG 1008, "Characteristics of Shipboard Electrical Power Systems in Warships of the NATO Navies", NATO, Edition 9, 24 Aug. 2004.
3. USA MIL-STD-1399(NAVY), "Interface standard for Shipboard systems – Section 300A – Electric Power, Alternating Current".

4. Howard A., Smolleck Satish J., Ranade Nadipuram R., Prasad Rudolph, O. Velasco, “Effects of Pulsed – Power Loads upon an Electric Power Grid”, IEEE/PSS 1990 Sumner meeting, Minneapolis, Minnesota, July 15-19, 1990.
5. F.D. Kanellos, I.K. Hatzilau, J. Prousalidis, E. Styvaktakis, “Simulation of a Shipboard Electrical Network (AES) comprising Pulsed Loads”, Engine as a Weapon II, IMarEST, Dec. 2006, London.
6. F.D. Kanellos, I.K. Hatzilau, J. Prousalidis, “Investigation of voltage/frequency modulation in ship electric networks with pulsed loads according to STANAG 1008 design constraints”, All Electric Ship Conference 2007, London.
7. G. J. Tsekouras, F.D.Kanellos, J.M. Prousalidis, I.K. Hatzilau, “STANAG 1008 design constraints for pulsed loads in the frame of the All Electrical Ships”, Nausivios Chora, A journal in Naval Sciences and Technology, vol. 3, 2010, pp. 115-154.
8. F.D.Kanellos, G. J. Tsekouras, J. Prousalidis, I.K. Hatzilau, “An effort to formulate frequency modulation constraints in Ship-Electrical Systems with Pulsed Loads”, IET Electrical Systems in Transportation, vol. 1, issue 1, 2011, pp. 11-23.
9. F.D.Kanellos, G. J. Tsekouras, J. Prousalidis, I.K. Hatzilau, “Effort to formulate voltage modulation constraints in ship-electrical systems with pulsed loads”, IET Electrical Systems in Transportation, vol. 2, issue 1, 2012, pp. 18-28.
10. P. Krause, “Analysis of Electric Machinery”, McGraw-Hill, 1986.
11. Chee-Mun Ong, “Dynamic Simulation of Electric Machinery using Matlab/Simulink”, Prentice Hall PTR, 1998.
12. H. Gremmel, G. Kopatsch. “Switchgear Manual”, ABB AG Germany, 11th edition, 2008.